UNCOVERING MECHANISMS THAT CONTROL MYOSIN-1A MEMBRANE BINDING AND TARGETING DYNAMICS

By

Jessica Nicole Mazerik

Dissertation

Submitted to the Faculty of the

Graduate School of Vanderbilt University

in partial fulfillment of the requirements

for the degree of

DOCTOR OF PHILOSOPHY

in

Cell and Developmental Biology

August 2013

Nashville, Tennessee

Approved:

Professor James R. Goldenring

Professor Charles R. Sanders, II

Professor Matthew J. Tyska

Professor Susan R. Wente

ACKNOWLEDGEMENTS

First and foremost, I would like to thank my mentor, Matt Tyska. During the course of my graduate career, he has offered advice, enthusiasm and encouragement and has supported my scientific endeavors and related extracurricular activities. He has trained me to ask questions that address “big picture” problems, interpret data critically and thoughtfully, and present results in ways relay coherent and interesting stories. He has an amazing ability to describe scientific problems and findings clearly and with contagious excitement. Watching him communicate so brilliantly has inspired me to transition into a science communications career. His leadership and personality have also fostered an excellent training environment: My present and past lab mates and I are close friends, and I owe them much gratitude for being unbelievable colleagues.

I want to thank my committee members, Drs. Susan Wente, Jim Goldenring, Chuck Sanders, and Shane Hutson. Throughout my training they have offered me invaluable advice, direction, and support, especially in regards to career development, and I am blessed that such a talented group of scientists helped me along this path. Although they were not members of my committee, I want to thank Drs. Puck Ohi and Melanie Ohi for helping me learn new techniques and providing critical feedback about my project as it progressed, and Dr. Anne Kenworthy and Lewis Kraft, with whom we have collaborated closely over the past year. I would also like to thank the Epithelial Biology Center for funding equipment that was vital to my project, and the American Heart Association and Molecular Biophysics Training Grant for funding.

Finally, I'd like to thank my family for being so supportive through this process. This includes Mom and Dad, my husband Drew, my sisters, Christina and Colie, my brother, Mike, my in-laws DS, Susan, and Stacey, my Columbus friends, and the friends I have made here in Nashville. Over the past six years, we have made many memories and shared many fun experiences. I cherish these relationships and am grateful for each and every one of them.

TABLE OF CONTENTS

Page

LIST OF FIGURES

LIST OF TABLES

LIST OF ABBREVIATIONS

Acan	Acanthamoeba
ADP	Adenosine di-phosphate
APC^{min}	Adenomatous polyposis coli
Arp 2/3	Actin-related protein 2/3
ATP	Adenosine tri-phosphate
BHB	Basic hydrophobic basic
CaM	Calmodulin
CaMKII	Calmodulin dependent protein kinase II
CL4	LLC-PK1-CL4
CTM	Carboxyl-terminal targeting motif
DOPC	1,2-dioleoyl-*sn*-glycero-3-phosphocholine
DOPE	1,2-dioleoyl-*sn*-glycero-3-phosphoethanolamine
DOPS	1,2-dioleoyl-*sn*-glycero-3-phospho-L-serine
EGFP	Enhanced green fluorescent protein
EPEC	Enteropathogenic *Escherichia coli*
FEM	-Fold Enrichment in Microvilli
FL	Full length
FPLC	Fast protein liquid chromatography
FRAP	Fluorescence recovery after photobleaching
Lact-C2	Lactadherin-C2
LPS	Lipopolysaccharide
LV	Lumenal vesicle

MSD	Mean squared displacement
Myo1a	Myosin-1a
Myo1x	Myosin-1x (x = letter that defines the myosin isoform)
NMI	Nuclear myosin I
NTM	Amino-terminal targeting motif
PAK	p21 activated kinase
PH	Pleckstrin Homology
P_i	Inorganic phosphate
PI 3-kinase	Phosphatidylinositol 3-kinase
PI $(3,4,5)P_3$	Phosphatidylinositol 3,4,5 –triphosphate
PI $(4,5)P_2$	Phosphatidylinositol 4,5 –bisphosphate
PLCδ	Phospholipase C delta
rDNA	Ribosomal deoxyribonucleic acid
RFP	Red fluorescent protein
RNA	Ribonucleic acid
SH3	SRC homology 3
SM	Single molecule
TH1	Tail homology 1
TH2	Tail homology 2
TH3	Tail homology 3
TIF1A	Transcription initiation factor 1A
TIRF	Total internal reflection fluorescence
WASP	Wiskott-Aldrich syndrome protein

WIP	WASP interacting protein

CHAPTER I.

INTRODUCTION

Myosins: diverse molecular machines

Myosin motor proteins are actin-based molecular machines that use energy derived from ATP hydrolysis to transduce forces in order to perform diverse functions in cells. Humans express over 35 myosin genes; the actin-binding amino-terminal motor region is the unifying domain structure of these molecules, while their neck regions and carboxyl-terminal cargo binding tail regions vary greatly across classes (Odronitz and Kollmar, 2007). While expression patterns and functions are diverse across myosin superfamily members, all of these motors share general structural features. Myosins are categorized based on their ability to bind actin filaments through an interaction with an ATP-hydrolyzing amino-terminal motor region and have actin-activated ATPase activity (Richards and Cavalier-Smith, 2005). An alpha-helical neck extends from the back of the motor domain and functions as a force transducing lever arm. The neck region may contain coiled-coil motifs that participate in homodimerization, and IQ motifs, with consensus sequence IQXXXRGXXXRK, that facilitate light chain binding (McNally et al., 1991; Mooseker and Cheney, 1995). These motifs bind regulatory proteins such as calmodulin (CaM) or a variety of CaM-like, calcium sensitive, or signaling proteins (Houdusse and Cohen, 1995). At their carboxyl-termini, myosins have “tail” regions that usually play roles in cargo binding and help define localization and function [Fig. 1-1, adapted from (McConnell and Tyska, 2010)].

This introduction will focus on class I myosins and provide a historical

perspective of their biochemical and biophysical properties. The main focus, however, is the recent literature that has provided insight as to how specific properties prime certain motors for different physiological roles in cells, the challenges associated with those roles, and how the cellular functions of this subfamily manifest in human pathologies when misregulated. This introduction will provide insight as to what our studies with vertebrate Myosin-1a (Myo1a) have taught us overall about class I myosins, how our work fits in to the big picture being painted in the class I myosin field and how our findings have contributed to progressing the field forward.

Class I myosins are primordial actin based molecular motors

As the largest family of unconventional myosins, class I myosins are one of three ancient myosin subfamilies; the membrane binding tail homology 1 (TH1) domain is the defining feature of this ancestral class of motors (Richards and Cavalier-Smith, 2005). Myosins-I were lost by plants but are found in higher eukaryotes and lower eukaryotes, including yeast, amoeba, fungi, worms, and flies (Richards and Cavalier-Smith, 2005; Thompson and Langford, 2002). Because of their presence in such a wide diversity of eukaryotes, myosins-I are probably one of the original members of the myosin superfamily (Richards and Cavalier-Smith, 2005). Evolution has preserved these molecules and they have diversified over the years, for example through the addition of SRC homology 3 (SH3) domains to the tail regions in some cases (Richards and Cavalier-Smith, 2005). It is clear that their roles in processes such as vesicle tethering, membrane/cytoskeletal adhesion, channel gating and vesicle shedding, are essential to maintain proper cellular physiology. Understanding the structures, properties, and functions of these motor proteins will provide insight on their conservation and

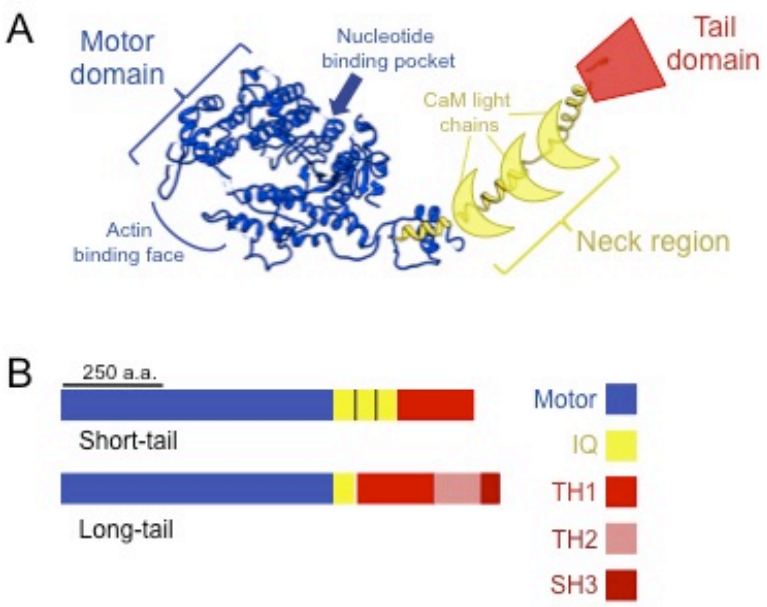

Figure 1-1. Myosin-I domain structure. A, Predicted structure of Myo1a motor and neck regions based on homology with other myosin structures. The neck region (yellow), which binds varying numbers of calmodulin molecules, connects the actin binding motor domain (blue) and the cargo binding tail domain (red). B, Cartoons representing a prototypical short tail and long tail myosin-1. Adapted from (McConnell and Tyska, 2010).

importance in organisms from single cell eukaryotes to lower vertebrates and humans.

Domain organization of class I myosins: implications for regulation & function

The domain structure for myosins-I from yeast to humans is similar, with diversifications having significant implications for functions. These proteins share the general domain features of the myosin superfamily: they have amino-terminal motor domains and carboxyl-terminal tail domains, which are linked together through their neck regions (Odronitz and Kollmar, 2007). All of these myosins are monomeric and have highly conserved motor domains (Richards and Cavalier-Smith, 2005). The neck region, which is essential for mechanochemical force transduction, consists of varying numbers of IQ

motifs and binds to calcium sensing proteins such as CaM and other light chains that have EF-hand motifs (Khoroshev et al., 1999; Mooseker and Cheney, 1995). The neck region is also a site of splicing, for example in vertebrate Myo1b, where alternative splicing results in isoforms with four, five, or six IQ motifs (Ruppert et al., 1993). Myosins-I are subdivided into short tail and long tail groups. Both groups have membrane binding TH1 domains, but long tailed myosins-I have additional protein interacting regions such as glycine, proline, alanine rich (GPA) tail homology 2 (TH2) domains and SH3 (also called TH3) domains (Richards and Cavalier-Smith, 2005; Thompson and Langford, 2002) [Fig. 1-1, adapted from (McConnell and Tyska, 2010) and Table 1-1]. As molecules that link membrane cargos to the cytoskeleton, these motors are uniquely positioned to perform a variety of functions at the membrane/cytoskeletal interface.

Domain structure and general properties- the motor domain

Class I myosins bind to actin in an ATP-dependent manner, hydrolyze ATP to generate energy and translate that energy into force using mechanochemical coupling between the motor and neck regions. A small conformational change in the motor domain is translated through the lever arm and results in a large rotation of the carboxyl-terminal tail. Upon binding to a new ATP molecule, the motor domain releases from the actin filament, starting the ATPase cycle. ATP is hydrolyzed to ADP-P_i, and the motor rebinds to the filament. P_i release corresponds to a lever arm rotation, or “power stroke,” which translates force from the motor region through the neck region and results in a physical displacement of the carboxyl-terminal tail domain. Release of ADP corresponds with a strongly bound state, or rigor. When a new ATP molecule binds, the cycle starts over (Bagshaw et al., 1974; Johnson and Taylor, 1978; Lymn and Taylor, 1971).

Table 1-1. Table of class I myosin isoforms and domain structures across species. Summary of class I myosins that are primarily discussed in this introduction. *Sc* is Saccharomyces cerevisiae and *sp* is Schizosaccharomyces pombe.

Organism	Isoform	# of IQs	Tail Length
Vertebrate (Human)	Myo1a	3	Short
	Myo1b	4, 5 or 6	Short
	Myo1c	3	Short
	Myo1d	2	Short
	Myo1e	1	Long
	Myo1f	1	Long
	Myo1g	3	Short
	Myo1h	2	Short
Drosophila	Myo31DF	2	Short
	Myo61F	3	Short
Yeast	Myo3p (*sc*)	2	Long+Acidic peptide
	Myo5p (*sc*)	2	Long+Acidic peptide
	Myo1p (*sp*)	2	Long+Acidic peptide
Dictyostelium	Myo1A	2	Short
	Myo1B	1	Long
	Myo1C	3	Long
	Myo1D	1	Long
	Myo1E	2	Short
	Myo1F	2	Short
Acanthamoeba	Myo1A	1	Long
	Myo1B	1	Long
	Myo1C	1	Long

Myosins-I are plus-end directed motors and ensembles are able to move actin filaments *in vitro*. However, single molecules are not predicted to walk for long stretches on actin bundles in cells (De La Cruz and Ostap, 2004). This prediction is supported by two general characteristics of the class I myosins. First, they are low duty ratio motors, meaning that during a single ATP hydrolysis cycle, they spend only a small

fraction of the total cycle strongly bound to actin (De La Cruz and Ostap, 2004). Kinetic studies have revealed that in the presence of ATP, their interactions with actin filaments are transient, with total bound time varying between ~5 ms for *Dictyostelium* myosins-I and ~500 ms for vertebrate Myo1b (Greenberg and Ostap, 2013). Second, class I myosins demonstrate slow actin movement (10-150 nm/s) and slow ATP turnover rates ($0.3 – 3\ s^{-1}$) (McConnell and Tyska, 2010). Because of kinetic properties they display, these motors are thought to function as ensembles rather than independently when doing work in cells (Leibler and Huse, 1993).

Although not processive as single molecules, class I myosins display relatively large lever arm rotations, which in some cases allows them to have step sizes that cover surprisingly long distances. Vertebrate and myosins-I from lower eukaryotes share this trait. The Myo1d lever arm is only 2 IQ motifs (~7 nm), yet it rotates ~ 90° to facilitate its large (14 nm) step size (Kohler et al., 2003). Structural evidence suggests that large changes in rotational angles occur concurrent to the power stroke for vertebrate Myo1a and *Dictyostelium* Myo1E as well. In Myo1a, ADP release corresponds to a lever arm rotation that results in a large (~63°) displacement of the tail domain (Jontes and Milligan, 1997a, b; Jontes et al., 1995). For Myo1E, the position of the converter domain in relation to the actin filament results in a prepower stroke position that appears to facilitate a large angular rotation of the lever arm (Kollmar et al., 2002).

Myosin motor domains, which are responsible for the actin activated ATPase activities, are structurally conserved. Variations at the level of primary amino acid sequences are predicted to provide diversity in biochemical and biophysical properties

(Uyeda et al., 1994). Structural data obtained using cryoelectron microscopy for actin bound *Acanthamoeba (Acan)* Myo1B and brush border myosin (Myo1a) from chicken support this idea. These molecules have motor regions that are structurally similar, yet variations in the primary sequence manifest in a ~10° difference in the angle at which these molecules protrude from actin filaments (Jontes et al., 1998). A crystal structure for the motor domain of *Dictyostelium* Myo1E provides the only high-resolution information available for a class I myosin motor domain to date (Kollmar et al., 2002). Comparison of this structure with a structure of the *Dictyostelium* myosin II motor domain revealed minor differences in domain conformations and loop positions, but generally the overall structure was similar, supporting the idea that structural organization of the motor domain is similar for all members of the myosin superfamily (Milligan, 1996; Vale and Milligan, 2000). The main structural features are the globular upper 50 kDa and lower 50 kDa domains which form the actin binding interface, several loops that aid in actin binding and others that facilitate nucleotide binding, hydrolysis, and release, a relay helix that communicates the nucleotide state to the converter, and a converter region that participates in mechanical transduction (Rayment et al., 1993). The actin binding interfaces and active sites are also well conserved at the level of primary sequence. Key variations in amino acids have functional and regulatory consequences and allow for diversity of biochemical properties exhibited across and within myosin classes.

Domain structure and general properties - the lipid binding tail domain

Although protein interacting partners have been identified for some class I myosins, the most ubiquitous cargo for this family of molecules is membrane. In 1989, Adams and

Pollard first verified directly that *Acan* myosins-I are *bona fide* membrane binding proteins (Adams and Pollard, 1989). Shortly after that, Hayden and colleagues isolated Myo1a from chicken intestines and performed similar *in vitro* membrane binding experiments (Hayden et al., 1990). Both studies clearly showed these molecules bind negatively charged phospholipids and suggested the interactions, most likely mediated by the carboxyl-terminal region, are electrostatic and of reasonably high affinity (~100-300 nM). These early studies supported the notion that TH1 might support an interaction with membrane for all class I myosins.

Almost two decades passed before a putative class-wide membrane binding mechanism was proposed. Detailed studies revealed that vertebrate Myo1c binds with high affinity and specificity to phosphatidylinositol 4,5, -bisphosphate ($PI(4,5)P_2$) through an interaction with a putative Pleckstrin Homology (PH) domain in the TH1 (Hokanson et al., 2006; Hokanson and Ostap, 2006). Mutations to two highly conserved signature basic residues in the PH region abolish this interaction and membrane localization in cells. Sequence homology analysis revealed that other vertebrate class I myosins share these residues and the putative PH region (Hokanson et al., 2006).

These initial studies lay important groundwork for understanding the TH1/membrane interaction. Subsequent work showed that *Dictyostelium* Myo1D, Myo1E, and Myo1F localize to the leading edge of cells during chemotaxis through an interaction with phosphatidylinositol 3,4,5 triphosphate ($PI(3,4,5)P_3$) that is mediated by the PH domain and IQ motifs (Chen et al., 2012; Zhang et al., 2010). Vertebrate Myo1b also binds $PI(4,5)P_2$ with high affinity *in vitro*, and intact signature basic residues are required for peripheral membrane targeting in cells for Myo1b, Myo1g, and Myo1f

(Komaba and Coluccio, 2010; Olety et al., 2010; Patino-Lopez et al., 2010). However, Myo1e, Myo1a, and *Acan* myosins-I are not reliant on the signature PH domain residues to localize properly in cells, indicating an alternative membrane binding mechanism facilitates targeting for these motors. They instead bind membrane through electrostatic interactions; $PI(4,5)P_2$ and other anionic phospholipid species contribute to the interaction, albeit not stereospecifically (Brzeska et al., 2008; Feeser et al., 2010; Mazerik and Tyska, 2012). In *Acan* and some *Dictyostelium* myosins-I, motifs alternative to the PH are required for interactions with membranes. These regions, called basic-hydrophobic-basic (BHB) motifs, are presumably unstructured and contain alternating basic and hydrophobic residues (Brzeska et al., 2012; Brzeska et al., 2010). Although the alternative lipid binding motifs identified in vertebrate Myo1a and Myo1g were not tested directly for ordered structure, similar sequences is found in lipid binding regions outside the myo1-PH domains (Mazerik and Tyska, 2012; Patino-Lopez et al., 2010). Overall, these studies highlight the multisite nature and diversity in membrane binding mechanisms used in the class I myosin family.

From a functional standpoint, the tail domains of vertebrate class I myosins are required for proper subcellular localization. In some cases, the motor enhances localization, but in general a functional motor domain cannot target without a tail (Benesh et al., 2010; Patino-Lopez et al., 2010; Ruppert et al., 1995; Tang and Ostap, 2001; Tyska and Mooseker, 2002). The lifetime of the tail/membrane interaction can be long lived; transient kinetic assays and fluorescent recovery after photobleaching (FRAP) experiments suggest the interaction lasts several seconds, or at least long enough to remain attached for the full duration of one or more ATPase cycles (Feeser et

al., 2010; McKenna and Ostap, 2009; Tang et al., 2002; Tyska and Mooseker, 2002). This interaction is substantially longer than the measured duration of the strongly bound interaction between the motor domain and actin during an ATPase cycle, which typically lasts several hundred milliseconds.

When liposomes containing physiologically relevant mixtures of lipid species are used to measure tail/membrane interactions for vertebrate Myo1c and Myo1e, transient kinetic methods reveal decreases in dissociation rates (i.e., increases in bound lifetimes) when compared to rates measured when liposomes composed of 2% $PI(4,5,)P_2$ in a neutral background are used (Feeser et al., 2010; McKenna and Ostap, 2009). This effect was more substantial for Myo1e, perhaps because of the electrostatic nature by which it interacts with membranes (versus the ability of Myo1c to bind $PI(4,5)P_2$ stereospecifically). In the case of Myo1c, additional negative charge greatly decreases the dissociation rate. In live cell FRAP studies on vertebrate Myo1a-TH1 in brush borders of polarized epithelial cells, slow recovery takes ~40 seconds. Impressively, full-length Myo1a recovers at the same rate, indicating at the level of ensemble analysis TH1 dominates the cellular dynamics. These data also revealed subtle differences in the total immobile fractions between these two proteins, but its significance is unclear (Tyska and Mooseker, 2002). Overall, these results suggest that in physiological lipid environments myosins-I total bound lifetimes can be long.

Other biochemical properties

Biochemical and biophysical studies have revealed properties that may provide unique insight as to how class I myosins perform their duties *in vivo*. For example, early biochemical studies using *Acan* myosins-I revealed that these motors are actin

crosslinkers, a feature that results in a biochemical cycle that is titrated by varying concentration of actin in solution (Albanesi et al., 1985a; Albanesi et al., 1985b; Fujisaki et al., 1985). The GPA regions of these molecules interact with actin in an ATP-independent fashion; this results in an actin-activated ATPase cycle that is 'triphasic' (Albanesi et al., 1983; Lynch et al., 1989; Pollard and Korn, 1973). Intriguingly, when bound to lipid, the actin interaction with the ATPase independent actin binding site is inhibited, suggesting the tail domains of these molecules bind either lipid or actin, but not both at the same time (Miyata et al., 1989). The actin crosslinking mechanism for *Acan* myosins-I appears to be unique to long tail class I myosins, as vertebrate Myo1e also displays this triphasic activation and an ATP-insensitive actin binding site in the tail (Stoffler and Bahler, 1998), which is absent in other isoforms.

Regulation by phosphorylation

In yeast, *Acan* and *Dictyostelium* myosins-I, phosphorylation of the motor domain is required for ATPase activity and movement of actin filaments (Bement and Mooseker, 1995; Redowicz, 2001). One highly conserved regulatory site has threonine, glutamate, aspartate or serine, and is known as "TEDS." Negative charge at the TEDS site is required for activation. Vertebrate motors have glutamate or aspartate residues and are constitutively active, while myosins with serine or threonine require phosphorylation. Members of the p21 activated kinase (PAK) family confer this phosphorylation (Redowicz, 2001).

The TEDs site is in the cardiomyopathy loop, a stretch of amino acids in the upper 50 kDa domain that is so named because mutations in this loop in human cardiac muscle myosin II are associated with hypertrophic cardiomyopathies (Geisterfer-

Lowrance et al., 1990). The negative charge in this position causes the loop to undergo a conformational change that speeds the rate of phosphate release (Redowicz, 2001). *Dictyostelium* myosins-I absolutely require an intact functional phosphorylation site to properly fulfill their roles in cell growth and pinocytosis (Novak and Titus, 1998). In yeast, however, mutations to the phosphorylation site result in defects in fast, ligand-induced endocytosis, but have little effect on constitutive, slow endocytosis (Grosshans et al., 2006). These results point to the highly specific regulation of the various *in vivo* functions for this class of motors.

Phosphorylation of vertebrate Myo1c is required for this motor to fulfill its role in vesicle trafficking in adipocytes. Myo1c is phosphorylated by calmodulin-dependent protein kinase II (CaMKII) at residue S701; this induces the loss of at least one calmodulin from the neck region, stimulates ATPase, and facilitates an interaction with 14-3-3 (Yip et al., 2008). Although Myo1c is ubiquitously expressed, the interaction with 14-3-3 is not evident in rat muscle cells (Yip et al., 2008). Furthermore, Myo1c, but not CaMKII, is still required for vesicle docking in these cells (Boguslavsky et al., 2012), suggesting the mechanism that regulates this process may be cell-type dependent.

Regulation by inter- and intramolecular interactions

Intramolecular interactions or interactions with CaM and other light chains modulate biochemical and biophysical properties of myosins-I. These interactions have been heavily investigated *in vitro*. The myosin-I neck region is an alpha helix that acts as a lever arm and provides an excellent regulatory switch. Rigidity of the neck, which is required for force transduction, is primarily achieved through interactions with the Ca^{2+} binding protein, CaM (Mooseker and Cheney, 1995). Because CaM undergoes a

conformational change upon binding to Ca^{2+} (Yap et al., 1999), the neck region is highly susceptible to regulation by Ca^{2+}/CaM interactions. The neck region is inherently flexible in the absence of CaM, and some myosins fold through a conformational change in the neck region that results in an interaction between the motor and tail domains.

The overall effects of calcium on the ATPase activity and mechanical ability of myosins-I have been studied extensively *in vitro* and reviewed at length elsewhere (Greenberg and Ostap, 2013; McConnell and Tyska, 2010). Generally, low micromolar levels of Ca^{2+} increase ATPase rates, but decrease or prevent the ability to move actin filaments. The latter effect is rescued by including additional exogenous CaM (Adamek et al., 2008; Lin et al., 2005; Williams and Coluccio, 1994; Wolenski et al., 1993b). Together with structural studies (Whittaker and Milligan, 1997), this suggests that at least one CaM dissociates from the neck region in the presence of Ca^{2+}.

Although regulation is needed to conserve cellular energy, and Ca^{2+}/CaM interactions seem likely candidates to regulate these processes based on *in vitro* studies, little is known about how class I myosins limit motor activity or membrane binding activity in cells. Several members of the myosin superfamily, including myosins II, V, VII and X, undergo a conformational change in the neck region that results in folding and a head-tail interaction that regulates ATPase activity (Ikebe, 2008; Sellers and Knight, 2007; Taylor, 2007; Umeki et al., 2011; Umeki et al., 2009; Yang et al., 2009). In some cases, interactions between the light chains and neck regions mediate this shape change, while in other cases the resulting conformation is stabilized by head/tail interactions. Cryoelectron microscopy studies have shown that upon CaM

dissociation in vertebrate Myo1a, TH1 undergoes a large displacement in space (Whittaker and Milligan, 1997). This structure was obtained when Myo1a was actin bound and does not conclusively show that this molecule can fold, but it suggests that the neck has the flexibility needed to undergo a large change in conformation that may lead to folding. *In vitro* studies investigating vertebrate Myo1e ATPase also hint that class I myosins may fold. For vertebrate Myo1e, the tail domain regulates ATPase activity (Stoffler and Bahler, 1998). In solution ATPase assays, addition of tail binding antibodies increases both the basal and actin-activated ATPase rates, presumably by relieving the tail's inhibitory effects. These results support the idea that the tail may be folding back to interact with the motor domain, but structural evidence to confirm this idea is lacking, and the contribution of any Ca^{2+}/CaM interaction were not investigated. For the long tailed motor *Acan* Myo1C, a structural change that results in a folded molecule has been confirmed using nuclear magnetic resonance. The carboxyl-terminus folds back on itself and results in an interaction between the SH3 domain and a more amino-terminal PH domain in the tail's basic region (Hwang et al., 2007; Ishikawa et al., 2004). However, the site that facilitates this interaction is in the tail rather than the neck region. While folding appears to be important to limit activity in other myosins, further studies are needed to determine if this is also a class-wide feature of myosins-I and to understand the interplay between folding and CaM/ Ca^{2+} interactions in cells.

Regulation by mechanical loading

Some myosins-I produce their working stroke in two steps, a feature that suggests regulation by mechanical force. This model was first supported when kinetic data

verified that ADP release occurs in two biochemically distinct steps (Jontes et al., 1997). Optical trapping experiments with Myo1a, Myo1b, and Myo1c later showed that these molecules do in fact produce their working stroke in two steps (Batters et al., 2004; Veigel et al., 1999). However, despite its unusually large lever arm rotation, the secondary step was not detected for Myo1d (Kohler et al., 2003). These early studies led to the hypothesis that myosins-I with a two-step working stroke are able to sense and respond to tension. In this model, a resistant load on these molecules could lead to inhibition of the biochemical event that precedes detachment (ADP release) and thus greatly increase the duration of the strongly bound state.

Recently, such strain dependence was confirmed for vertebrate Myo1b and Myo1c (Greenberg et al., 2012; Laakso et al., 2008) [Fig. 1-2, A and B; adapted from (McConnell and Tyska, 2010)]. Optical trapping experiments were used to measure actin attached durations for single molecules under load. While under applied forces, both of these molecules transition into high duty ratio motors. Interestingly, there are notable differences between Myo1b and Myo1c force sensing, which have been analyzed in detail elsewhere (Greenberg and Ostap, 2013). First, Myo1b transitions from a low duty ratio motor to a high duty ratio motor at very small forces (<1pN). The actin attached lifetimes for Myo1b molecules under these small loads increases from ~0.05 s to ~50 s (Laakso et al., 2008; Lewis et al., 2006). This force transition is abolished in the presence of low micromolar calcium, and is linearly related to the length of the neck. (Laakso et al., 2010; Lewis et al., 2012). The shorter splice forms of Myo1b are not efficient tension sensors, which might alter or affect their roles *in vivo.* Myo1c transitions to a high duty ratio motor only at forces >2.5 pN and can generate much

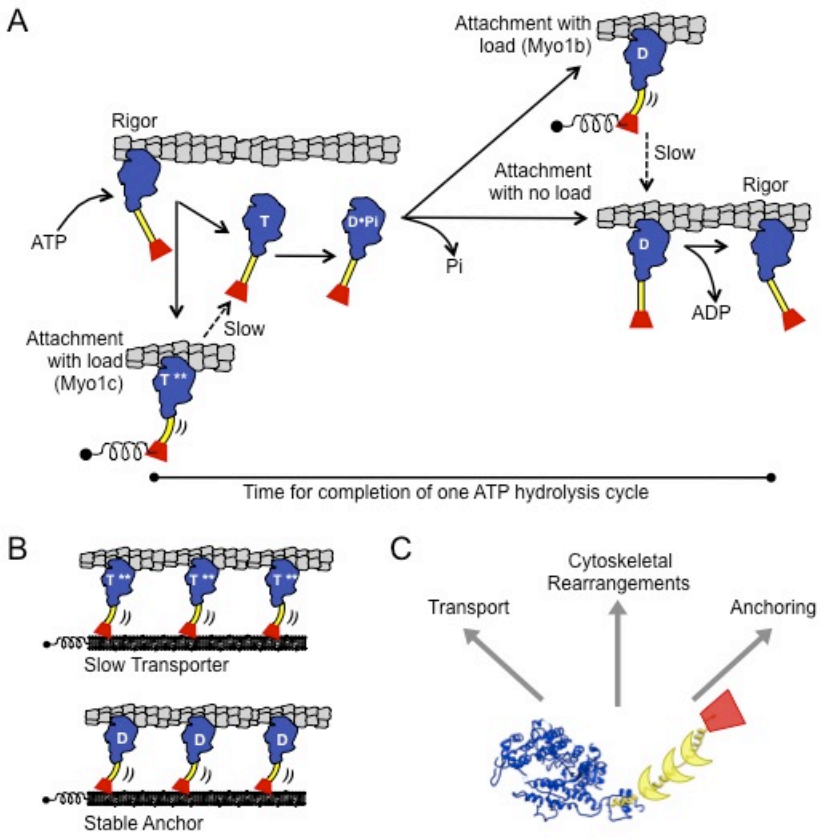

Figure 1-2. The myosin ATPase cycle. A, Cartoon of the mechanochemical cycle for class I myosins. Force sensitive steps (ADP release for Myo1b and ATP isomerization for Myo1c) are indicated B, Force sensitive transition steps for Myo1b and Myo1c lead to altered actin attachment durations and are predicted to alter actin-attached behavior. Adapted from (McConnell and Tyska, 2010).

more power over a large range of forces compared to Myo1b (Greenberg et al., 2012). The force-sensitive kinetic step is also different for these two motors. For Myo1b, the ADP release rate is altered under load, while in Myo1c, ATP isomerization (i.e., the rate of ATP binding and transition into a state that promotes myosin dissociation from the filament) is altered. Because of these differences, Myo1c is expected to function in longer range transport, while Myo1b is predicted to act as a true tethering motor in cells

(Greenberg and Ostap, 2013). Whether Myo1a has the ability to transition to a high duty ratio motor is yet to be explored, but as these studies highlight, motors with similar kinetics behave quite differently under load, leading to differences that could further explain the diversification of their cellular functions.

Physiological roles for class I myosins

Since the first class I myosin was discovered in *Acan* in the early 1970s (Pollard and Korn, 1973), decades of research have provided biochemical, biophysical, and cell biological insight on the *in vivo* functions of these motors. In recent years, many studies have suggested that vertebrate class I myosins are "tension sensitive" molecules that act as dynamic linkers between the membrane and cytoskeleton (McConnell and Tyska, 2010). In light of the most recent *in vitro* studies using optical trap assays to directly measure this tension sensitivity for Myo1b and Myo1c, we review the last decade of *in situ* and *in vivo* studies, highlighting how these motors may exploit tension sensing to carry out specific tasks in cells [Fig. 1-3, adapted from (McConnell and Tyska, 2010)].

I*n vitro* experiments suggest some class I myosins may be more finely adjusted to sense load and become a rigid tether (Myo1b) (Laakso et al., 2008), while others are adapted to play more dynamic roles in transport-related processes in cells (Myo1c) (Greenberg et al., 2012). We will therefore discuss possible functional roles for myosins-I that are characterized as either 'anchoring' and 'transporting' [Fig. 1-2 C, adapted from (McConnell and Tyska, 2010)]. Here, anchoring is any process where myosins-I are required for membrane stabilization, and myosins-I involvement in vesicle or membrane movement is defined as transport. There is no direct evidence that Myo1c (or any class I myosin) functions as a *bona fide* transporter in cells. However, in

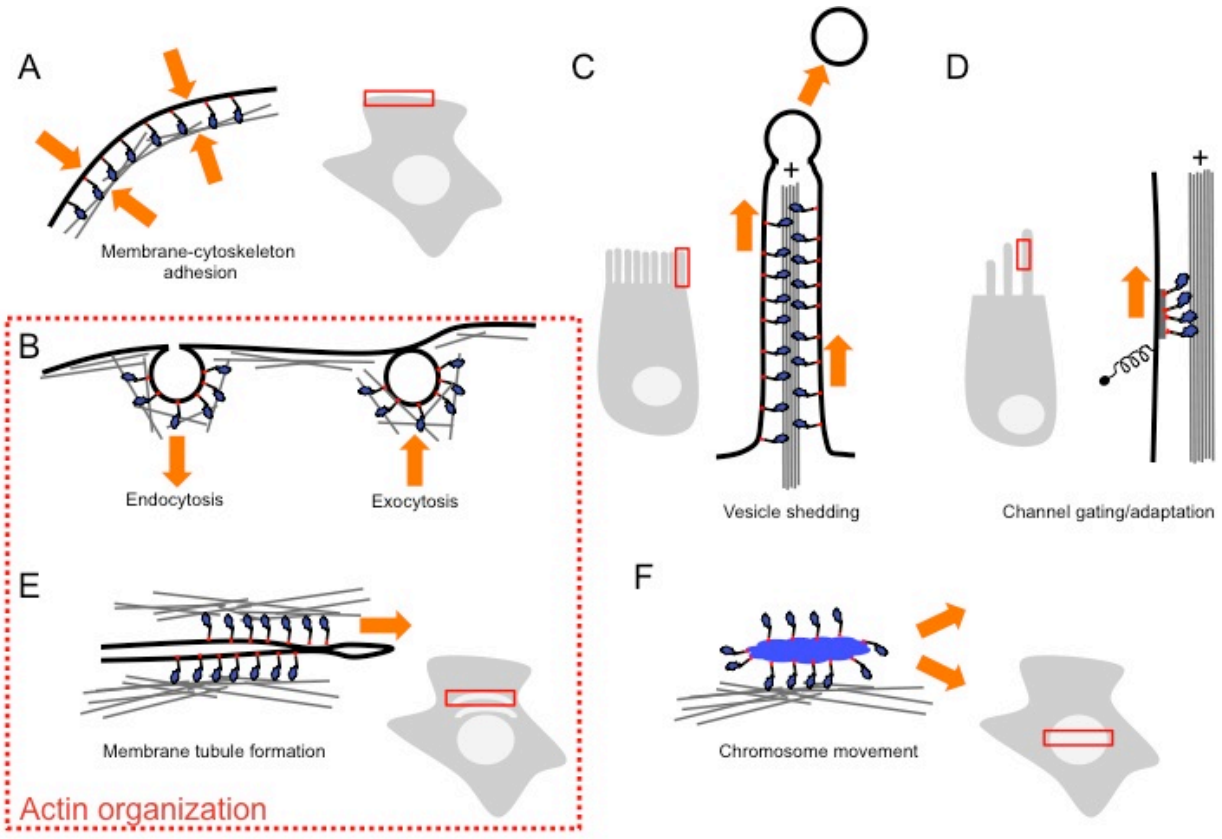

Figure 1-3. Class I myosins regulate cellular functions at the actin/membrane interface. A, Myosins-I dynamically link the plasma membrane to the actin cytoskeleton to regulate cellular adhesion. B, To facilitate endo- and exocytosis, myosins-I shape the membrane and actin. C, Myosin-I in protrusions on the apical surfaces of enterocytes contributes to membrane movement that results in vesicle shedding. D, Myosin-I in stereocilia plays a role in hearing by helping to maintain tension between tip links. E, Myosin-I reorganizes the actin cytoskeleton and aids in membrane tubule formation at the golgi. F, Chromosome movement is dependent on the actin cytoskeleton and nuclear myosin-I. Adapted from (McConnell and Tyska, 2010).

combination with the biophysical evidence described above, some studies discussed below support this role for Myo1c. Likewise, there is no direct evidence for tension sensing events *in vivo:* studies have not directly shown that myosins-I under load in cells alter their kinetics during specific tasks. Studies examined here show that some

myosins-I act as anchors, which supports the idea that myosins-1 have the ability to respond to tension while performing functions in cells.

Next, we will touch on the ability of class I myosins, especially in lower eukaryotes, to influence the arrangement of the actin cytoskeleton [Fig. 1-2 C, adapted from (McConnell and Tyska, 2010)]. Yeast and *Dictoystelium* myosins-I interact directly with actin polymerizing proteins and thereby influence the cytoskeleton during certain processes. In *Drosophila*, genetic modification of myosins-I expression results in *situs inversus*. This phenotype is striking, but the underlying mechanism is less clear.

Finally, we will discuss recent literature that describes roles for vertebrate myosins-I in human diseases and pathologies. These studies are part of a growing body of literature that is continually highlighting the importance and evolutionary impact of class I myosins.

Anchoring

Control of cellular tension

Maintenance of cellular membrane tension, the ability to resist deformation, is vital to cellular processes such as endocytosis, exocytosis, cell division, and motility (Dai and Sheetz, 1995; Raucher and Sheetz, 2000). Often, a fine balance and adjustability between low tension and high tension is required to permit a cell to undergo these functions. Because myosins-I are at the actin/cytoskeletal interface and interact directly with the actin cytoskeleton (which itself provides structure, shape and support), they are uniquely positioned to regulate membrane tension in cells.

Experiments using *Dictystelium* in the 1990s first showed directly that myosins-I are required for whole-cell tension maintenance. Loss of Myo1A and Myo1B resulted in

defects in chemotaxis: in the absence of either one of these motors, the cells simultaneously extend multiple psuedopods, turn more frequently, and exhibit decreases in velocity of directed motility (Titus et al., 1993; Wessels et al., 1991). Although genetically eliminating more than one myosin-I from *Dictyostelium* does not cause more severe motility phenotypes, it does result in defects in non-receptor mediated fluid phase uptake, or macropinocytosis, and increases in the number of actin protrusions associated with this process (Jung et al., 1996; Novak et al., 1995). *Dictyostelium* cells that overexpress Myo1B also have motility defects and lack the ability to rearrange cytoskeletal components (Novak and Titus, 1997). Together, these studies suggest that the proper concentration of myosin-I at the cortex is critical for maintaining tension needed to perform basic cellular functions. Indeed, micropipette aspiration assays were later used to show that cortical tension drops in cells lacking at least two myosin-I isoforms (Dai et al., 1999). These studies, however, measured overall cellular deformability and did not directly tease out the differences between myosins-I acting as dynamic membrane/cytoskeletal adhesion molecules or direct regulators of the actin cytoskeleton. Those studies came later, using vertebrate class I myosins.

Even the earliest electron micrographs hinted at a role in structural maintenance for vertebrate class I myosins. Specifically, images revealed that Myo1a, which is expressed primarily in the small intestine, is found in the ideal position for this role: it directly links the actin cytoskeleton to the plasma membrane in the epithelial cells that line the small intestine. Striking electron micrographs of the brush border, a densely packed array of parallel, membrane-enclosed actin structures on the apical surfaces of

gut enterocytes, revealed lateral cross bridges that link the core actin bundles to the overlying plasma membrane (Mooseker and Tilney, 1975). The early images clearly showed molecules connecting actin to membrane but did not report on the dynamicity of this cross linker. Later studies using Myo1a isolated from chicken small intestines showed that the 'lateral bridges' are actually Myo1a, and revealed that the molecules possess actin-activated ATPase activity and display plus end directed (albeit slow) motility on actin filaments (Conzelman and Mooseker, 1987). Years later, the Myo1a knockout mouse was developed and Myo1a was further implicated in regulating membrane tension. Although these mice do not have overt physiological defects, close examination of the microvillar structure unearthed significant perturbations. Occasionally, scanning electron micrographs revealed large, protruding membrane herniations, where, in the absence of Myo1a, the membrane is completely disassociated from the underlying core actin bundles (Tyska et al., 2005). The lack of an obvious phenotype in the Myo1a knockout mice was attributed to the redistribution and redundant function of other class I motors, Myo1c and later Myo1d (Benesh et al., 2010; Tyska et al., 2005). Although these motors clearly could not completely and exactly replace Myo1a, their redundancy indicated that membrane tension regulation might be a class wide function.

Optical trapping assays provided direct measurement of the adhesion capacity of several vertebrate myosins-I, including Myo1a, b, c, d and e, and verified that they do in fact modulate tension (Nambiar et al., 2009). Interestingly, Myo1e provides the most membrane stabilization, followed by Myo1c, Myo1b, Myo1d and then Myo1a. This study also directly compared brush borders isolated from wild type mice and Myo1a knockout

mice for the ability to resist membrane deformation. Not surprisingly, wild type brush borders resist much greater forces than those isolated from Myo1a knockout animals. Likewise, in living epithelial cells that have endogenous Myo1a, overexpression of Myo1a induces an increase in response to tension, while expression of Myo1a-TH1, which acts as a dominant negative, reduces membrane tension to levels lower than that of cells expressing EGFP alone (Nambiar et al., 2009). Myo1g knock down was later shown to increase the elasticity of Jurkat cells (Olety et al., 2010), which added to the evidence that membrane tension maintenance is a class-wide feature.

An interesting side effect of linking the cytoskeleton to the plasma membrane is the potential to influence interactions between other proteins or membrane components and the actin network. The brush border is highly specialized for nutrient processing and absorption, and proper localization of enzymes and channels that facilitate these functions is critical for these processes to be carried out properly. It turns out that Myo1a is not only important for maintaining membrane tension and structure of the brush border, but is also required to retain a key nutrient processing enzyme in the apical domain. A transient interaction between Myo1a and sucrase isomaltase is necessary for the proper localization of this protein. Overexpressing the dominant negative Myo1a-TH1 in epithelial cells that have protein composition very similar to that of *bona fide* brush borders breaks this interaction and sucrase isomaltase is lost from the brush border (Tyska and Mooseker, 2004). This indicates that the membrane/cytoskeletal link facilitated by Myo1a is required to maintain proper composition in the apical domains of enterocytes. About 20% of total brush border Myo1a is associated with detergent resistant membranes, where integral and

transmembrane processing proteins are usually found (Tyska and Mooseker, 2004). It is interesting to speculate that these membranes might impart force onto this population of Myo1a. This could result in altered motor kinetics that increase actin attachment lifetime and decrease the dynamics of Myo1a-bound sucrase isomaltase to retain this protein in microvilli.

Directing traffic at the golgi

Although several myosins-I have been implicated in endocytosis, exocytosis, or other aspects of membrane trafficking, we will focus on the role of vertebrate Myo1b in these processes because this motor has unique load-sensing abilities. The wide expression of Myo1b--- in the lungs, liver, heart, and brain (Ruppert et al., 1993; Sherr et al., 1993)--- suggests this motor is a good candidate to participate in a process common to many cell types. Recently, Myo1b was shown to facilitate transport of receptors from the trans-golgi network to endosomes and plasma membrane (Almeida et al., 2011; Coudrier and Almeida, 2011). Knockdown of Myo1b substantially slows these processes and also results in morphological changes in golgi stacks. Live cell imaging experiments showed that these defects are caused by a reduction in the post golgi carriers that normally transport these proteins. These carriers start from membrane tubules, to which Myo1b and actin are recruited, elongate, then undergo a scission event to continue in the trafficking process. In the absence of Myo1b, tubule formation is decreased, as are the actin foci with which they normally associate (Almeida et al., 2011). These results indicate that Myo1b might act on the membrane, the actin, or both. In an earlier report, expression of Myo1b resulted in tubular membrane structures on multivesicular endosomes, further supporting the ability of Myo1b to generate

membrane tethers (Salas-Cortes et al., 2005).

These data support a model where Myo1b is required to tether membrane tubules to a stable F-actin structure. Live cell imaging showed Myo1b is indeed recruited to these structures. *In vitro*, Myo1b can lock up on an actin filament for ~50 s (Laakso et al., 2008). If Myo1b is under load in the tethering scenario, one possibility is that a long actin- and membrane- attachment would allow Myo1b molecules to properly orient the F-actin, thus giving Myo1b influence over the arrangement of actin foci. Interestingly, Arp2/3 complex knockdown phenocopies the loss of actin foci also seen upon Myo1b knockdown (Almeida et al., 2011), which could suggest a more direct interaction between Myo1b and recruitment of actin polymerization proteins. Although the plasma membrane is thought to be the primary cargo for most class I myosins including Myo1b, another possibility is that Myo1b could recruit Arp2/3 or interacting proteins either directly or by retaining certain protein/lipid environment through its membrane interaction. Direct high resolution imaging of Myo1b on these structures is needed to determine if Myo1b is acting as a static tether or participating in dynamic rearrangement of the actin cytoskeleton.

Mechano-electrical transduction channel gating in the cochlea

Although Myo1c is ubiquitously expressed, one of its most well studied and highly debated functions is in the structures that facilitate balance and hearing. Hair cells in the inner ear respond to stimuli such as sound waves or movements through deflection of stereocilia, rows of actin-based protrusions that decrease step-wise in height and are linked together by tip links, which provide constant tension in the structure (Hudspeth, 2005). Upon deflection caused by sound waves or head movement, tip links act like

loaded springs to open gated ion channels and allow an influx of calcium. The signal is instantaneously transmitted into an electrical signal, and the system returns to its baseline mechano-sensitive, high-tension state through an adaptation response (Hudspeth, 2005). Myo1c is proposed to facilitate both fast adaptation, which happens in several milliseconds, and slow adaptation, which generally takes tens of milliseconds (Holt et al., 2002; Stauffer et al., 2005). Chemical-genetic strategies showed that in the presence of an ADP analog that transitions a population of the Myo1c motors into a strongly bound state and acts as a dominant negative for the still-functional motors, both fast and slow adaptation are blocked. While Myo1c is likely involved in both adaptation responses in some way, growing evidence suggests that the model for Myo1c as *the* adaptation motor should be refined.

One piece of evidence that contradicts the model is the location where calcium enters the stereocilia in relation to the location of Myo1c positioning for both slow and fast adaptation responses. The current model suggests that Ca^{2+} rushes into the channel, which is thought to be located at the lower tip link density, and disengages Myo1c, which is localized to the upper tip link channel This results in a drop of tension and channel slippage associated adaptation (Gillespie and Muller, 2009). This means that Ca^{2+} likely enters the stereocilia at the channel opposite from where Myo1c is proposed to act. Furthermore, the distances that Ca^{2+} diffuses during adaptation responses has been measured in turtle hair cells (Ricci et al., 1998), and Myo1c is located outside the radii of diffusion for both slow and fast adaptation. Although the distance between upper tip link and lower tip link varies in different organisms, these results suggests that Ca^{2+} is unlikely to reach Myo1c in time to provide a regulatory

switch (Gillespie and Muller, 2009). Furthermore, the overall effects that calcium would have on Myo1c under load *in vivo* have not been tested. Unloaded, calcium results in decreased motility for Myo1c in gliding filament assays. Under load, however, it is not clear how detachment kinetics would be altered. Whereas Myo1b working stroke and thus actin attachment lifetimes (i.e., tension sensing) decrease in the presence of calcium (Lewis et al., 2012), Myo1c working stroke increases in the presence of calcium (Batters et al., 2004) and therefore may respond differently under load (Greenberg et al., 2012). While more biophysical experiments are needed to determine if this is the case, the recent optical trapping experiments suggest that Myo1c is not exquisitely sensitive to load (Greenberg et al., 2012) and therefore may be more fit to maintain overall tension of this specialized auditory system through constant power generation rather than respond to the fluctuations in tension.

Transport?

A role in the nucleus

Not long after actin was implicated in diverse functions in the nucleus (Rando et al., 2000), the ubiquituously expressed Myo1c was identified as a nuclear myosin (Nowak et al., 1997; Pestic-Dragovich et al., 2000). Three isoforms of Myo1c have been found in the nucleus to date, including the originally discovered isoform that is predominantly thought to be cytoplasmic. The Myo1c gene on chromosome 11 has multiple start sites, which results in three distinct gene products (Ihnatovych et al., 2012; Pestic-Dragovich et al., 2000). The shortest gene product is commonly referred to as ‘cytoplasmic’ Myo1c (although it is also found in the nucleus under the ideal conditions (Dzijak et al., 2012)), while the two other gene products have amino terminal extensions of 36 and 16

additional amino acids, respectively (Ihnatovych et al., 2012; Pestic-Dragovich et al., 2000). A nuclear import sequence in the neck region and the importins beta, 5 and 7 are required to shuttle Myo1c into the nucleus (Dzijak et al., 2012). Interestingly, this implies that the nuclear localization of Myo1c is regulated by CaM binding. In the presence of CaM, the nuclear localization sequence is likely inaccessible, thus preventing transition into the nucleus (Dzijak et al., 2012). In the nucleus, Myo1c (called NMI upon nuclear localization) complexes with RNA polymerase II (Pol II) and is critical in the process of transcription, as antibodies against NMI inhibit *in vitro* transcription in nuclear extracts (Pestic-Dragovich et al., 2000). NMI also is important for Pol I transcription of ribsosomal RNA genes (rDNA) in nucleoli (Philimonenko et al., 2004). NMI and actin both associate with rDNA. While actin is required for later steps in transcription, NMI is required early for initiation and complexes with rDNA via an interaction with phosphorylated transcriptional initiation factor, TIF-IA. Microinjection of antibodies against either actin or NMI specifically inhibits rDNA transcription, and knockdown of NMI leads to a reduction in rRNA products (Philimonenko et al., 2004). Other data suggest NMI also plays a role in chromatin remodeling through its association with B-WICH, a protein that works post-initiation to open a gene that is being actively transcribed by Pol I (Percipalle and Farrants, 2006). Clearly, NMI interactions with other proteins are involved in its transcription regulation, but NMI motor activity is also required (Ye et al., 2008). In scenarios in the nucleus, Myo1c might be trading in its membrane interaction to instead act as a dynamic linker between protein complexes and actin.

An interesting observation in light of the recent mechanical studies of Myo1c is

that NMI has also been implicated in chromosome movement during interphase (Chuang et al., 2006). Under an inducible system that allows for visualization and imaging of chromosome movement, chromosomes start at the periphery of the nucleus and move into a more central position over time. During periods of rapid directional movement their average velocity is ~0.3 μm/min (0.005 μm/s) (Chuang et al., 2006). Actin is required for the chromosome movement, and NMI is required to make the transport efficient. A mutation to NMI predicted to result in weak actin binding causes a 3-hour delay in chromosome movement (Chuang et al., 2006). It is unclear exactly how NMI is facilitating the translocation of chromosomes. One possibility is that NMI dynamically links the chromosome to the actin cytoskeleton, facilitating its directed transport. In *in vitro* motility assays, ensembles of Myo1c move actin filaments at a velocity of 0.3-0.5 μm/s (Zhu et al., 1996), velocities that suggest NMI transporting chromosomes is feasible, however, movement of the motor was not observed directly. High resolution imaging studies of NMI in the nucleus are needed to determine if its role is to facilitate directed transport or simply tether proteins to chromatin once they are properly targeted, thereby aiding in Pol I and Pol II transcription.

Membrane trafficking, exocytosis and endocytosis

Several class I myosins have been implicated in trafficking roles. Vertebrate Myo1d, which is found in most tissues throughout the body and is highly expressed in the nervous system (Bahler et al., 1994; Benesh et al., 2012), is involved in the transfer of early endosomes to recycling endosomes (Huber et al., 2000). Long tail myosins, including yeast myo3p and myo5p, and vertebrate Myo1e, are necessary for endocytosis, most likely through their abilities to influence the actin cytoskeleton (Cheng

et al., 2012; Sun et al., 2006). Vertebrate Myo1c is required for translocation of exocytic vesicles containing the glucose transporter, GLUT-4 (Bose et al., 2002; Bose et al., 2004). Because a growing amount of literature is dedicated toward Myo1c's involvement in this process, and because we now have a better understanding of the biophysical underpinnings of this motor, we will focus our discussion on GLUT-4 trafficking.

In adipocytes and muscle cells, increased insulin levels activate p110-type phosphatidylinositol 3-kinase (PI 3-kinase), which stimulates the translocation of GLUT-4 containing vesicles to the plasma membrane (Czech and Corvera, 1999). Myo1c is found on GLUT-4 vesicles and is required for GLUT-4 presentation on the surfaces of cells and for glucose uptake in both fat and muscle cells (Bose et al., 2002; Toyoda et al., 2011). Inhibition of PI 3-kinase causes GLUT-4 vesicles to aggregate at the cell periphery, presumably because they are unable to fuse with the plasma membrane, an effect that is overridden by overexpressing Myo1c (Bose et al., 2004).

In recent years, the signal pathways involved in regulating Myo1c during GLUT-4 exocytosis have been elucidated. In adipocytes, insulin stimulates PI 3-kinase signaling, which results in CaMKII kinase phosphorylation at residue S701 in the first IQ motif, a decrease in calmodulin binding, and subsequent 14-3-3 binding to Myo1c (Yip et al., 2008). Myo1c phosphorylation and motor activity are required for surface presentation of GLUT-4. Although insulin activates CaMKII, this activation is not PI 3-kinase dependent (Yip et al., 2008). Myo1c phosphorylation is, however, suggesting PI 3-kinase might prime Myo1c for phosphyorylation in some way. Interestingly, another study showed that Myo1c binding to RalA, a G-protein also found on GLUT-4 vesicles,

is another PI 3-kinase dependent interaction that is required for successful GLUT-4 trafficking (Chen et al., 2007). The interaction between Myo1c and RalA only occurs in the presence of calcium-bound CaM, indicating the calcium induced conformational change in CaM may expose a binding site. It is still unknown how these two regulatory mechanisms are related, if at all. It is interesting to speculate that they are intertwined, especially given the calcium/CaM dependent activation of CaMKII. The CaMKII-mediated regulation is specific to adipocytes, and although both mechanisms occur in adipocytes, the RalA mechanism may be more universal and occur in muscle cells as well.

While these studies clearly show that the role of Myo1c in GLUT-4 exocytosis is tightly regulated, they provide little evidence as to what that specific role is. Early dynamics studies revealed that Myo1c overexpression causes membrane ruffling at localized sites of GLUT-4 vesicle fusion (Bose et al., 2004). Recently, studies that employed total internal reflection fluorescence (TIRF) microscopy have expanded on this result. While Myo1c is not required for translocation of GLUT-4 vesicles from the perinulcear region to the cytoplasm, this motor is needed to retain and immobilize the vesicles at the cell periphery, suggesting it is probably involved in membrane tethering (Boguslavsky et al., 2012). Another intriguing observation made in this study is that Myo1c knockdown abolishes insulin-induced reorganization of the actin cytoskeleton. Determining the exact role for Myo1c in this docking and fusion process will require live cell analysis of Myo1c molecules at these sites. One possibility is that two differentially regulated populations of Myo1c are at work during these processes. While membrane bound at the cell periphery, one population of Myo1c might cycle constantly, pulling on

actin filaments to recruit and rearrange the cytoskeleton, while a second, vesicle bound population, might act as a slow transporter, constantly cycling to facilitate the navigation of the vesicles through the dense, insulin-stimulated actin network at the cell periphery.

Microvillar vesicle shedding in the gut

Studies on vertebrate Myo1a, which is specifically found in the small intestine in the brush borders of enterocytes, provide convincing evidence of directed membrane transport powered by this motor. Brush borders are made up of actin based protrusions called microvilli, which have parallel actin bundles oriented plus end out. Therefore, they present a unique structure in which to study the use of actin as a track by Myo1a, which is the most abundant motor found in this compartment (Benesh et al., 2010). When isolated from tissue, brush borders' structure and composition are maintained, making them amenable to experimentation even after they are detached from cell surfaces.

Experiments using this isolated brush border system revealed that Myo1a uses the core microvillar actin bundles as tracks to move membrane. In the presence of ATP, brush border membrane is translocated toward the plus ends of the actin bundles (McConnell and Tyska, 2007). This results in the formation, budding, and shedding of small membrane-bound vesicles. The membrane moves at ~20 nm/s, which is consistent with the velocity of a class I myosin. When the same experiment is performed on Myo1a knockout brush borders, shedding activity is reduced by ~95%, definitively demonstrating that this transport is a Myo1a dependent process (McConnell and Tyska, 2007). The residual activity observed in the absence of Myo1a might be due to the redistribution of Myo1c and Myo1d into the brush border in the Myo1a knockout tissue (Benesh et al., 2010; Tyska et al., 2005). If this is the case, this lack of

compensation by other class I myosins is a clear example of the refined differences in their physiological functions that manifest from differences in biophysical properties, even though their structural and biochemical properties seem similar.

This *in vitro* reconstitution of vesicle shedding brought about some intriguing questions: does vesicle shedding happen *in vivo*, and if so, what is the purpose of these vesicles? The answers to these questions came from experiments that used differential centrifugation to isolate vesicles from mouse small intestine flushate (McConnell et al., 2009; Shifrin et al., 2012). Scanning electron micrographs revealed vesicles budding from microvillar tips in native tissue, and biochemical analysis confirmed that the vesicles are oriented with the same topology as microvillar membrane and contain catalytically active brush border enzymes (McConnell et al., 2009). These 'lumenal' vesicles (LVs), which are ~100 nm in diameter and loaded with the enzyme alkaline phosphatase, are deployed through a seemingly regulated process in wild type mice, but LVs from Myo1a knockout mice are reduced in number, highly irregular in size and lack the protein distribution characteristic those from wild type mice (McConnell et al., 2009). The misregulation of this process in Myo1a knockout mice emphasizes this motor's role in vesicle shedding *in vivo*.

The enrichment of alkaline phosphatase on LVs provided a clue that their *in vivo* function is to help maintain gut homeostasis (Shifrin et al., 2012). This enzyme is a regulator of gut microbiota (Malo et al., 2010) and detoxifies the bacterial toxicity factor, lipopolysaccharide (LPS) (Bates et al., 2007; Koyama et al., 2002). Indeed, native LVs isolated from rat small intestinal contents physically interact with bacteria and detoxify purified LPS, inhibit the growth of native bacterial cultures and enteropahtogenic

Escherichia coli (EPEC), and when added to cultured cells, greatly reduce the ability of EPEC to attach and infiltrate the epithelial sheet (Shifrin et al., 2012). EPEC also stimulate shedding in cultured epithelial cells, a response that is abolished when the Myo1a dominant negative tail domain is expressed in the cells (Shifrin et al., 2012).

From these elegant studies, it is clear that Myo1a is intimately involved in the LV shedding process. *In vitro*, Myo1a appears to be the sole driver of membrane translation toward the microvillar tips. *In vivo,* however, the process may not be quite as straightforward. The alkaline phosphatase enrichment implies that Myo1a may be somehow regulating which membrane components are released in the LVs. Because alkaline phosphatase is an outer leaflet GPI-anchored protein, it is unlikely that Myo1a is directly transporting this enzyme. A more likely scenario is that Myo1a is able to control LV composition by retaining certain proteins in microvilli, while others diffuse freely into portions of the membrane that are released on LVs. This may be through direct (albeit transient) interactions with membrane proteins (Tyska and Mooseker, 2004) or through stronger interactions with membrane compartments, such as lipid rafts, that contain these proteins. Studies that examine Myo1a dynamics *in vivo* will help elucidate the exact mechanisms by which this motor facilitates the shedding process.

Shaping the actin cytoskeleton

Because of their abilities to bind both membrane and actin simultaneously, myosins-I are in a unique position to participate in many cellular events that involve membrane movement or deformation, or actin polymerization and rearrangement, or both. This section is focused on different mechanisms by which class I myosins are able to shape

the actin cytoskeleton. Here, we highlight the changes in the actin cytoskeleton that appear to be myosin-I dependent or are apparent during a myosin-I dependent process.

In *Dictyostelium*, myosins-I are required for functions that result from actin cytoskeletal rearrangements, such as macropinocytosis and motility. As discussed above, the actin cytoskeleton is more dynamic (ie, more pseudopods simultaneously extended, more protrusions) in *Dictyostelium* lacking myosins-I. Moreover, F-actin staining using fluorescent phalloidin revealed visible differences between the actin cytoskeleton in wild type *Dictyostelium* as compared to the double myosin-I mutants (Novak et al., 1995). Through their interactions with CARMIL, a WASP-interacting protein, myosins-I have the ability to rearrange actin structures (Jung et al., 2001). Myosins-ID, E and F also interact with $PI(3,4,5)P_3$ at the leading edge during cytokinesis and phagocytosis, thereby connecting membrane signaling to actin reorganization associated with these events (Chen et al., 2012). The phenotypes observed in *Dictyostelium* that are lacking myosins-I could therefore be a result of their abilities to directly manipulate the cytoskeleton, which could then indirectly influence overall cortical tension in these organisms.

In yeast, deletion of myosins-I results in several phenotypes that are associated with the integrity of the actin cytoskeleton. Primarily these mutants have defects in depolarization of actin patches, or active, dynamic sites associated with growth, polarization, and endocytosis (Kim and Flavell, 2008). Through interactions with the carboxyl-termini acidic domains, yeast myosins-I bind to Bee1p/Las17p and Vrp1p, homologues to human Wiskott-Aldrich Syndrome protein (WASP) and WASP-interacting protein (WIP). It is likely that myosins-I in yeast shape the actin cytoskeleton

by localizing these proteins, which are essential to polymerization, to the cell cortex (Kim and Flavell, 2008) and by organizing the rapidly polymerizing actin at sites of active endocytosis (Kaksonen et al., 2006).

Like their long tail counterparts in yeast, vertebrate Myo1e and Myo1f both influence the actin cytoskeleton. While Myo1e is expressed in the immune system and various other tissues including lung, kidney and small intestine, Myo1f is more confined to the immune system and is specifically found in neutrophils (Kim et al., 2006). Neutrophils from Myo1f knockout mice have an extra dense cortical actin cytoskeleton and exhibit increased granule exocytosis of β2 integrin, which is necessary for migration. These phenotypes lead to defects in immune response to the human bacterial pathogen, *Listeria monocytogenes* (Kim et al., 2006). While the exact mechanisms underlying these problems are unclear, it is possible that Myo1f directly or indirectly influences the actin network at exocytic sites. Myo1f might somehow regulate cortical tension at these sites by imparting antagonistic forces on the underlying cytoskeleton, thereby preventing excessive exocytosis.

Given its broader expression compared to Myo1f and its similarity to long-tailed yeast myosins, it is perhaps not surprising that Myo1e plays a role in trafficking processes at the cell surface through mediation of actin polymerization activity (Cheng et al., 2012; Schietroma et al., 2007). In frog oocytes, Myo1e is involved in cortical granule exocytosis (Schietroma et al., 2007). During clathrin mediated endocytosis in a variety of other cell types, Myo1e is involved in internalization at the cell surface and in transferring internalized membranes to early endosomes in the perinulcear region (Cheng et al., 2012). Myo1e is targeted to sites of endocytosis through interactions

between its SH3 domain and two proteins intimately involved with endocytosis, synaptojanin-1 and dynamin (Krendel et al., 2007). The SH3 domain and TH1 interaction with membranes are both necessary for targeting. The isolated tail domain targets properly and expression of this region alone acts as a dominant negative, presumably displacing endogenous full-length Myo1e, and inhibits endocytosis, indicating that the full-length molecule is required for this process (Krendel et al., 2007). Upon depletion of Myo1e, the rate of endocytosis is reduced and the lifetimes of clathrin and dynamin at endocytic sites increase significantly (Cheng et al., 2012), which suggests Myo1e may regulate overall dynamics at these sites. Intriguingly, Myo1e might do so through its ability to influence actin assembly and organization. When Myo1e is tagged with a mitochondrial targeting domain, it localizes to mitochondria and facilitates formation of actin networks at these sites through recruitment of Arp2/3 activating proteins (Cheng et al., 2012). The protein recruitment and subsequent actin polymerization at mitochondria are dependent on the SH3 domain of Myo1e (Cheng et al., 2012). Although it remains unknown whether the SH3 domain directly interacts with proteins involved in actin polymerization, future studies addressing these interactions and how they influence the interactions between SH3 and clathrin/dynamin will provide important information as to the exact mechanism by which Myo1e contributes to endocytosis.

Among other activities, vertebrate Myo1c might alter the actin cytoskeleton during GLUT-4 exocytosis (Bose et al., 2004). Not surprisingly then, Myo1c facilitates actin assembly during cortical granule exocytosis, and is thus required for compensatory endocytosis (Sokac et al., 2006). In this system, knockdown of Myo1c

results in unregulated actin assembly, suggesting that, similar to myosins-I in *Dictyostelium*, Myo1c might refine or restrict the shape and structure of the actin cytoskeleton during granule exocytosis in frog oocytes (Titus, 2006). An interesting and obvious difference between Myo1e and Myo1c is that Myo1e appears to regulate cytoskeletal-dependent processes and dynamics via interactions between the SH3 domain and other proteins. Myo1c lacks such a domain, and although protein-protein interactions are still possible (as indicated by the GLUT-4 literature, discussed above) it will be interesting to pursue the exact mechanism by which Myo1c executes these functions. One recent study suggests that Myo1c might recruit G-actin to the leading edge of cells (Fan et al., 2012). This finding is worth following up, although it is unclear how this particular recruitment would enable Myo1c to restrict polymerization or contain and control the shape of the actin network involved in exocytosis.

Left/right asymmetry in gut looping

Class I myosins in *Drosophila melanogaster* exert influence over the actin cytoskeleton to regulate the formation of left/right asymmetry. When *myo31DF* (the ortholog to vertebrate Myo1d) is genetically removed from flies, looping of tubular organs such as the gut and spermiduct is inverted (Hozumi et al., 2006; Speder et al., 2006). The resulting phenotype, counter-clockwise or sinistral rotation, indicates that Myo1d, perhaps through an interaction with the *Drosophila* homolog of β-catenin, is responsible for clock-wise, or dexteral, rotation in invertebrates (Speder et al., 2006). Strikingly, this inversion is rescued when the Myo1c ortholog, *myo61F*, is overexpressed in Myo1d deficient flies. Furthermore, overexpression of Myo1c in wild type flies results in dexteral gut looping (Hozumi et al., 2006).

In Myo1d and Myo1c double knockout flies, sinistral gut looping prevails, rather than a “no rotation” phenotype, which would be expected if Myo1c were responsible for sinistral gut looping (Petzoldt et al., 2012). This suggests Myo1c has an antagonistic effect on Myo1d in this system, an activity which is thought to be mediated through interactions between these class I myosins and adherins junctional components (Petzoldt et al., 2012). Myo1d binds directly to DE-cadherin, another protein that plays a role in left/right asymmetry (knockout of DE-cadherin results in a no rotation phenotype). Although Myo1c and DE-cadherin do not seem to interact directly, reduction of DE-cadherin causes an increase in Myo1c protein levels and a decrease in Myo1d expression, indicating that DE-cadherin regulates both of these proteins in some way (Petzoldt et al., 2012).

The idea that Myo1d and Myo1c share a common regulator is also supported by a study that used chimeric myosins to investigate gut looping. In a Myo1d knockout background, overexpression of Myo1d rescues symmetry defects in the hindgut and posterior midgut, while overexpression of Myo1c rescues foregut looping defects. Exchanging of IQ/tail domains between these two molecules did not change the specificity in rescuing the defects above, which the authors interpreted to indicate that the motor domain directs the organ specificity these motors demonstrate (Hozumi et al., 2008). In light of the hypothesis that Myo1c antagonizes Myo1d, this could mean that the IQ/tail domains have the same binding partners in both the foregut and midgut/ hindgut. While a direct interaction between DE-cadherin and Myo1c was not observed (Petzoldt et al., 2012), competitive interaction could be lipid based or mediated through another junctional component that also interacts with DE-cadherin. This would allow the

chimeric molecule to properly target regardless of which IQ/tail are attached. While the genetic data convincingly implicate both Myo1c and Myo1d in the fundamental process of gut looping in this invertebrate system, mechanistic details of the roles these two motors play in this system remain unclear and require closer investigation. Notably, this activity is likely specific to *Drosophila*, because asymmetry in vertebrates is directed by nodal cilia (Speder and Noselli, 2007). These structures are composed of microtubules, meaning that these actin-based motors probably are not directly involved in symmetry breaking in higher organisms. However, a recent study demonstrated the surprising ability of vertebrate Myo1c to generate counterclockwise movement of actin filaments *in vitro* on supported lipid bilayer containing physiological levels of $PI(4,5)P_2$ (Pyrpassopoulos et al., 2012). This result indicates that transducing molecular chirality to the cellular level is a potential functional feature of Myo1c even in higher organisms.

Human pathologies

Despite our quickly growing understanding of the specific functions that myosins-I carry out in cells, relatively little is known about how defects in vertebrate class I myosins directly contribute to human disease states. Genetic screens have revealed mutations in class I myosins that are potentially associated with deafness. Mutations are found in the MYO1A gene in Italian individuals with hearing loss (Donaudy et al., 2003). One of these identified mutations manifests as an E to D transition at residue 385 (E385D), which contributes to a salt bridge in the active site and results in uncoupling ATP hydrolysis from force transduction (Yengo et al., 2008). Motors with this mutation hydrolize ATP at slower rates than wild type Myo1a molecules and are unable to translocate filaments in actin gliding assays. Importantly, fluorescently tagged E385D

mutant molecules do not target to microvilli (Yengo et al., 2008). The original study identifying MYO1A mutations as possible causes underlying deafness showed that Myo1a mRNA is found in the mouse inner ear during embryogenesis (Donaudy et al., 2003). However, Myo1a protein in developed hair cells has not been detected, which may indicate that Myo1a functions prenatally in this context.

Several hearing associated mutations have been identified in the MYO1C gene as well (Zadro et al., 2009). The effects of R156W, a mutation in the switch 1 loop near the nucleotide binding site, were recently analyzed. At high surface densities, this mutant moves actin filaments at the same velocity as wild type Myo1c, but at lower densities of R156W, actin detaches from the glass rather than moving at higher velocities, as is the case for wild type Myo1c (Lin et al., 2011). The authors propose that this effect is the result of a decrease in R156W duty ratio (which means the motor is spending less time attached to actin). The precise function of Myo1c in stereocilia might be debatable, but it is clearly prominent in the inner ear and therefore is a likely candidate as a deafness gene.

Two mutations in Myo1e, A159P, which is also in the switch 1 region, and a nonsense mutation that affects Y695 and results in truncation after the motor domain and subsequent protein degredation, are associated with kidney disease (Mele et al., 2011). Specifically, these mutations are found in certain cases of childhood familial focal segmental glomerulosclerosis, or scarring of glomuleri, the filtering centers of the kidney. Indeed, tissue samples from patients with the Y695 mutation lack Myo1e and have histological characteristics similar to samples from Myo1e knockout mice; the tissue samples show thickening and disorganization of the basement membrane. In

cultured human podocytes, endogenous and recombinant wild type Myo1e localize to the cell periphery, while A159P is soluble (Mele et al., 2011). Podocyte specific knockout of Myo1e in mice also results in ultrastructural and filtration defects, further underlining the importance of Myo1e in proper kidney function (Chase et al., 2012). The morphological changes observed in podocytes lacking Myo1e are consistent with possible defects in trafficking or cytoskeletal rearrangements, two cell biological roles for which this motor has been implicated previously.

In patients with adenocarcinomas of the gut, Myo1a is sometimes mutated, resulting in more invasive tumors (Mazzolini et al., 2012). The mutation found in patients conveys a premature stop codon that results in the last 11 carboxyl-terminal amino acids becoming 7 different amino acids. When this recombinant protein is expressed in colon-derived epithelial cells, it is soluble and unable to target to brush borders. In tumor growth assays, Myo1a knockdown interferes with cell polarization and differentiation. Although Myo1a knockout alone does not increase tumor formation in these mice, when Myo1a knockout mice are crossed with the APC^{min} mice (that already have a cancer-driving mutation) the tumor number increases and the survival rate decreases as compared to mice with only the APC^{min} mutation. In patients, higher expression levels of Myo1a correspond to better survival (Mazzolini et al., 2012). The authors interpret these results to mean that Myo1a has tumor suppressor activity through its ability to maintain cell polarization. Similarly, Myo1a displays tumor suppressor activity in the gastric epithelium (Mazzolini et al., 2013).

Performing mechanical work on a fluid lipid bilayer

Inherently, myosins are force-generating molecules. In examining the cell biological

functions discussed above, proper function clearly requires class I myosins to transduce force onto their cargos or respond to tension imparted by cargos. Often times, these cargos are cellular membranes. Some particular examples where class I myosins need to generate force on the membrane include Myo1a in vesicle shedding (McConnell and Tyska, 2007), Myo1b in tubule formation at the golgi (Almeida et al., 2011), Myo1c in GLUT-4 trafficking (Bose et al., 2004) or tension regulation and channel gating in stereocilia (Gillespie and Muller, 2009). A rigid interaction between the myosin I tail and membrane also seems necessary for a molecule that is providing directionality to an assembling actin cytoskeleton. The general problem with generating force on the membrane (or vise versa, where the membrane "pulls" on the myosin) is that membranes often display characteristics of fluid substrates.

Force transduction on a fluid surface is seemingly unproductive: when the myosin undergoes a powerstroke while membrane bound, it is likely that the tail would slip and the force would dissipate into the plane of the bilayer. Indeed, membrane binding proteins that interact with a lipid head group with 1:1 stereospecificity diffuse freely with the lipid (Knight and Falke, 2009; Knight et al., 2010). It is difficult to imagine how a diffusing protein could effectively transfer force. One way to increase force transduction efficiency is to make the membrane a rigid platform. Slowing or immobilizing the diffusion of the molecule, slowing or immobilizing the lipids within the bilayer, or a combination of both, could achieve this.

The tail/membrane affinities for class I myosins are often quite high and likely support long-lived interactions. However, a tight interaction does not imply low lateral mobility, which is necessary for preventing forces generated by the myosin powerstroke

from dissipating into the bilayer. One mechanism by which diffusion is slowed is to establish multiple points of contact between membrane and protein (Knight et al., 2010). In this case, as the number of 1:1 interactions between a PH domain and PI (3,4,5)P_3 in a supported lipid bilayer increase, protein mobility decreases (Knight et al., 2010). This is an interesting possibility to consider using Myo1c as an example. Myo1c interacts stereospecifically with PI(4,5,)P_2, but this interaction alone does not result in a membrane bound lifetime that is long enough to account for lifetimes measured under physiological conditions involving a mix of lipid species (Hokanson and Ostap, 2006; McKenna and Ostap, 2009). These data suggest an additional binding site may be involved in the membrane interaction, which could alter the velocity at which Myo1c diffuses on membrane.

Although membrane binding sites in addition to the Myo1c-PH domain have not been identified, another informative experiment revealed that Myo1c powers actin motility on supported bilayers (Pyrpassopoulos et al., 2012). At physiological concentrations of PI(4,5,)P_2, Myo1c moves actin filaments counterclockwise at velocities expected for a class I myosin. Upon addition of other negatively charged lipids to bilayers, which increases affinity and could involve additional tail interactions with alternative membrane binding sites, this motility decreased (Pyrpassopoulos et al., 2012). If Myo1c has less lateral mobility when more negatively charged lipid species are included in the bilayer, one possibility is that the membrane more efficiently imparts force onto the molecule under these circumstances. This would increase the duty ratio for Myo1c and perhaps result in altered kinetics that increase power output and decrease motility (Greenberg et al., 2012). Although Myo1c dynamics were not

observed directly in these experiments, the results could suggest that the interaction between Myo1c and the membrane could tune motor activity.

Another method to rigidify the membrane is to change the lipid composition such that diffusion in the bilayer becomes slower, thus causing the diffusion of membrane bound proteins to slow as well. This mechanism could be at work in the brush border, where Myo1a is needed for vesicle shedding, an activity that clearly requires generating force onto the plasma membrane. The brush border has high concentrations of cholesterol, which decreases membrane fluidity and could feasibly decrease membrane-bound protein diffusion. When expressed exogenously, the *bona fide*, well-characterized phosphatidylserine (PS) binding domain, lactadherin-C2, and Myo1a-TH1 compete for binding sites in microvilli, suggesting these proteins share some similar membrane binding properties (Mazerik and Tyska, 2012; Yeung et al., 2008). Indeed, addition of cholesterol to supported bilayers slows diffusion of membrane bound lactadherin-C2 (Kay et al., 2012). Furthermore, PS itself diffuses more slowly in cells when cholesterol is added exogenously (Kay et al., 2012), supporting the idea that high cholesterol content will influence the dynamics of other PS binding proteins, such as Myo1a-TH1. Understanding the membrane binding dynamics of class I myosins both *in vitro* and *in vivo* should be the next step in this field, as these studies will provide critical information about how these molecules might transduce and sense force in their cellular environments.

Summary

Over the past decade, several important functions of class I myosins have surfaced. This is especially true for Myo1a, which clearly contributes to structure, function and

physiology in the brush border small intestine. Its main roles are maintaining microvillar structure and membrane tension (Nambiar et al., 2009; Tyska et al., 2005) and regulating the process of vesicle shedding (McConnell and Tyska, 2007). These physiological processes require proper localization of this motor and a strong interaction between the tail and microvillar membrane. The goal of this thesis is to provide high resolution, mechanistic detail as to how Myo1a binds membrane and targets in cells, and how Myo1a cellular dynamics are controlled. We find that Myo1a targets to the brush border of epithelial cells through electrostatic interactions that involve basic residues in two independent regions and the anionic lipid species, PS (Chapter III). *In vitro*, peptides encoding these regions compete with Myo1a for binding sites on negatively charged liposomes containing PS, indicating these regions are *bona fide* membrane binding motifs. Strikingly, the PS binding protein, lactadherin-C2 (Yeung et al., 2008), competes with Myo1a-TH1 for brush border localization, showing that this interaction is also relevant in cells. Based on these studies and biochemical studies indicating the short-lived interaction between Myo1a motor domain and actin, we hypothesized that Myo1a-TH1 is the master regulator of dynamics for this molecule. To test this idea, we used live cell single molecule total internal reflection fluorescence (TIRF) microscopy in combination with single particle tracking and mean squared displacement (MSD) analysis to measure and compare lateral mobility for Myo1a and Myo1a-TH1 (Chapter IV). Using this approach, we discovered that Myo1a displayed lower overall lateral mobility and had a larger population of near-immobile molecules. Some of these low mobility events are long-lived, and are absent from analysis of Myo1a-TH1. These data suggest the motor domain makes an unexpected contribution

to controlling the dynamics of this molecule at the membrane/cytoskeletal interface. Structure/function analysis confirmed this result and further suggests that these Myo1a events may be instances where the molecule is under load, or tension sensing. This is the first study to examine dynamics for any class I myosin in live cells at single molecule resolution, and the results are surprising and unexpected. With a new emphasis on whole-molecule function, we were interested in how brush border targeting might be regulated in the context of full-length Myo1a. To this end, we explored the regulation by which Myo1a properly localizes (Chapter V). We find that Myo1a-TH1 displays "unregulated" membrane binding and has a smaller soluble pool than Myo1a. The neck region plays a role in regulating the localization of Myo1a, perhaps through CaM/calcium interactions. Our data suggest a possible conformational change may be responsible for regulating Myo1a brush border targeting, but further investigation is needed to confirm this. The results presented within this thesis provide novel insight as to how Myo1a cellular targeting and dynamics are controlled, and how biochemical and biophysical properties of Myo1a manifest in cells to help this molecule carry out its physiological roles in the brush border.

CHAPTER II.

MATERIALS AND METHODS

Molecular biology

Truncation constructs and point mutants were cloned using the previously described pEGFP-tagged human Myo1a or Myo1a-TH1 (residues 772-1043) as a template (gene accession number AF009961) (Tyska and Mooseker, 2002); each new construct was confirmed by sequencing before expression in cells. Truncations included the following amino acids: NΔ49, residues 821-1043; NΔ66, residues 838-1043; NΔ87, residues 859-1043; CΔ49, residues 772-994; CΔ21, residues 772-1022; CΔ15, residues 772-1028; CΔ10, residues 772-1033. Myo1a-Neckless was a deletion of residues 694-764, which removed the three IQ motifs. Point mutagenesis was performed using a QuikChange Lightning Mutagenesis kit (Qiagen), and mutations were verified by sequencing. EGFP-lactadherin-C2, developed by the Grinstein laboratory (Yeung et al., 2008), was obtained from Addgene. PLCδ1-PH-GFP was a generous gift from Tamas Balla (Balla and Varnai, 2009; Szentpetery et al., 2009).

Cell culture

LLC-PK1-CL4 (CL4) cells were cultured at 37°C and 5% CO_2 in Dulbecco's Modified Eagle Medium with high glucose (Invitrogen), 2 mM L-glutamine (Invitrogen), and 10% defined fetal bovine serum (Atlantic Biosciences) as described previously (Tyska and Mooseker, 2002). SF9 insect cells were cultured at 27°C in Grace's Insect Media (Invitrogen) with 1% Pluronic F-68 solution (Sigma) and 1% antibiotic-antimycotic (Invitrogen).

Microscopy

Confocal microscopy: CL4 cells were transfected using Lipofectamine 2000 according to the manufacturer's protocols (Invitrogen). After 4-5 hour incubation in transfection media with DNA, CL4 cells were processed for microscopy. For steady state targeting assays, cells were washed two times in warm PBS, fixed for 15 minutes in 4% paraformaldahyde, permeabilized for six minutes in 0.1% Triton X-100 (Sigma) in PBS, and stained with AlexaFluor 568 labeled phalloidin (Invitrogen Molecular Probes) at 1:100 in PBS. For antibody labeling, cells were fixed as above, permeabilized for 10 minutes in 0.2% saponin or 0.01% Triton X 100, respectively, in PBS, blocked in 5% BSA in PBS for 30 minutes, incubated in anti-PS (1:50, Millipore) or anti-myo1a (4P1) overnight at 4°C, washed three times for five minutes each in PBS, incubated at RT for 30 minutes in donkey anti-mouse Alexa 568 secondary (1:200) (Invitrogen Molecular Probes), then washed again. Coverslips with fixed cells were mounted on slides using Prolong Gold with DAPI (Invitrogen/Molecular Probes) and sealed using clear nail polish. Cells were imaged using a Leica TCS SP5 LASER scanning confocal microscope equipped with 63x and 100x objectives. Images were smoothed, contrast enhanced, and pseudo-colored using ImageJ v.1.43u (http://rsb.info.nih.gov/ij/; NIH).

Live cell single molecule TIRF microscopy (SM-TIRF): Myo1a, Myo1a-TH1 and selected variants were tagged with three tandem copies of mCitrine (3x-mCitrine) using a previously described vector (a generous gift from K. Verhey) (Cai et al., 2007), and verified by sequencing. CL4 cells expressing constructs of interest were plated sparsely in glass bottom imaging dishes. Cells were gently washed two times in Ringer's buffer

(10 mM HEPES/KOH, 155 mM NaCl, 5 mM KCl, 2 mM $CaCl_2$, 1 mM $MgCl_2$, 2 mM NaH_2PO_4, 10 mM glucose, pH 7.2) (Cai et al., 2009; Cai et al., 2007) and kept in the same buffer for imaging experiments. TIRF microscopy was performed on a Nikon TiE inverted light microscope equipped with a Nikon TIRF illuminator, a 100x/1.49 NA TIRF objective (used in combination with a 1.5x optivar), a Hamamatsu ImagEM-CCD camera, and MetaMorph software to control image acquisition. Calibrated pixel size was 75 nm/pixel. Fluorescence was excited using a 50 mW 491 nm diode LASER operating between 20-30% of maximum power. Single molecule membrane binding events appeared as bright diffraction limited spots on the ventral surface of the cell. The presence of tandem fluorescent proteins was confirmed by observations of multi-step photobleaching at high LASER power. Cells expressing exceedingly low levels of each construct were chosen for analysis to improve the signal-to-noise ratio of single molecule detection; image stacks consisting of 250 frames (12.5 sec) were captured at 20 frames per second and then subject to contrast enhancement and two frame rolling average using ImageJ. Image stacks were then processed using DiaTrack (Vallotton et al., 2003) to extract the lifetimes of spots with intensities above background, which typically exhibited a grayscale value of 70-80. Using a TIRF system such as this, spot lifetimes will be limited by the detachment rate of 3x-mCitrine fusion proteins or the photobleaching of mCitrine fluorescent proteins. Because photobleaching is a stochastic event, the likelihood of observing a simultaneous triple photobleaching event is small (Cai et al., 2009; Cai et al., 2007). Moreover, imaging was carried out at reduced LASER power to minimize the impact of mCitrine photobleaching on observed spot lifetimes (i.e. kinetics were dominated by detachment from the membrane rather than

photobleaching). In support of this point, we frequently observed events that persisted for the full 12.5 sec recording (Fig. 3-6C-2). Importantly, long-lived events were difficult to resolve in cells expressing 3x-mCitrine empty vector.

SM-TIRF modifications (Chapter IV) and MSD analysis: Single molecule imaging was performed on live cells using a slightly modified variation of a published procedure. In our previous studies, imaging procedures were focused on collecting lifetime data. For the present study, data acquisition, processing and analysis were tailored to collect mobility (diffusion) measurements. Briefly, the TIRF system was similar to that previously described (Mazerik and Tyska, 2012), but a Photometrics Evolve EM-CCD camera was used to collect image stacks, and image acquisition was controlled with Nikon Elements software. Calibrated pixel size was 110 nm/pixel. A 488-nm LASER was used to excite constructs of interest tagged with 3x-mCitrine and a 561-nm LASER was used to excite mCherry-Espin, which served as a label for the actin cytoskeleton. Data were collected using 2x averaging at 50 frames per second for 400 frames (8.1 sec). This fast frame rate made it necessary to use a higher LASER power than previously published (Mazerik and Tyska, 2012). Kymograph analysis was performed on image stacks using ImageJ. Max projections of 3x-Citrine constructs (green) and mCherry-Espin (red) image stacks were made and then contrast enhanced, merged, and pseudo-colored using ImageJ. For single particle tracking, ImageJ was used to contrast enhance and then threshold image stacks to include only the brightest particles on the ventral surface, which typically exhibited a grayscale value of 120-130. Particles were then tracked using DiaTrack (Vallotton et al., 2003). For each construct, trajectories were taken from 20-40 cells. Trajectories produced in DiaTrack were

subjected to further analysis using software programmed in MatLab. The mean squared displacement for each trajectory with lifetime greater than or equal to 10 frames was calculated using all pairs of points with the appropriate lag times. For *N* time points, the *n*th average is,

$$\left\langle r^2(n)\right\rangle = \frac{1}{N}\sum_{i=0}^{N-1}\left[r(i+n)-r(i)\right]^2$$

The mean squared displacement was cut off at one-half of the total number of time steps before fitting to a two-dimensional simple diffusion model weighted by the inverse variance,

$$\left\langle r^2(t)\right\rangle = 4Dt$$

Trajectories greater than 10 frames were divided into lengths of 10 and fit individually (Saxton, 1997). Final diffusion coefficients and lifetimes matched to each D value were exported from MatLab and plotted in SigmaPlot. Notably, lifetime data were plotted in relationship to diffusion coefficient, D, and were not fit to obtain membrane binding rates. Changes made to data acquisition were aimed to obtain high quality mobility data (i.e., fast frame rate and high LASER power) and resulted in decreases in the frequency of long lived events that were previously observed using modified imaging conditions and are representative of the "productive" binding events that are physiologically interesting.

Fold enrichment in microvilli quantification

X-Z (i.e. vertical) section images were used to quantify EGFP-Myo1a-TH1 construct targeting to microvilli. For each construct, 6-13 cells from 2-4 experiments were

analyzed to obtain 'Fold Enrichment in Microvilli' (FEM) values. FEM values were generated as follows: for a given cell, microvilli were first localized using the F-actin (phalloidin) channel. In the corresponding EGFP channel image, the intensity of Myo1a-TH1 was measured at 5-7 points that mapped to the position of microvillar F-actin labeling. Another 5-7 intensity points were acquired from a region that corresponded to non-nuclear cytosol. Intensity values from microvillar and cytosolic regions were averaged separately and the resulting means were used to obtain microvilli:cytosol intensity ratios (i.e. FEM). Errors for FEM values were calculate as $SD/\sqrt{n}$ where n corresponds to the number of averaged FEM values for a given construct. A FEM value of 1 (dashed line, Fig. 3-3) is the enrichment threshold, the value for a protein that partitions equally between the microvilli and cytosol (Patino-Lopez et al., 2010). Constructs with FEM values above this threshold are enriched in microvilli, while constructs with FEM values below 1 are enriched in the cytosol. Similar quantification methods were used previously to assay the structural basis of membrane enrichment for Myo1g (Patino-Lopez et al., 2010), mDia2 (Gorelik et al., 2011), and lactadherin-C2 (Fairn et al., 2011a).

Protein purification

Full length Myo1a tagged with a Myc-FLAG epitope (Yengo et al., 2008) and calmodulin (CaMΔall, a generous gift from K. Trybus) (Krementsov et al., 2004), were coexpressed in SF9 insect cells and Myo1a-myc-FLAG was purified using affinity chromatography as described previously (Yengo et al., 2008). Briefly, infected cells were collected by centrifugation at 300 x *g* and lysed using a dounce in lysis buffer (10 mM Tris-Cl pH 7.5, 200 mM KCl, 1 mM EGTA, 1 mM EDTA, 1 mM $MgCl_2$, 2 mM ATP, 0.1% NP-40, 5%

sucrose, 1 mM dithiothreitol, pefabloc, leupeptin, phenylmethanesulfonyl fluoride). Lysate was then centrifuged at 186,000 x *g* in a Type 45 Ti rotor using a Beckman ultracentrifuge. Myo1a-myc-FLAG was collected from resulting supernatant using immobilized M2 FLAG resin (Sigma), washed with twenty-five column volumes of wash buffer (10 mM Tris-Cl pH 7.5, 200 mM KCl, 1 mM EGTA, 1 mM EDTA, 1 mM $MgCl_2$, 2 mM ATP, 1 mM dithiothreitol, pefabloc, leupeptin, phenylmethanesulfonyl fluoride) containing 5 μg/mL purified bovine calmodulin (CalBiochem), eluted using FLAG peptide (Sigma) in calmodulin-free wash buffer, and dialyzed overnight into binding buffer (10 mM HEPES, 100 mM KCl, 1 mM EGTA). Purified protein was either flash frozen and stored at –80° C or stored on ice for up to one week.

Liposome preparation

Liposomes were prepared by extrusion according to slightly modified published protocols (Brzeska et al., 2008; Frost et al., 2008; Hokanson and Ostap, 2006). Lipids [1,2-dioleoyl-*sn*-glycero-3-phosphocholine (DOPC), 1,2-dioleoyl-*sn*-glycero-3-phosphoenthanolamine (DOPE), 1,2-dioleoyl-*sn*-glycero-3-phospho-L-serine (DOPS), phosphatidylinositol-4,5-bisphosphate ($PI(4,5)P_2$), Avanti Polar Lipids] in $ChCl_3$ were mixed in glass vials to desired concentrations and dried under a stream of nitrogen with gentle vortexing. Lipid mixtures were resuspended in binding buffer and subjected to five freeze-thaw cycles. We noted that sucrose loaded liposomes, which are frequently used for cosedimentation studies, appeared multilamellar by negative stain electron microscopy. Additionally, sucrose loaded liposomes require dialysis to remove sucrose from the resuspension buffer, which resulted in an extensive loss of liposome product. Therefore, liposomes for cosedimentation experiments were prepared in the absence of

sucrose. Mixtures were then pushed through an extruder fit with a 100 nm filter 16-20 times. Total loss of lipid during the extrusion process was calculated in control experiments using liposomes containing 2% β-BODIPY-500/510 hexadecanoyl-*sn*-glycero-3-phosphate (Invitrogen) and final concentrations were adjusted accordingly. Liposomes were stored on ice and used for up to three days.

Liposome binding assays

Cosedimentation assays for measuring Myo1a binding to liposomes were performed as described previously (Komaba and Coluccio, 2010). To clear any protein aggregates, purified Myo1a (2-5 μM) was centrifuged at 4° C for 30 minutes at 352,000 x *g* using a TL100 Beckman centrifuge and a TLA100 rotor. Centrifuge tubes were pre-coated with 100 μM DOPC and 100 μg/mL BSA. Myo1a-myc-FLAG (50 nM) was then incubated at room temperature with increasing concentrations (0-100 μM) of liposomes composed of varying mol percentages of either DOPC/DOPS, DOPC/DOPE, or DOPC/DOPE with $PI(4,5)P_2$ in a final volume of 200 μL buffer. After incubation, liposome-protein complexes were centrifuged at 352,000 x *g* for 30 minutes at 25° C. Then, 170 μL were removed and the remaining 30 μL 'pellet' was resuspended in 10 μL boiling sample buffer. Although liposomes were not sucrose loaded, using fluorescent liposomes, we determined >90% of the liposomes sedimented under these conditions. Protein was analyzed by SDS-PAGE and Coomassie Blue (BioRad) staining, and then visualized with an Odyssey infrared imaging system (LI-COR Biosciences). All individual data points were normalized to the percent Myo1a bound to 100 μM 80% DOPS and are expressed as a function of lipid concentration. Data points are averages of two to six experiments. Competition experiments were performed using liposomes composed of

20% DOPC/80% DOPS (50 μM). Peptides (GenScript) corresponding to the NTM (KLCASELFKGKKASYPQSVP, residues 847-866), the CTM (GDNSKLRYKKKGSHCLEVTV, residues 1023-1042), or a region from the motor domain (negative control, LLEGSVGVEDLVLLEPLVEE, residues 3-22) at varying concentrations (25-400 μM) were incubated with liposomes and Myo1a, and then processed as described above. Total percent bound Myo1a in the presence of control peptide was equal to the percent bound in the absence of peptide; therefore, for each sample containing NTM or CTM peptide, percent Myo1a bound was calculated using the control peptide condition as 100% bound. Binding data were fit to hyperbolae using SigmaPlot (Systat Software Inc).

Chromatography

Full length Myo1a was purified as described above, loaded with exogenous CaM, and dialyzed into solution A' (150 mM KCl, 20 mM Imidazole, 2mM EGTA, 2.5 mM MgCl2, 0.02% Na-Azide, pH 7.2) in the presence or absence of 1 mM $CaCl_2$. The protein was run through a HiLoad 16/60 Superdex 200 prep grade column (GE Healthcare Biosciences) at a flow rate of 0.5 mL/ min using a DuoFlow FPLC system (BioRad). Fractions were collected and protein content was analyzed using SDS-PAGE and Coomassie Blue (BioRad) staining, visualized with an Odyssey infrared imaging system (LI-COR Biosciences), and band densities were quantified using ImageJ.

CHAPTER III.

MYOSIN-1A TARGETS TO MICROVILLI USING MULTIPLE MEMBRANE BINDING MOTIFS IN THE TAIL HOMOLOGY 1 (TH1) DOMAIN

Jessica N. Mazerik and Matthew J. Tyska

Department of Cell and Developmental Biology, Vanderbilt University Medical Center, Nashville, TN

Keywords: brush border, actin, phosphatidylserine, liposome, TIRF

To whom correspondence should be addressed:
Matthew J. Tyska, PhD
Associate Professor
Department of Cell and Developmental Biology
Vanderbilt University Medical Center
3150A Medical Research Building III
465 21st Avenue South
Nashville, TN 37232-8240
Phone: (615) 936 5461
Fax: (615) 936 5673
Email: matthew.tyska@vanderbilt.edu

Previously published as:
Mazerik, J.N. and Tyska, M.J., 2012. *Myosin-1a targets to microvilli using multiple membrane binding motifs in the tail homology 1 (TH1) domain*. J Biol Chem 287, 13104-13115.

Abstract

One of the most abundant components of the enterocyte brush border is the actin-based monomeric motor, myosin-1a (Myo1a). Within brush border microvilli, Myo1a carries out a number of critical functions at the interface between membrane and actin cytoskeleton. Proper physiological function of Myo1a depends on its ability to bind to microvillar membrane, an interaction mediated by a C-terminal tail homology 1 (TH1) domain. However, little is known about the mechanistic details of the Myo1a-TH1/membrane interaction. Structure-function analysis of Myo1a-TH1 targeting in epithelial cells revealed that an N-terminal motif conserved among class I myosins, and a C-terminal motif unique to Myo1a-TH1, are both required for steady state microvillar enrichment. Purified Myo1a bound to liposomes composed of phosphatidylserine (PS) and phosphoinositol (4,5) bisphosphate [$PI(4,5)P_2$], with moderate affinity in a charge-dependent manner. Additionally, peptides of the N- and C-terminal regions required for targeting were able to compete with Myo1a for binding to highly charged liposomes *in vitro*. Single molecule total internal reflection fluorescence (TIRF) microscopy showed that these motifs are also necessary for slowing the membrane detachment rate in cells. Finally, Myo1a-TH1 co-localized with both lactadherin-C2 (a PS-binding protein) and PLCδ1-PH (a $PI(4,5)P_2$-binding protein) in microvilli, but only lactaderin-C2 expression reduced brush border targeting of Myo1a-TH1. Together, our results suggest that Myo1a targeting to microvilli is driven by membrane binding potential that is distributed throughout TH1 rather than localized to a single motif. These data highlight the diversity of mechanisms that enable different class I myosins to target membranes in distinct biological contexts.

Introduction

Class I myosins are monomeric, membrane-binding, actin-based motor proteins that comprise a major fraction of the myosin superfamily (Odronitz and Kollmar, 2007). All myosin-1 isoforms contain at least three core domains: an N-terminal motor domain that coordinates ATP hydrolysis with actin binding and force generation; a central neck region made up of varying numbers of IQ motifs, which bind calmodulin or calmodulin-like proteins; and a tail region which includes a highly basic C-terminal tail homology 1 (TH1) domain that is responsible for membrane binding (Fig. 3-1 A) (Coluccio, 2008; Krendel and Mooseker, 2005; McConnell and Tyska, 2010; Nambiar et al., 2010). Vertebrates express eight class I myosins, which are found in diverse cell types and tissues; because these motors simultaneously bind to actin and membrane, they provide a dynamic linkage between the cytoskeleton and the overlying plasma membrane in a variety of biological contexts (Coluccio, 2008; Krendel and Mooseker, 2005; McConnell and Tyska, 2010; Nambiar et al., 2010). While numerous studies have contributed to our understanding of the biochemical and mechanical properties of class I myosins, only recently have the detailed mechanisms of membrane binding become the focus of intense investigation (Brzeska et al., 2010; Brzeska et al., 2008; Feeser et al., 2010; Hokanson et al., 2006; Hokanson and Ostap, 2006; Komaba and Coluccio, 2010; McKenna and Ostap, 2009; Olety et al., 2010; Patino-Lopez et al., 2010; Tang et al., 2002).

Myo1a is expressed in the enterocytes that line the small intestine, where it localizes to the apical brush border (Collins and Borysenko, 1984; Matsudaira and Burgess, 1979; Skowron and Mooseker, 1999). This domain is defined by an extensive

array of actin-supported membrane protrusions, referred to as microvilli, which extend into the lumen of the gut (Mooseker and Tilney, 1975). In addition to maintaining brush border composition (Tyska et al., 2005; Tyska and Mooseker, 2004), structure (Tyska et al., 2005), and regulating microvillar membrane tension (Nambiar et al., 2009), Myo1a also plays a role in powering the release of vesicles from the tips of microvilli, an activity that may hold important implications for gut host defense (McConnell et al., 2009; McConnell and Tyska, 2007). Although membrane binding is expected to be critical for all of these functions, little is known about the mechanisms underlying Myo1a membrane interactions. Previous studies with chicken Myo1a showed that TH1 is a *bona fide* membrane-binding domain that interacts with liposomes composed of negatively charged phospholipids with moderate affinity (Hayden et al., 1990). Myo1a-TH1 is also sufficient for targeting to microvilli in cultured epithelial cells (Tyska and Mooseker, 2002). However, the structural motifs that govern Myo1a-TH1 membrane binding and the lipid species relevant to these interactions *in vivo* have not been identified.

Reports published in the past several years have identified a myosin-1 pleckstrin homology (Myo1-PH) domain as a conserved region within the TH1 domain that may contribute to membrane binding (Hokanson et al., 2006; Hokanson and Ostap, 2006; Komaba and Coluccio, 2010; Olety et al., 2010; Patino-Lopez et al., 2010). The Myo1-PH domain was originally identified in Myo1c, which binds stereospecifically to $PI(4,5)P_2$ via interactions with two conserved signature basic residues that flank this motif (Hokanson et al., 2006; Hokanson and Ostap, 2006). When these signature residues are mutated to alanine in Myo1c, Myo1b, Myo1g, and Myo1f, targeting to the membrane

is abolished (Hokanson et al., 2006; Komaba and Coluccio, 2010; Olety et al., 2010; Patino-Lopez et al., 2010). These studies highlight the importance of the Myo1-PH domain and in some cases, specific interactions with phosphoinositides such as $PI(4,5)P_2$ in the membrane binding mechanism of these class I myosins. However, other characterized isoforms such as *Acanthamoeba* myosin-1c (*Acan* Myo1c) and vertebrate Myo1e appear to target membranes using a mechanism that does not require stereo-specific phosphoinositide recognition (Brzeska et al., 2008; Feeser et al., 2010); instead, these myosins appear to bind membranes through less specific electrostatic interactions with a variety of acidic phospholipids.

In this study, we used a cell-based targeting screen to identify putative membrane binding motifs in Myo1a-TH1. Microvillar targeting assays in cultured cells revealed that Myo1a-TH1 does not depend solely on the Myo1-PH domain for enrichment to microvilli. However, we identified two other regions that are essential for targeting to microvilli at steady state: an N-terminal targeting motif (NTM) that is conserved across short-tailed class I myosins, and a C-terminal targeting motif (CTM) that is less well conserved. Cosedimentation studies revealed that purified Myo1a bound to liposomes composed of the acidic phospholipids PS and $PI(4,5)P_2$ with moderate affinity in a charge-dependent manner. *In vitro,* NTM and CTM peptides were able to compete with Myo1a for binding to highly charged liposomes, confirming that the motifs identified in our cell-based targeting screen represent *bona fide* lipid binding regions. Single molecule TIRF microscopy assays in live cells indicate that mutations to either the NTM or the CTM reduce the Myo1a-TH1 membrane bound lifetime. Finally, although Myo1a-TH1 co-localizes with both the PS binding protein, lactadherin C2

(Yeung et al., 2008; Yeung et al., 2009), and the PI(4,5)P_2 binding protein, PLCδ1-PH (Balla and Varnai, 2009; Szentpetery et al., 2009), only lactadherin C2 is able to compete with Myo1a for targeting to microvilli. Together, our results suggest that Myo1a targeting to microvilli is driven by membrane binding potential that is distributed throughout TH1 rather than localized to a single motif. Importantly, these findings suggest that different class I myosins may rely on distinct membrane-targeting mechanisms, which could provide a basis for the diversity of cellular functions carried out by these motors.

Results

Dissecting the mechanism of Myo1a-TH1 targeting in cultured epithelial cells

Our initial goal was to identify regions within Myo1a-TH1 (defined here as a.a. 772-1043 of *Human* Myo1a) that are needed for targeting to brush border microvilli. Targeting is expected to be at least partially driven by direct interactions with the apical membrane (Hayden et al., 1990). We reasoned that once critical targeting motifs were identified, we could then use other more direct *in vitro* biochemical methods to assess their contribution to membrane binding. To this end, we developed a microvillar-targeting assay using the LLC-PK1-CL4 (CL4) epithelial cell model system (Tyska and Mooseker, 2002). CL4 cells polarize quickly and build a brush border with densely packed apical microvilli; they are also highly transfectable, which makes them ideal for large-scale structure-function studies and screening numerous Myo1a-TH1 mutants and truncation constructs. Previous studies employed CL4 cells successfully to investigate the targeting determinants of full length Myo1a and other microvillar components (Loomis et al., 2003; Nagata et al., 2008; Tyska and Mooseker, 2002).

Using confocal microscopy we acquired X-Y and X-Z images of cells expressing EGFP-tagged Myo1a-TH1 constructs. In the X-Y orientation, constructs that target to microvilli appear punctate in the apical domain. Images in the X-Z plane provided simultaneous access to microvillar and cytosolic intensity levels and were used to quantify 'Fold Enrichment in Microvilli' (FEM), the ratio of microvillar:cytosolic signal. The lower limit for enrichment, or FEM value for a protein that partitions equally between microvilli and cytosol, is 1 (dashed line, Fig. 3-3) (Patino-Lopez et al., 2010). As controls, we expressed EGFP-Myo1a, EGFP-Myo1a-TH1, and EGFP in CL4 cells and analyzed localization (Fig. 3-2 A-C). EGFP-Myo1a and EGFP-Myo1a-TH1 were both enriched in microvilli as previously reported (Tyska and Mooseker, 2002) (FEM = 1.56 ± 0.10, 2.63 ± 0.14, respectively; Fig. 3-3 A) while EGFP was soluble and showed no microvillar targeting (FEM = 0.17 ± 0.02; Fig. 3-3 A). To further validate this approach, we examined the FEM scores of other proteins that are expected to be enriched in the brush border. For example, F-actin, which forms the core of the microvillus, exhibits extremely high enrichment in this assay (FEM = 4.14 ± 0.36). Moreover, the PLCδ1-PH domain was also highly enriched in microvilli (FEM = 2.61 ± 0.21), whereas a mutant deficient in membrane-binding, PLCδ1-PH-R40L, was not (FEM = 0.47 ± 0.02) (Ferguson et al., 1995; Varnai and Balla, 1998). Thus, the FEM assay provides a simple and robust readout on the microvillar enrichment of constructs of interest.

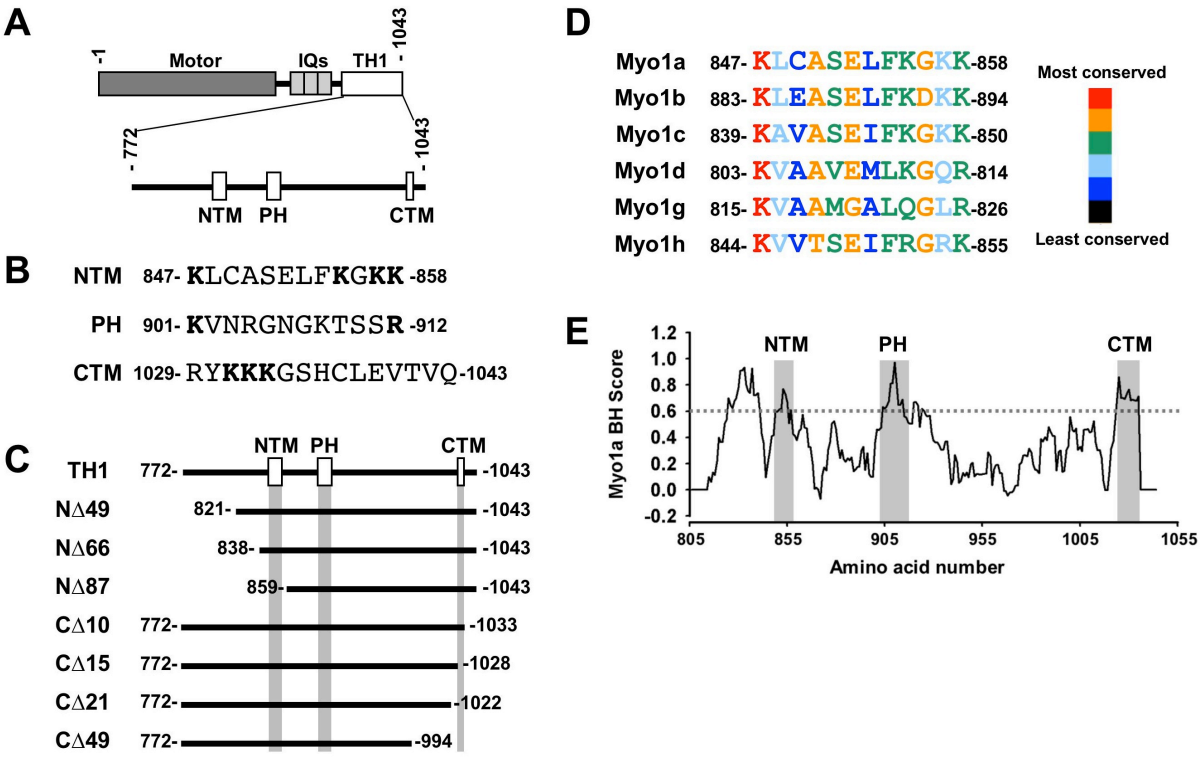

Figure 3-1. Domain organization of Myo1a and constructs used in this study. (*A*) Bar diagram representing the structural domains of Myo1a and regions of interest in Myo1a-TH1. (*B*) Sequence from the N-terminal targeting motif (NTM), Pleckstrin homology (PH) domain, or C-terminal targeting motif (CTM); residues in bold were mutated to alanine in structure-function studies of EGFP-Myo1a-TH1. (*C*) Bar diagrams representing EGFP-tagged Myo1a-TH1 N-terminal and C-terminal truncation constructs; boxes representing the NTM, PH, and CTM are drawn to scale. (*D*) MegAlign alignment of the region representing the NTM from human short-tailed class I myosins. *(E)* A BH plot of the Myo1a-TH1 domain (a.a. 805-1043); regions corresponding to the NTM, PH domain, and CTM are indicated.

Myo1-PH domain is not essential for the enrichment of Myo1a-TH1 in microvilli

Previous studies on multiple vertebrate class I myosins show that when the signature basic residues in the Myo1-PH are mutated to alanine, targeting to membrane is abolished (Hokanson et al., 2006; Komaba and Coluccio, 2010; Olety et al., 2010; Patino-Lopez et al., 2010). To determine if the Myo1-PH was necessary for Myo1a-TH1 targeting, we mutated the equivalent conserved residues, K901 and R912, to alanine (Fig. 3-1 A,B) and expressed the mutant constructs in CL4 cells. Although Myo1-PH

point mutants K901A and R912A, and double point mutant K901A/R912A reduced microvillar targeting of EGFP-Myo1a-TH1, all three constructs were still above the enrichment threshold (FEM = 1.34 ± 0.03, 2.00 ± 0.08, 1.64 ± 0.12, respectively; Figs. 3-2 D-F and 3-3 B). This result is reminiscent of experiments with vertebrate Myo1e and *Acan* Myo1c, which revealed that mutations to signature PH residues do not significantly impact subcellular targeting (Feeser et al., 2010) or binding to liposomes *in vitro* (Brzeska et al., 2008; Feeser et al., 2010). From these experiments, we conclude that a functional Myo1-PH is not necessary for Myo1a-TH1 enrichment in microvilli.

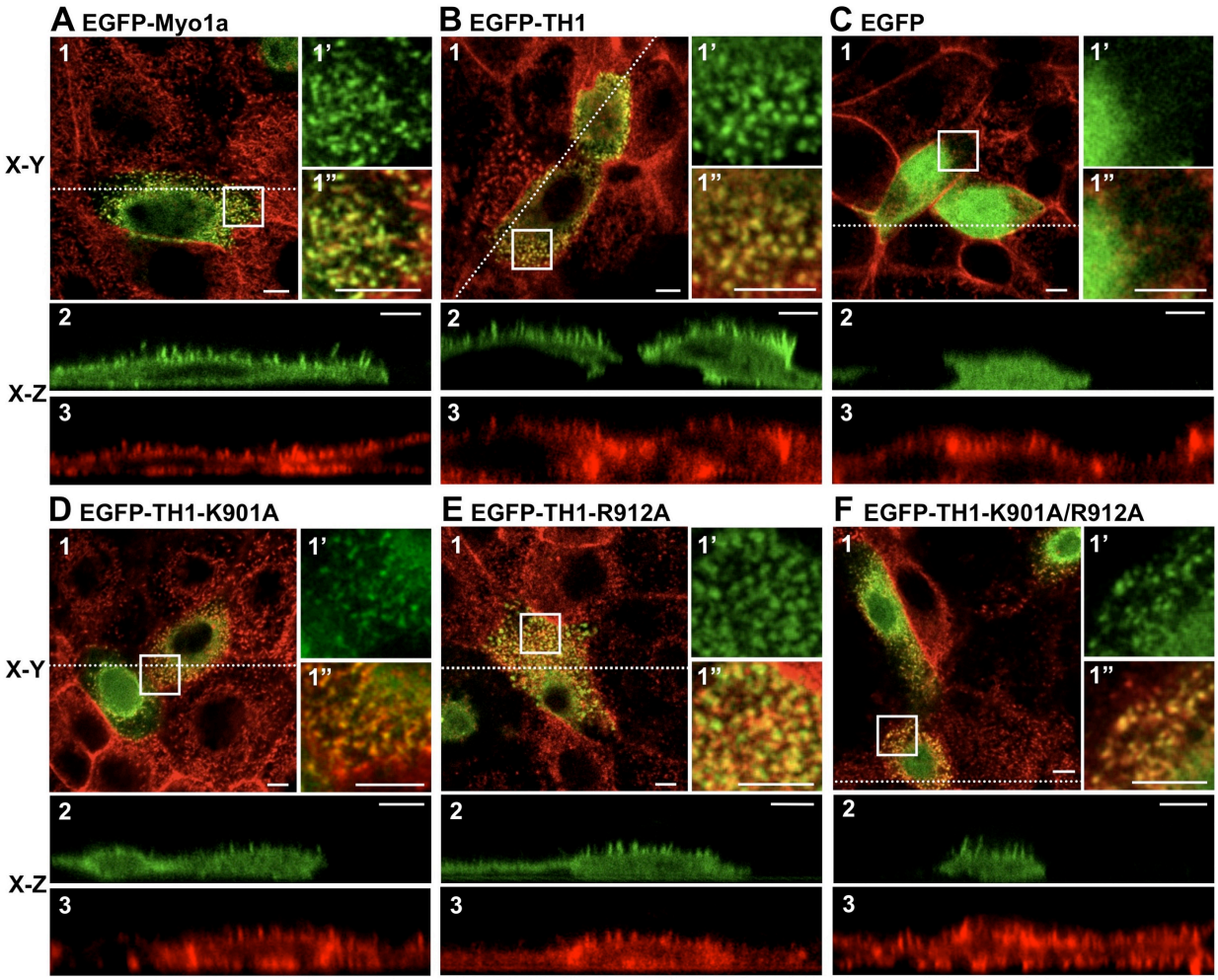

Figure 3-2. Analysis of EGFP-Myo1a, EGFP-Myo1a-TH1, and EGFP-Myo1a-TH1-PH domain mutant targeting to microvilli. *A-C*, Representative confocal images show EGFP-Myo1a (*A*) and EGFP-Myo1a-TH1 (*B*) are enriched in microvilli, but EGFP (*C*) is soluble. *D-F*, Representative confocal images show EGFP-Myo1a-TH1-K901A (*D*), EGFP-Myo1a-TH1-R912A (*E*), and EGFP-Myo1a-TH1-K901A/R912A (*F*) are enriched in microvilli. Here, 1 represents an apical *en face* view of EGFP-tagged construct (green) merged with Alexa568-phalloidin labeled F-actin (red); the boxed area in 1 is shown in 1' (EGFP or EGFP-tagged construct) and 1" (merge with phalloidin). X-Z (vertical) sections show EGFP-tagged constructs (green, 2) or F-actin (phalloidin, red, 3). Dashed line in 1 represents location in the cell where X-Z section was imaged. Bars are 5 μm.

Discovery of novel microvillar targeting motifs in Myo1a-TH1

Because mutations to the signature PH domain residues in Myo1a-TH1 did not abolish microvillar enrichment, we sought to identify other motifs that might contribute to the targeting of Myo1a to the brush border. To this end, we truncated Myo1a-TH1 from the N-terminus (Fig. 3-1 C), expressed EGFP-tagged truncation constructs in CL4 cells, and assessed microvillar targeting. EGFP-Myo1a-TH1-NΔ49 and EGFP-Myo1a-TH1-NΔ66 both targeted at levels above the enrichment threshold (FEM = 1.88 ± 0.13, 1.10 ± 0.08, respectively; Fig. 3-3 C). However, when we further truncated Myo1a-TH1 by an additional 20 amino acids (EGFP-Myo1a-TH1-NΔ87), targeting to microvilli was completely lost (FEM = 0.22 ± 0.05; Fig. 3-3 C). We compared Myo1a-TH1 primary sequence to other short-tailed myosin-1 TH1 domains to identify conserved residues between NΔ66 and NΔ87 that might contribute to targeting. We found several residues that appear conserved from humans to *Dictyostelium* (Fig. 3-1 D). We also used the basic-hydrophobic (BH) scale to examine the predicted membrane binding potential of this region (Brzeska et al., 2010). Recent development of the BH algorithm followed the identification of a potentially unstructured non-PH domain membrane-binding site, rich in basic and hydrophobic residues, in the *Acan* Myo1c TH1 domain (Brzeska et al., 2008). BH analysis of Myo1a-TH1 revealed a moderate peak corresponding to this

region (Fig. 3-1 E). In light of these analyses, we chose to focus additional mutagenesis on the basic residues in this region for two reasons: (i) recent studies show that in the context of Myo1g, the conserved basic residues that flank this region are required for membrane targeting in Jurkat cells (Patino-Lopez et al., 2010), and (ii) early studies with chicken Myo1a determined that binding to charged liposomes is attenuated as ionic strength is increased, implying an electrostatic mechanism (Hayden et al., 1990). We made single or double alanine substitutions to conserved lysine residues K847, K855, K857, and K858 in order to determine their significance in Myo1a-TH1 targeting (Fig. 3-1 B). The single point mutant K847A had a minor impact on enrichment (FEM = 0.88 ± 0.07), whereas K847A/K855A and K847A/K858A abolished targeting to microvilli (FEM = 0.56 ± 0.03 and 0.22 ± 0.02, respectively; Fig. 3-3 C and 3-4 A-C). From this point forward, we refer to this region as the N-terminal targeting motif (NTM, Myo1a-TH1 residues 847-858).

To explore targeting contributions from the C-terminus of Myo1a-TH1, we carried out a similar truncation analysis on this end of molecule (Fig. 3-1 C). Truncations CΔ49 and CΔ21 both abolished microvillar targeting (FEM = 0.20 ± 0.02 and 0.25 ± 0.03, respectively; Fig. 3-3 D). Interestingly, the region encompassing the last 15 residues of Myo1a-TH1 scored highly on the BH scale (Fig. 3-1 E). Deletion of the C-terminal hydrophobic residues in this region (CΔ10, Fig. 3-1 C) reduced targeting to just below the enrichment threshold (FEM = 0.85 ± 0.08; Fig. 3-3 D and *3*-4 D-F). Further truncation to removed a cluster of four basic residues (CΔ15, Fig. 3-1 C) abolished targeting (FEM = 0.24 ± 0.02; Fig. 3-3 D and *3*-4 D-F). For this reason, we focused site-

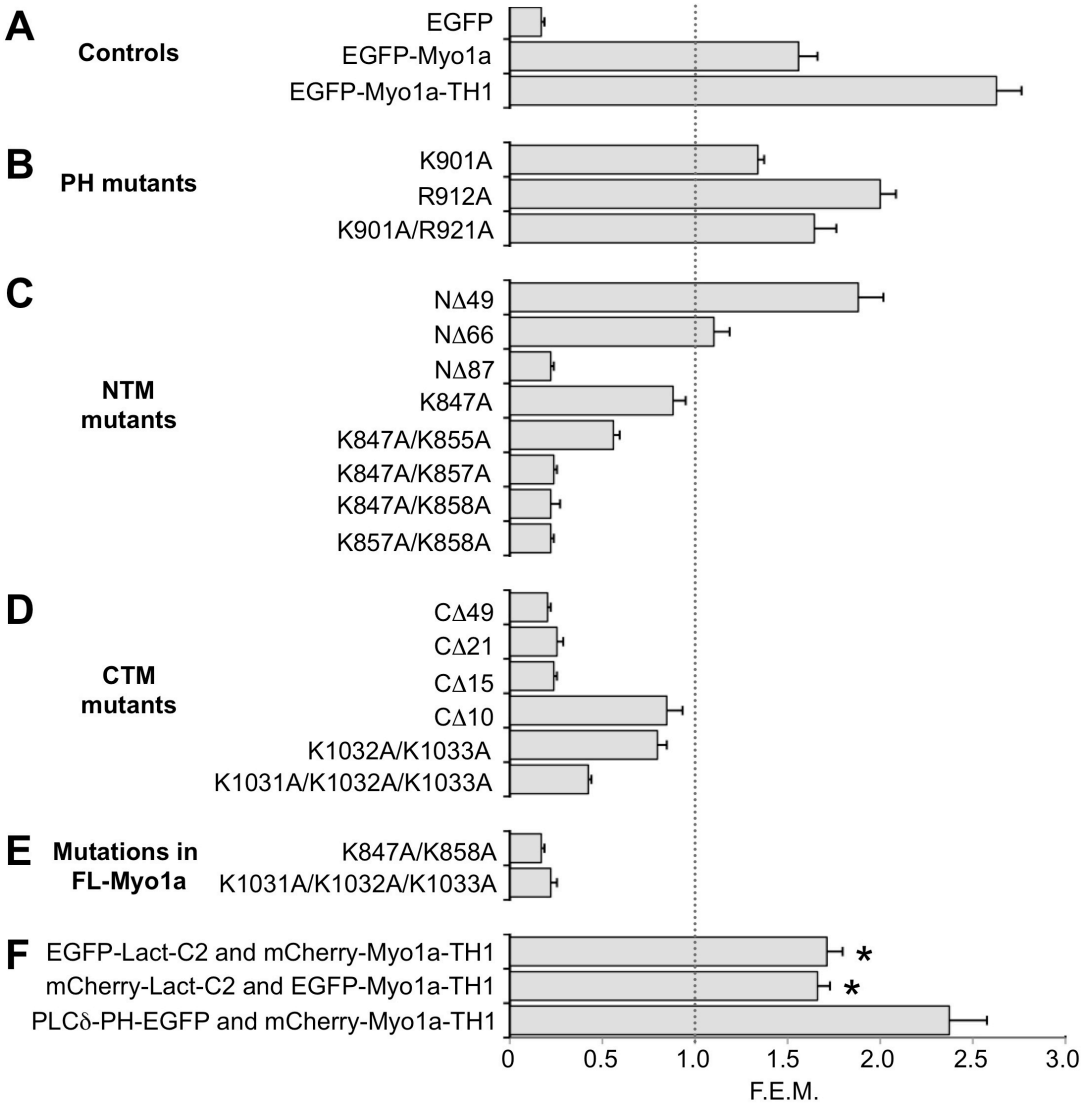

Figure 3-3. Fold Enrichment in Microvilli (FEM) for various Myo1a-TH1 mutant constructs. Control constructs (*A*), EGFP-Myo1a-TH1 constructs with point mutations to the PH region (*B*), EGFP-Myo1a-TH1 constructs with truncations or mutations to the NTM (*C*) or CTM (*D*), or EGFP-Myo1a full length molecules with mutations to the key lysine residues identified in TH1 (*E*) were expressed individually in CL4 cells and analyzed for microvillar targeting. (*F*) Myo1a-TH1 was coexpressed with Lact-C2 or PLCδ1-PH, and TH1 targeting was quantified in the presence of each construct. Lact-C2, but not PLCδ1-PH, reduced TH1 targeting to microvilli. *p<<0.0001 vs. EGFP-Myo1a-TH1 alone. Plotted FEM values represent the average microvillar intensity:cytosolic intensity ratio. Gray dashed line represents the 1:1 enrichment threshold; constructs with FEM values below this level are not enriched in microvilli. Error bars represent mean ± sem.

directed mutagenesis on these residues, making alanine substitutions to one, two, or three of the lysines in this region. Only the triple point mutation, K1031A/K1032A/K1033A (Fig. 3-1 B), abolished enrichment of EGFP-Myo1a-TH1 in microvilli (FEM = 0.42 ± 0.02; Fig. 3-3 D and 3-4 D-F). Sequence alignments revealed that the C-terminal region is well conserved among vertebrate Myo1a isoforms, but not class I myosins in general. Thus, these experiments identify a second region required for Myo1a-TH1 microvillar targeting, the C-terminal targeting motif (CTM, Myo1a-TH1 residues 1029-1043), which appears unique to Myo1a.

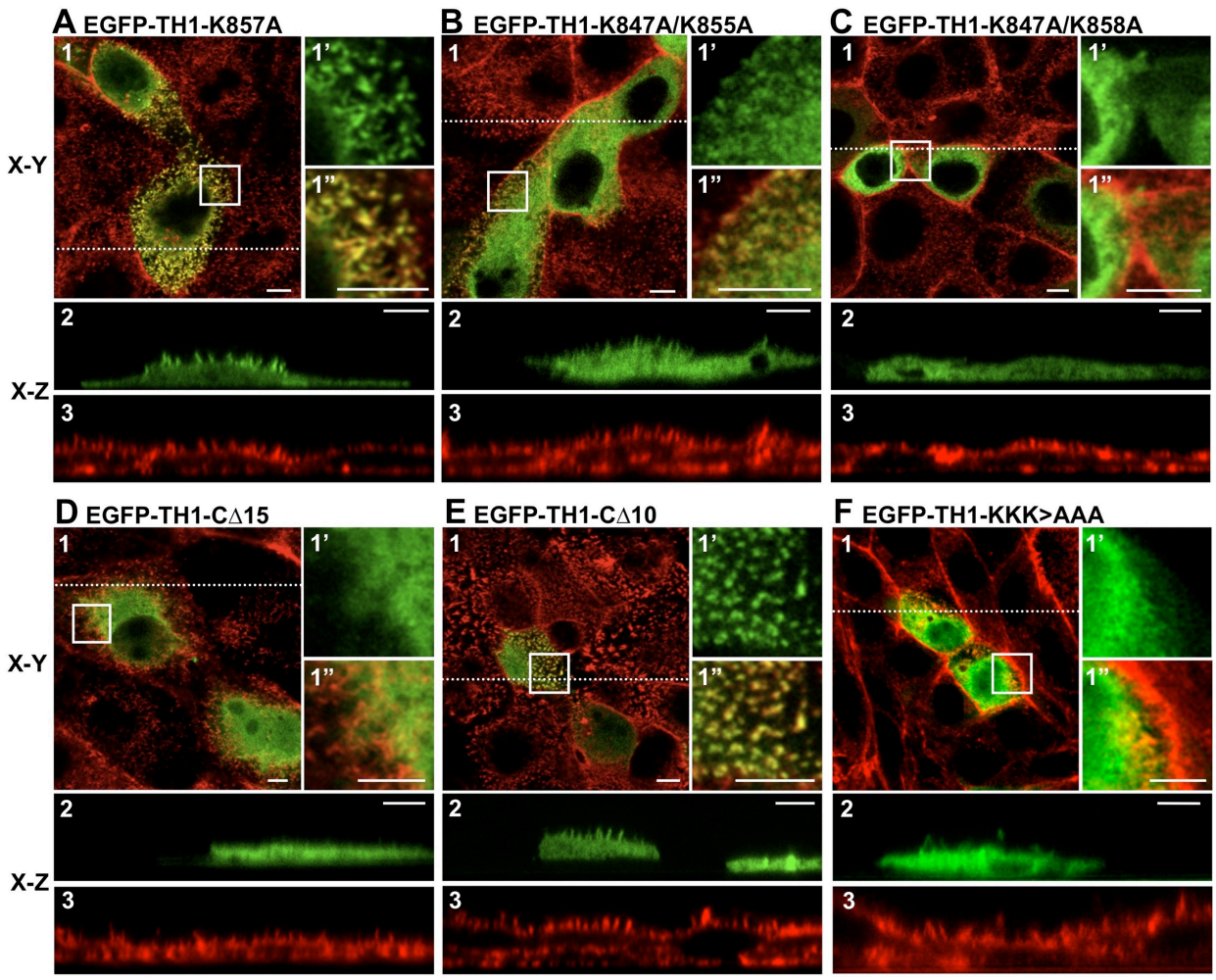

Figure 3-4. NTM and CTM are required for Myo1a-TH1 targeting to microvilli. (*A*-*C*) Representative confocal images of a subset of expressed NTM mutant constructs. EGFP-Myo1a-TH1-K857A is enriched in microvilli (*A*), while EGFP-Myo1a-TH1-K847A/K855A (*B*) and EGFP-Myo1a-TH1-K847A/K858A (*C*) do not target to microvilli. (*D*-*F*) Representative confocal images of a subset of expressed CTM mutant constructs. EGFP-Myo1a-TH1-CΔ15 does not target to microvilli (*D*), while EGFP-Myo1a-TH1-CΔ10 exhibits reduced enrichment (*E*). (*F*) A construct with alanine mutations to the three lysine residues in the CTM, EGFP-Myo1a-TH1-K1031A/K1032A/K1033A (KKK>AAA), does not localize to microvilli. Here, 1 represents an apical, *en face* view of EGFP-tagged construct (green) merged with Alexa568-phalloidin labeled F-actin (red); the boxed area in 1 is shown in 1' (EGFP or EGFP-tagged construct) and 1" (merge with phalloidin). X-Z sections show EGFP-tagged constructs (green, 2) or F-actin (phalloidin, red, 3). Dashed line in 1 represents location in the cell where X-Z section was imaged. Bars are 5 μm.

Whereas the structure-function studies described above were carried out using the Myo1a-TH1, we next sought to determine if the targeting motifs identified with this approach also played a role in the microvillar enrichment of full length (FL) Myo1a. We created EGFP-tagged variants of FL-Myo1a expressing mutations in the NTM or CTM, which eliminated Myo1a-TH1 enrichment in microvilli (K847A/K858A or K1031A/K1032A/K1033A, respectively, Fig. 3-1 B). FEM analysis of both mutants revealed major reductions in steady state microvillar targeting (FEM = 0.17 ± 0.02 and 0.22 ± 0.03, respectively**;** Fig. 3-3 E). This suggests that similar to Myo1a-TH1, FL-Myo1a also targets to the microvillus using a mechanism that involves the NTM and CTM.

Myo1a binds to acidic phospholipids in vitro

Previous studies have shown that several class I myosins from lower and higher eukaryotes, including chicken Myo1a (Hayden et al., 1990), are *bona fide* membrane binding proteins (Coluccio, 2008). We sought to determine if this is also the case for human Myo1a. To this end, we examined the lipid binding ability of purified full-length

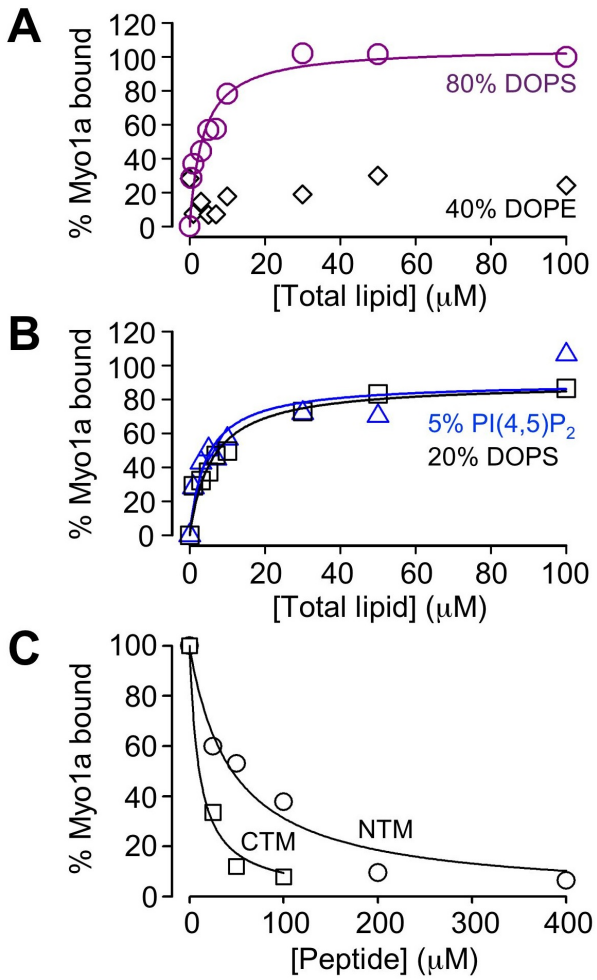

Figure 3-5. NTM and CTM compete with Myo1a for binding to negatively charged liposomes *in vitro*. (*A*) Cosedimentation assays using Myo1a-myc-FLAG (50 nM) and liposomes composed of varying lipid species (0-100 μM). Myo1a binds to liposomes composed of 20% DOPC/80% DOPS with moderate affinity (purple symbols and line, K_D = 3.6 ± 0.9 μM). Additionally, Myo1a did not show significant binding to liposomes composed of 60% DOPC/40% DOPE (black diamonds). (B) Myo1a bound similarly to liposomes composed of either 40% DOPE, 55% DOPC, and 5% PI(4,5)P_2 (blue symbols and line, K_D = 4.5 ± 1.7 μM) or 80% DOPC/20% DOPS (black symbols and line, K_D = 6.0 ± 1.4 μM), suggesting the interaction between Myo1a and membrane is electrostatic rather than stereospecific. Data were normalized to the percent bound value for 100 μM 80% DOPS and fit to hyperbolae using SigmaPlot. (*C*) Peptides corresponding to a control sequence from the Myo1a motor domain, the NTM, or the CTM were incubated with 50 nM Myo1a-myc-FLAG and 50 μM liposomes composed of 80% DOPS/20% DOPC. In the presence of NTM or CTM peptides, but not the control peptide, Myo1a binding to liposomes was significantly reduced. Percent bound Myo1a was calculated by dividing total bound Myo1a for each condition by total bound in the presence of control peptide. Data are averages from two (NTM peptide, 200 and 400 μM) or three independent experiments. Fits to hyperbolic decays yield IC_{50} values of 47 ± 9 μM for the NTM and 10 ± 2 μM for the CTM. Errors represent standard errors of the fit parameter.

human Myo1a using co-sedimentation assays (Fig. 3-5 A,B). Myo1a bound with moderate affinity to liposomes composed of DOPS at a physiologically relevant concentration (20% DOPS; K_D = 6.0 ± 1.4 μM; Fig. 3-5 B). Increasing the concentration of DOPS 4-fold increased the affinity slightly (80% DOPS; K_D = 3.6 ± 0.9 μM; Fig. 3-5 A). Moreover, liposomes containing 5% $PI(4,5)P_2$ produced binding similar to that observed with 20% DOPS vesicles, which are equivalent in total charge (Fig. 3-5 B). No significant binding was observed with liposomes containing 2% $PI(4,5)P_2$ (data not shown). These results suggest that in contrast to vertebrate Myo1b and Myo1c (Hokanson and Ostap, 2006; Komaba and Coluccio, 2010), Myo1a does not demonstrate a binding preference for $PI(4,5)P_2$. Instead, Myo1a likely binds to membranes via non-stereospecific electrostatic interactions driven by the density of negative charge, similar to vertebrate Myo1e and *Acan* Myo1c (Brzeska et al., 2008; Feeser et al., 2010).

NTM and CTM peptides compete with Myo1a for binding to acidic phospholipids *in vitro*

Because mutations to NTM and CTM basic residues abolished Myo1a-TH1 and FL-Myo1a targeting to microvilli, and our co-sedimentation data indicates that human Myo1a binds liposomes containing acidic phospholipids *in vitro*, we sought to determine if either of these newly discovered motifs possessed membrane binding activity. Purified Myo1a was mixed with 50 μM liposomes composed of 20% DOPC/80% DOPS in the presence of NTM peptide, CTM peptide, or a peptide of comparable length obtained from a random region in the motor domain (negative control); co-sedimentation was used to assess the extent of Myo1a liposome binding in each reaction. Although Myo1a

binding was unaffected by the control peptide, binding decreased in a dose-dependent manner when NTM or CTM peptides were included in reactions (Fig. 3-5 B). Interestingly, the CTM peptide was a more potent inhibitor of Myo1a liposome binding (IC_{50} = 10 μM) compared to the NTM (IC_{50} = 47 μM), but this was not due to a higher charge density as both NTM and CTM peptides have a pI of ~9.5. These results indicate that both NTM and CTM peptides interact directly with membranes composed of acidic phospholipids, and further suggest that these motifs are capable of mediating Myo1a membrane binding in cells.

NTM and CTM regulate Myo1a-TH1 membrane-binding dynamics in live cells

If the NTM and CTM are capable of binding directly to membrane lipids, mutations to these motifs likely impact steady-state microvillar enrichment of Myo1a (Figs. 3-3 and 3-4) by reducing the amount of time this molecule spends in a membrane bound state. To explore this possibility, we used single molecule TIRF microscopy to measure the lifetimes of Myo1a-TH1 molecules bound to the plasma membrane of live cells. For these studies, we tagged Myo1a-TH1 and two non-targeting Myo1a-TH1 mutants (K847A/K858A and K1031A/K1032A/K1033A) with three tandem copies of mCitrine (3x-mCitrine), and expressed these constructs in CL4 cells. Previous studies exploited this approach to examine the dynamics and directed movement of single kinesin molecules in live cells (Cai et al., 2009; Cai et al., 2007). TIRF imaging was performed on the ventral surface of sparsely plated, unpolarized CL4 cells. Observing cells with extremely low expression levels of 3x-mCitrine-tagged constructs allowed us to image single molecule binding events, which appeared as bright diffraction limited spots on the ventral cell surface (Fig. 3-6 A*, inset*). Fluorescence spots in image stacks were tracked

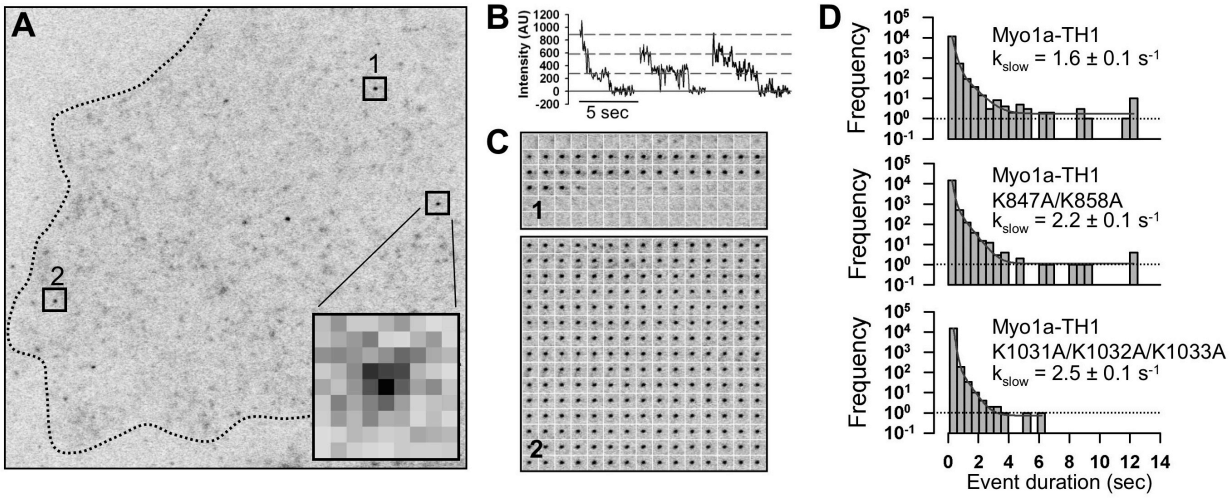

Figure 3-6. Single molecule TIRF microscopy reveals that the NTM and CTM contribute to long-lived membrane binding events. (*A*) A single time-point from a representative 250 frame (12.5 sec) image stack of a single CL4 cell expressing low levels of 3x-mCitrine-Myo1a-TH1. Dashed line traces the periphery of the cell. *Inset*, Enlarged diffraction limited spot representing a single molecule binding event (75 nm/pixel). (*B*) Multi-step photobleaching is observed for individual 3x-mCitrine molecules. (*C*) Montage of individual frames demonstrate the lifetimes of single molecules highlighted in *A* (see boxes 1 and 2). (*D*) Unitary membrane binding event lifetime distribution for 3x-mCitrine-Myo1a-TH1, 3x-mCitrine-Myo1a-TH1-K847A/K858A, and 3x-mCitrine-Myo1a-TH1-K1031A/K1032A/K1033A (KKK>AAA). Solid lines show fits to a bi-exponential decay; slow rate constants ± standard error of the fit parameter are given in each case.

using a 'FIONA'-based algorithm which enabled us to measure membrane bound lifetimes and assemble lifetime distributions (Fig. 3-6 D) (Toprak et al., 2010). Each record yielded thousands of individual binding events, the vast majority of which were rapid collisions between fluorescent molecules and the ventral cell surface. Single molecule lifetime measurements for 3x-mCitrine-Myo1a-TH1 revealed event durations that ranged from 100 ms (the shortest detectable event) to 12.5 sec (the entire 250 frame record) (Fig. 3-6 D). The longest events (> 10 sec) are consistent with lifetime estimates from previous studies (Tang et al., 2002; Tyska and Mooseker, 2002). We

assumed lifetime distributions consisted of two types of events: (i) short-lived non-specific interactions (fast component), and (ii) longer-lived 'productive' membrane binding events (slow component). Thus, fitting lifetime distributions to a bi-exponential decay revealed that Myo1a-TH1-K847A/K858A and Myo1a-TH1-K1031A/K1032A/K1033A both showed an increase in the rate of the slow component (k_{slow} = 2.2 ± 0.1 s^{-1} and 2.5 ± 0.1 s^{-1}, respectively; Fig. 3-6 D) relative to 3x-mCitrine-Myo1a-TH1 (k_{slow} = 1.6 ± 0.1 s^{-1}; Fig. 3-6 D). Other poorly targeting mutants with low FEM values (CΔ10 and K847A/K855A) produced similar results (data not shown). These experiments revealed that the NTM and the CTM likely contribute to membrane enrichment of Myo1a by slowing the rate at which Myo1a-TH1 detaches from the membrane.

Myo1a-TH1 interacts with PS in brush border microvilli

Our *in vitro* binding studies suggests that an electrostatic interaction with the plasma membrane may be the primary mechanism for Myo1a targeting to microvilli. Myo1a bound DOPS-containing liposomes *in vitro*, and PS is one of the most abundant negatively charged lipid species found in the inner leaflet of the plasma membrane (van Meer and de Kroon, 2011; van Meer et al., 2008). Thus, we sought to determine if PS colocalizes with Myo1a-TH1 in microvilli. As probes for observing the PS distribution, we used an antibody raised against PS and the PS sensor, lactadherin-C2 (Lact-C2). Lact-C2 is a PS-specific binding module and has been used previously to analyze PS localization in cells (Fairn et al., 2011b; Yeung et al., 2008; Yeung et al., 2009). Both PS probes revealed that Myo1a-TH1 and PS colocalized in microvilli (Fig. 3-7).

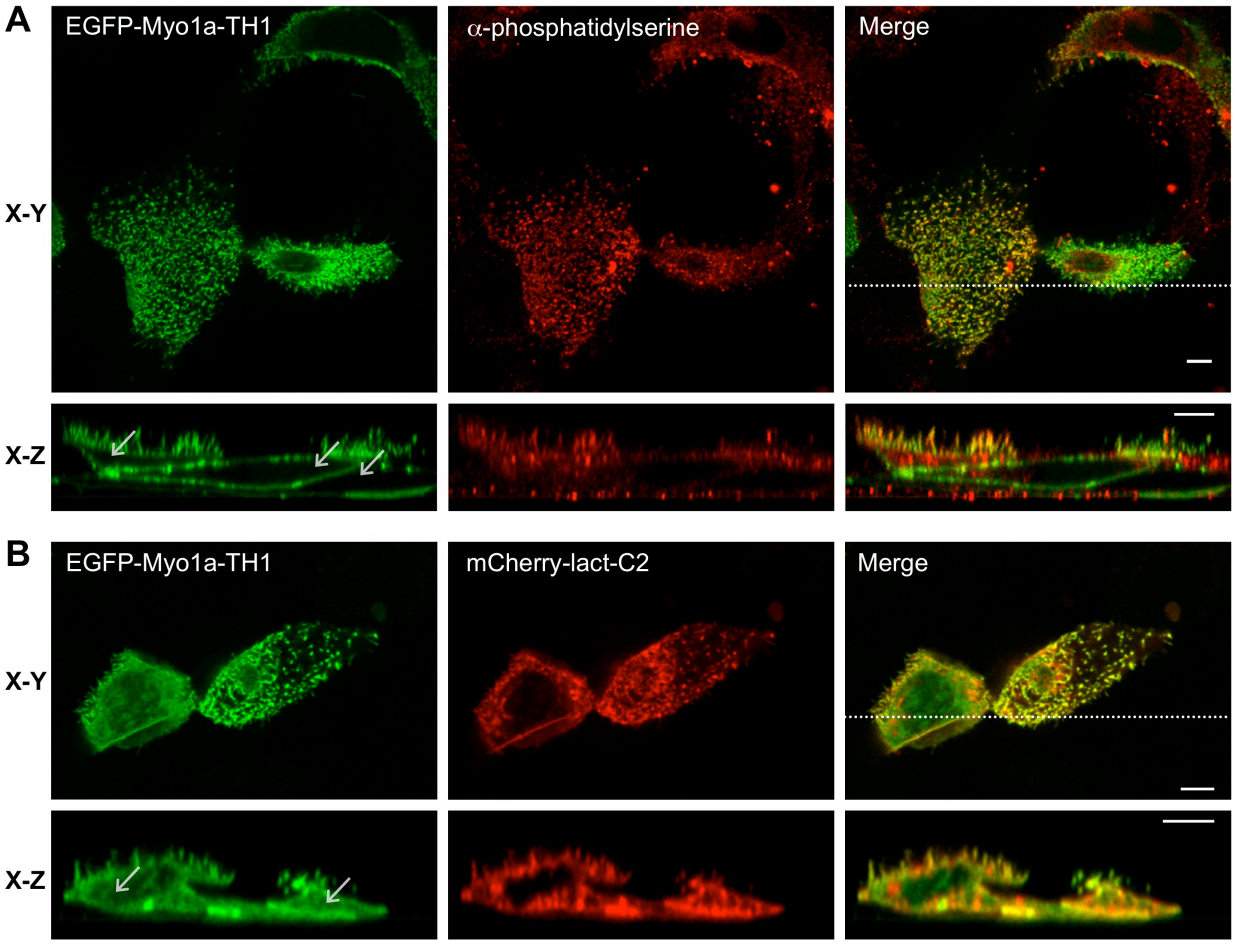

Figure 3-7. Myo1a-TH1 interacts with PS in microvilli. EGFP-Myo1a-TH1 colocalizes with antibody stained PS (*A*) and coexpressed PS-binding protein, mCherry-Lact-C2 (*B*), in microvilli. The cytosolic pool of EGFP-Myo1a-TH1 increases in the presence of Lact-C2 (compare white arrows in X-Z sections in *A and B*). Bars are 5 μm.

Whereas the anti-PS probe exhibited strong microvillar labeling with some minor staining of sub-apical material (likely biosynthetic vesicles; Fig. 3-7 A), Lact-C2 targeted to plasma membrane and intracellular vesicles throughout the cell as previously reported (Fairn et al., 2011b). The wider distribution of the Lact-C2 probe is most likely due to the fact that construct is over-expressed under these conditions. Surprisingly,

these studies also revealed that in the presence of Lact-C2, Myo1a-TH1 appeared much more soluble (Fig. 3-7 B, compare arrows in *A* and *B*, EGFP X-Z sections). FEM analysis of Myo1a-TH1 in cells coexpressing Lact-C2 revealed a significant decrease in microvillar enrichment, which was independent of the fluorescent protein tag used to visualize these molecules (EGFP-Myo1a-TH1, FEM = 1.66 ± 0.07 and mCherry-Myo1a-TH1, FEM = 1.71 ± 0.08; Fig. 3-3 F). Moreover, this effect was specific to the PS-binding protein; although Myo1a-TH1 co-localized with the $PI(4,5)P_2$ binding protein, PLCδ1-PH, microvillar enrichment of Myo1a-TH1 was not impacted by coexpression of this probe (FEM = 2.37 ± 0.20; Fig 3-3 F), despite the fact that PLCδ1-PH appears to bind liposomes composed of 2% $PI(4,5)P_2$ with higher affinity than Myo1a. These data suggest that $PI(4,5)P_2$ in the apical membrane makes only a minor contribution to Myo1a enrichment in microvilli. Instead, Myo1a-TH1 likely binds to PS in the brush border, and targeting of Myo1a to this sub-cellular domain is at least partially driven by this interaction.

Discussion

Dissecting the membrane binding mechanism of Myo1a-TH1

In this study, we used a cell-based screen to discover two regions in Myo1a-TH1 that are essential for normal microvillar targeting: the NTM (Myo1a-TH1 residues 847-858) and the CTM (Myo1a-TH1 residues 1029-1043; Figs. 3-1, 3-3, and 3-4). Loss of charge mutations to basic residues in either of these regions resulted in a significant loss of Myo1a-TH1 targeting to microvilli at steady state. Moreover, *in vitro* biochemical experiments showed Myo1a binds directly to acidic phospholipids with moderate affinity, and peptides encompassing either the NTM or CTM compete with Myo1a for binding to

liposomes composed of 80% DOPS/20% DOPC (Fig. 3-5), suggesting that these regions interact directly with membranes. Analysis of membrane binding dynamics in live cells using single molecule TIRF microscopy revealed that mutations to either of these motifs reduced the amount of time that Myo1a-TH1 spends in a membrane bound state (Fig. 3-6). This latter result provides a mechanism for the loss of steady state targeting observed in the initial structure-function experiments (Fig. 3-3). Finally, Myo1a-TH1 colocalizes with PS in the brush border; a PS-binding protein (Lact-C2), but not $PI(4,5)P_2$-binding protein (PLCδ1-PH), reduces Myo1a-TH1 enrichment in microvilli. Taken together, the data presented here indicate the NTM and CTM are *bona fide* membrane-binding motifs that contribute to electrostatic interactions between Myo1a-TH1 and acidic phospholipids such as PS, in the inner leaflet of the microvillar membrane.

The NTM identified in Myo1a-TH1 is predicted to be α-helical (data not shown) (Roy et al., 2010; Zhang, 2008) and is well conserved across vertebrate short-tailed class I myosins (Fig. 3-1 D), suggesting that this motif might represent a common membrane-binding feature. In support of this proposal, a region equivalent to the NTM in Myo1g (referred to as the 'pre-PH' domain) was shown to be critical for targeting of this motor in Jurkat cells; mutating either of the two conserved basic residues that flank this region (K815 and R826 in Myo1g, equivalent to K847 and K858 in Myo1a) significantly reduced the enrichment of Myo1g at the plasma membrane (Patino-Lopez et al., 2010). Helical wheel analysis of the NTM in Myo1g (Patino-Lopez et al., 2010) and Myo1a (not shown) reveals that the flanking basic residues are on the same face of a short a-helix and thus, well positioned to form a lipid binding interface. A folded

structure may help explain why a single point mutation (K847A) to the NTM impacts Myo1a-TH1 enrichment (Fig. 3-3 C), despite the modest BH score for this region (Fig. 3-1 E). Additional experiments will be needed to determine if the NTM functions as a general membrane binding motif in other class I myosins.

The CTM identified in Myo1a-TH1 exhibits poor sequence conservation with other class I myosins. Analysis of CTM secondary structure revealed a β-sheet prediction, although the confidence scores were weak, suggesting the region may be partially unstructured. This would be consistent with the broad BH peak observed for this motif (Fig. 3-1 E). Studies with BH motifs from *Acanthamoeba* and *Dictyostelium* myosins-1 revealed that mutations to either the basic or hydrophobic residues reduced binding to lipids (Brzeska et al., 2010; Brzeska et al., 2008). Consistent with these findings, removal of the hydrophobic residues at the C-terminus the CTM (Myo1a-TH1-CΔ10) or mutagenesis of the CTM basic cluster (Myo1a-TH1-K1031A-K1032A-K1033A), both had an impact on targeting to microvilli (Figs. 3-3 D, 3-4 E, F). These results further support the proposal that the CTM may function as a Myo1a-specific, unstructured lipid binding motif.

We also employed single molecule TIRF microscopy to investigate how the NTM and CTM contribute to the kinetics of unitary Myo1a-TH1 membrane binding events. Measurements of membrane bound lifetimes obtained from TIRF time-lapse data provide direct access to detachment rates (k_{OFF} = 1/bound lifetime). Imaging single molecule dynamics at the apical surface of polarized cells using TIRF is technically challenging due to the orientation of polarized cells grown in culture and the confinement of the TIRF excitation to the coverslip surface. Thus, we focused on the

ventral membrane of unpolarized CL4 cells, which is amenable to TIRF illumination and expected to contain many of the major acidic phospholipid species, including PS. These imaging data revealed that mutations to the NTM or CTM increased the membrane detachment rate for Myo1a-TH1. Together with our steady-state targeting data, these findings suggest that the NTM and CTM work together to produce long-lived membrane binding events.

Myo1-PH domain is not essential for Myo1a-TH1 targeting in cells

Previous studies with short-tailed class I myosins Myo1b, Myo1c, and Myo1g, have implicated the conserved Myo1-PH domain in the targeting of these motors to cellular membranes (Hokanson et al., 2006; Hokanson and Ostap, 2006; Komaba and Coluccio, 2010; Olety et al., 2010; Patino-Lopez et al., 2010). Biochemical studies with Myo1b and Myo1c have also revealed high affinity interactions with $PI(4,5)P_2$ (Hokanson et al., 2006; Hokanson and Ostap, 2006; Komaba and Coluccio, 2010). Unexpectedly, we find that the Myo1-PH domain and interactions with $PI(4,5)P_2$ are minor players in the mechanism that enables Myo1a-TH1 to become enriched on the microvillar membrane. This is supported by three principle findings: (1) mutations to signature Myo1-PH residues do not abolish the enrichment of Myo1a-TH1 in microvilli (Fig. 3-2 and 3-3 B), (2) Myo1a binds similarly to liposomes containing DOPS or $PI(4,5)P_2$ at levels that provide equivalent negative charge (Fig. 3-5 B), and (3) PLCδ1-PH does not compete with Myo1a-TH1 for binding sites in microvilli (Fig. 3-3 F). We note here that although Myo1a-TH1 variants with PH domain mutations are still enriched in microvilli, FEM values are reduced relative to control constructs (Fig. 3-3 B). Thus, in addition to the NTM and CTM, basic residues in the PH domain likely contribute to general electrostatic

interactions with the plasma membrane, similar to what has been proposed for *Acan* Myo1c (Brzeska et al., 2008).

Our findings are consistent with other recent results, which indicate that TH1 structural elements outside the Myo1-PH domain likely contribute to membrane binding. For example, the Myo1c PH domain interacts tightly and specifically with $PI(4,5)P_2$, yet transient kinetic and single molecule assays (McKenna and Ostap, 2009; Pyrpassopoulos et al., 2010) show this interaction alone cannot account for the long membrane bound lifetimes observed with more physiological mixtures of lipids (McKenna and Ostap, 2009). Vertebrate long-tailed Myo1e binds to liposomes composed of physiological concentrations of $PI(4,5)P_2$ with high affinity, yet mutations to PH domain signature residues do not disrupt *in vivo* targeting or liposome binding (Feeser et al., 2010). *Acan* Myo1c also binds to acidic phospholipids using motifs outside the PH domain (Brzeska et al., 2008). Finally, although Myo1g membrane targeting depends on the signature residues of the PH domain, the conserved residues of the NTM also contribute to localization of this isoform (Olety et al., 2010; Patino-Lopez et al., 2010). Differences in the role of the PH domain noted for these different myosin-1 isoforms are likely related to lack of uniform sequence conservation in this region, as previously pointed out by others (Feeser et al., 2010). Together with our work, however, these studies support a model where membrane binding motifs outside the Myo1-PH contribute to proper targeting of class I myosins.

PS as a lipid target for Myo1a-TH1 in microvilli

Our studies suggest that Myo1a-TH1 binds directly to PS in microvilli (Fig. 3-7, 3-3 F). PS is one of the most abundant phospholipid species found in the inner leaflet of the

plasma membrane (van Meer and de Kroon, 2011; van Meer et al., 2008), and is therefore a good candidate for supporting electrostatic interactions between Myo1a-TH1 and the microvillar membrane. Although the labeling methods used here show that PS and $PI(4,5)P_2$ are both found in microvilli, it is still unclear if these lipids compartmentalize into sub-domains along the microvillar axis. In bullfrog saccular hair cells, $PI(4,5)P_2$ is found strictly at the tips of stereocilia, while PS is more widely distributed along the length of these protrusions (Hirono et al., 2004). If such compartmentalization of lipid species is found in microvilli, it could provide one possible mechanism for polarizing the distribution of membrane associated proteins throughout this structure. Intriguingly, Myo1d, a second class I myosin found in the enterocyte brush border, targets to microvillar tips while Myo1a is distributed along the microvillar axis (Benesh et al., 2010). Further experimentation is needed to determine if differential distribution observed for these two class I myosins is based on the sorting of highly charged phospholipids along the microvillar axis. Moreover, elucidation of the brush border membrane 'lipidome' will allow us put the current results into context and help focus future studies on poorly characterized phospholipids that might also contribute to the targeting of class I myosins in this domain.

Functional implications of multiple membrane binding motifs

Although the NTM and CTM both contribute to Myo1a-TH1 membrane binding, our studies suggest that the binding affinities generated by each individual motif are below the threshold needed to create enrichment on the membrane. Indeed, mutations to either the NTM or CTM abolish enrichment on microvillar membrane and increase the membrane detachment rate (Figs. 3-3, 3-6), and peptides representing these motifs

bind to acidic phospholipids with a lower affinity than full length Myo1a (Fig. 3-5). These findings suggest that residues from both motifs are needed for full binding functionality. Multi-site binding mechanisms have been described for a number of peripheral membrane binding proteins and are hypothesized to provide several functional advantages (McLaughlin and Aderem, 1995; McLaughlin et al., 2002). For example, multi-site binding is able to create high binding affinities from relatively weak electrostatic interactions. This is because binding affinities are combined in a multiplicative (rather than additive) manner (Crothers and Metzger, 1972). Thus, two distinct sites that bind membrane weakly on their own, demonstrate a much higher binding affinity (and thus, longer membrane bound lifetimes) when tethered together in the same protein or protein complex (Knight et al., 2010; McLaughlin and Aderem, 1995; McLaughlin et al., 2002). Multi-site binding might also enable a protein to sequester lipids, thus reducing its diffusional mobility while bound to the inner leaflet (Knight et al., 2010). This would be advantageous for a motor such as Myo1a, which functions in processes that require force generation between the actin cytoskeleton and fluid plasma membrane.

How the NTM and CTM are arranged in the context of a folded TH1 domain, and how the spatial arrangement of these motifs impacts membrane binding, remains unclear. One possibility is that these two motifs fold into a single membrane binding site, although this was not supported by the results of *de novo* modeling studies using I-TASSER (Zhang, 2008), which reproducibly positioned these motifs on separate faces of the TH1 domain (not shown). Thus, a more likely possibility is that these motifs represent unique membrane-interacting regions. If the NTM and CTM are spatially

separated, it is tempting to speculate that these different sites could facilitate membrane binding during different phases of the Myo1a mechano-chemical cycle. For example, one binding site might be optimally engaged with the lever arm in a pre-power orientation, while the other binding site might be better oriented to bind membrane after the power stroke is complete. This would allow the TH1 domain to remain bound for the duration of the power stroke, despite the large conformational change that takes place during lever arm rotation (Jontes et al., 1995). High-resolution structural studies of the TH1 domain will be needed to develop our understanding of the spatial and functional relationships between the multiple membrane binding motifs identified in this and previous studies.

CHAPTER IV.

MYOSIN-1A MOTOR AND TAIL DOMAINS SYNERGISTICALLY MODULATE DYNAMICS IN CELLS

Abstract

Myosins-I are monomeric motor proteins that have diverse functional roles at the membrane/cytoskeletal interface in a wide variety of cellular systems. Localization and function require both motor/actin interactions and tail homology 1 (TH1)/membrane interactions, yet little is known about how these domains regulate local dynamics in cells. TH1 interactions with membranes are inherently long-lived and required for cellular targeting. Moreover, as low duty ratio motors, class I myosins spend little time strongly bound to actin, although under load this duration can increase. These characteristics lead to the basic prediction that membrane binding should control myosin-I dynamics in cells. However, dynamics studies to date have not explored how each domain contributes to myosin-I mobility in cells with precision and resolution necessary to characterize the behavior of single molecules. To this end, we used total internal reflection fluorescence microscopy in combination with single particle tracking and mean-squared displacement analysis to examine the dynamics of the well-characterized myosin-1a (Myo1a). These studies revealed that full length Myo1a exhibits limited dynamics relative to TH1 alone and that the motor domain makes an unexpected contribution to limiting Myo1a diffusion. Structure/function analysis further implicated the neck region as an additional regulator of mobility. These data are the first to explore myosin-1a dynamics at that single molecule level in cells and suggest a

model where the behavior of myosin-1a is controlled by synergistic interactions between the tail and motor domains, which are mediated by the neck region.

Introduction

Class I myosins are widely expressed, monomeric motor proteins that function at the actin/membrane interface in membrane tension maintenance (Nambiar et al., 2009), mechano-signal transduction (Gillespie and Cyr, 2004) and membrane remodeling and trafficking (Almeida et al., 2011; Bose et al., 2002). The eight vertebrate class I myosins exhibit diverse expression and localization but share defining structural features including a tail homology 1 (TH1) membrane binding domain, a force transducing neck region that binds varying numbers of calmodulin molecules, and an actin binding, ATP hydrolyzing motor domain that generates mechanical force. TH1 domains have long-lived interactions with membranes (McKenna and Ostap, 2009; Tang et al., 2002; Tyska and Mooseker, 2002) and are required for steady-state targeting in cells (Benesh et al., 2010; Patino-Lopez et al., 2010; Tang and Ostap, 2001; Tyska and Mooseker, 2002), even in the few cases where the motor domain enhances localization (Patino-Lopez et al., 2010; Tang and Ostap, 2001). Under unloaded conditions, myosins-I are low duty ratio motors that spend only a short duration of their total ATPase cycles strongly bound to actin (hundreds of milliseconds) (De La Cruz and Ostap, 2009; Greenberg and Ostap, 2013). However, recent *in vitro* single molecule optical trapping studies have determined that some class I myosins respond to load by altering their actin attachment kinetics (Greenberg et al., 2012; Laakso et al., 2008). For Myosin-1b, even small (<1pN) forces result in a large increase to the lifetime of the strongly bound state

(Laakso et al., 2008), while Myosin-1c alters its actin-attached kinetics over a range of larger (>2.5 pN) forces to transition to a slow power generator (Greenberg et al., 2012).

Myosin-1a (Myo1a) also exhibits kinetic properties that suggest a capacity for tension sensing (Jontes et al., 1997). Myo1a is primarily expressed in the small intestine where it localizes to the brush border: a highly ordered array of microvilli that extend from the apical surface of enterocytes (Mooseker, 1985). In the brush border, Myo1a links the core actin bundles of microvilli to the overlying plasma membrane and plays key roles in maintaining overall structure (Tyska et al., 2005), regulating membrane tension (Nambiar et al., 2009) and facilitating microvillar vesicle shedding (McConnell and Tyska, 2007). TH1 is required for Myo1a targeting to brush borders in cells (Tyska and Mooseker, 2002); our recent studies showed that two membrane binding motifs in this domain, the N-terminal motif (NTM) and C-terminal motif (CTM), facilitate this interaction. Mutations to basic residues in either of these regions decrease membrane bound lifetime (t_{ON}) and disrupt steady-state targeting (Mazerik and Tyska, 2012). Furthermore, in adenocarcinoma patients with mutated CTM regions, loss of epithelial polarity in the GI tract leads to increased tumor invasiveness and decreased overall survival (Mazzolini et al., 2012). These studies highlight the importance of TH1/membrane interactions and suggest a model where TH1 serves as a master regulator of myosin-I dynamics in cells.

Using Myo1a as a model class I myosin, we sought to test the hypothesis that the TH1 domain controls the dynamic behavior of myosin-I molecules in cells. To this end, we employed single molecule total internal reflection fluorescence (SM-TIRF) microscopy in combination with single particle tracking and mean squared displacement

(MSD) analysis. Our results show that the Myo1a motor and TH1 domains act synergistically to regulate the dynamics of this molecule in living cells. Moreover, these data indicate that actin/motor domain interactions makes an unexpected contribution to restricting the mobility of Myo1a at the cell periphery. We also find that full-length Myo1a demonstrates long-lived low mobility events that are eliminated by mutations to the motor, neck or tail and might represent molecules under load. Overall, this study is the first to explore myosin-I dynamics in cells and provides novel insight as to how to myosin-I mobility is controlled in the complex cellular environment.

Results

Myo1a exhibits restricted mobility in the membrane bound state

Previously, we measured lifetimes for the TH1/membrane interaction at the ventral surfaces of LLC-PK1-CL4 (CL4) epithelial cells using SM-TIRF. These experiments provided insight as to how two separate membrane binding motifs, NTM and CTM, govern TH1 membrane bound lifetime. They did not, however, explore lateral diffusion of TH1 or full-length Myo1a, or examine how different Myo1a domains contribute to these dynamics. Our goal was to gain a comprehensive understanding of how the dynamics of membrane bound Myo1a are controlled in cells. To this end, we employed SM-TIRF imaging in a manner similar to our published protocol (Mazerik and Tyska, 2012). Acquisition and data processing parameters were chosen to optimize temporal resolution, which enabled us to acquire time-lapse data at 50 fps. These included increased excitation LASER power and thresholding contrast enhanced image stacks to include the brightest spots, which exhibited 8-bit grayscale values of 120-130. We expressed 3x-Citrine tagged constructs (Fig. 4-1) in CL4 epithelial cells that stably

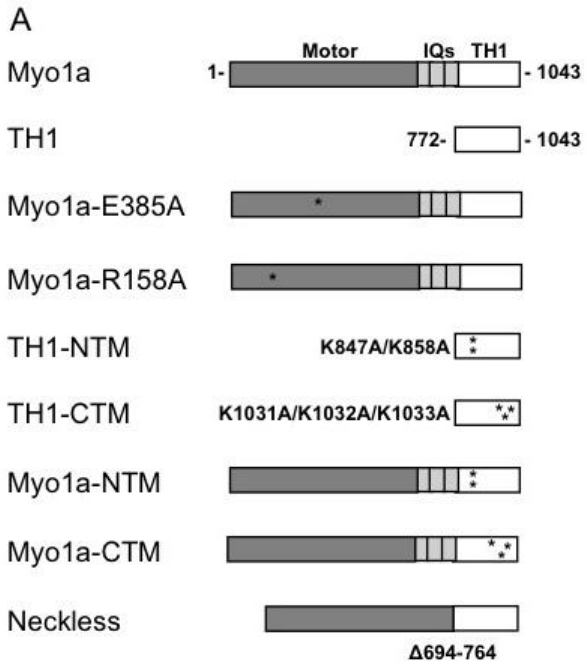

Figure 4-1. Diagrams of constructs used in this study. The mutations to the highly conserved residues in the motor domain, E385A and R158A, are predicted to result in weak actin binding. Both TH1 and Myo1a 'NTM' mutants have K to A mutations to key residues in this region (K847A/K858A). Similarly, TH1 and Myo1a 'CTM' mutants have K to A point mutations to key basic residues in this region (K1031A/K1032A/K1033A). Myo1a-Neckless has functional motor and tail domains, but the entire lever arm has been deleted.

expressed mCherry-Espin to co-label actin, and recorded single molecule membrane binding events over time at the ventral surface. From these image stacks, we used single particle tracking and MSD analysis to extract diffusion coefficients as readouts on molecular mobility. Diffusion coefficients (D) were obtained for each trajectory that lasted 10 frames (200 ms) and for each subsequent 10-frame interval, which resulted in multiple D values for individual trajectories lasting multiple 10-frame intervals. Individual diffusion coefficients for each construct were normalized and then plotted in histograms. We first examined the mobility of full length Myo1a and TH1. As a point of comparison, we also imaged the dynamics of Lactadherin-C2 (Lact-C2) (Yeung et al., 2008). Lact-

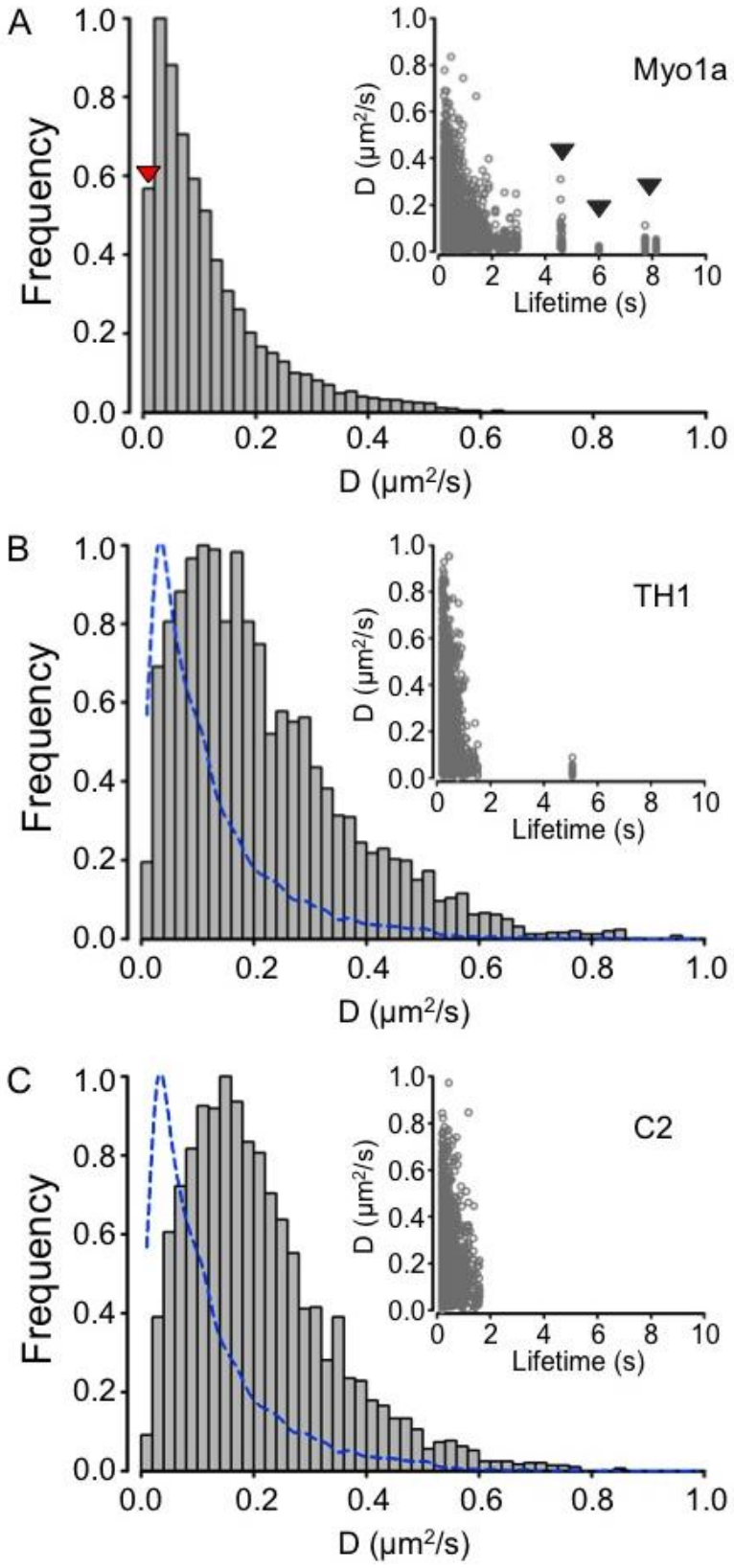
A
Myo1a
Frequency
D (μm²/s)
Lifetime (s)
B
TH1
Frequency
D (μm²/s)
Lifetime (s)
C
C2
Frequency
D (μm²/s)
Lifetime (s)

Figure 4-2. Comparing the dynamics of Myo1a, Myo1a-TH1, and Lact-C2. Individual constructs were tagged with 3x-mCitrine, expressed in CL4 cells, and imaged using TIRF. Images stacks were analyzed using single particle tracking and MSD analysis to determine diffusion coefficients (D) for each construct. D values were obtained for each trajectory lasting 10 frames (200 ms) and for each subsequent 10-frame interval (giving multiple D values for long-lived trajectories). The frequency of D values were normalized and plotted in histograms for Myo1a (A), Myo1a-TH1 (B), or Lact-C2 (C). Inset, plots of D versus lifetime associated with each trajectory fit to obtain D value. Myo1a displayed slower overall dynamics as compared to Myo1a-TH1 and Lact-C2. Numerous long-lived events with low mobility were detected for Myo1a (black arrowheads, inset) and were rarely detectable for Myo1a-TH1 and Lact-C2. Myo1a also displayed a shift toward slower mobility and had many more near-immobile events (red arrowhead). Blue dashed lines are traced outlines of Myo1a histogram density.

C2 competes with Myo1a-TH1 for binding sites in microvilli, and both proteins bind to phosphatidylserine (Mazerik and Tyska, 2012; Yeung et al., 2008). TH1 and Lact-C2 behaved similarly, demonstrating broad distributions in observed D values ranging from 0.01 – 0.95 μm^2/sec, with the peak of the distribution centered on 0.13 μm^2/sec (Fig. 4-2). Surprisingly, the distribution of full length Myo1a diffusion coefficients was shifted toward lower mobility relative to TH1 and Lact-C2, with D values ranging from 0.01 – 0.63 μm^2/sec with a sharp peak at 0.03 μm^2/sec. Myo1a also had a much larger population of events that were nearly immobilized (Fig. 4-2 A, red arrowhead). Additionally, Myo1a exhibited long-lived, low mobility events that were absent in TH1 and Lact-C2 datasets (Fig. 4-2, inset, arrowheads). These results suggest a fundamental difference in the diffusive properties between the membrane binding protein modules, TH1 and Lact-C2, and full length Myo1a, which can interact with both membrane and actin filaments. Indeed, kymograph analysis of Myo1a revealed striking examples of nearly immobilized (see white dashed lines to the left of representative events) molecules that co-localized with F-actin for several seconds (Fig. 4-3 A). In contrast, TH1 molecules demonstrated significant lateral movement and rarely co-

localized with actin filaments (Fig. 4-3 B). Together, these results suggest that the motor domain and/or neck regions (which the TH1 construct lacks) make significant contributions to restricting the lateral mobility of full length Myo1a.

The motor domain limits the lateral mobility of full length Myo1a

To determine if motor domain limits Myo1a dynamics in cells, we made single amino acid mutations in the full-length molecule to disrupt mechanochemical function (Fig. 4-1). Specifically, E385 and R158 are highly conserved residues found in the active site of all myosin superfamily members; mutations in these residues reduce ATPase activity and trap the motor in a state that only weakly interacts with actin filaments (Kambara et al., 1999; Lin et al., 2011; Sasaki et al., 2003; Shimada et al., 1997). If the lower mobility of full length Myo1a relative to TH1 is due to actin binding, alanine substitutions at these sites should cause the D distribution to shift toward higher values. Indeed, D observed for both Myo1a-E385A and Myo1a-R158A were shifted toward higher mobility with peaks broader than that of Myo1a centered at 0.09 μm^2/sec and 0.07 μm^2/sec, respectively (Fig. 4-4). The fraction of events demonstrating near immobilization (Fig. 4-2, red arrowhead) was also reduced (Fig. 4-4). Interestingly, the long-lived events that were present in Myo1a records (Fig. 4-2 A, inset) were absent from Myo1a-R158A and Myo1a-E385A (Fig. 4-4, inset). Together, these data suggest that the lower mobility observed for full length Myo1a is at least partially due to interactions between the motor domain and actin filaments at the cell surface.

TH1/membrane interactions also influence Myo1a dynamics

We next sought to determine the extent to which TH1/membrane interactions influence the dynamics of full length Myo1a in cells. Our previous studies showed that two

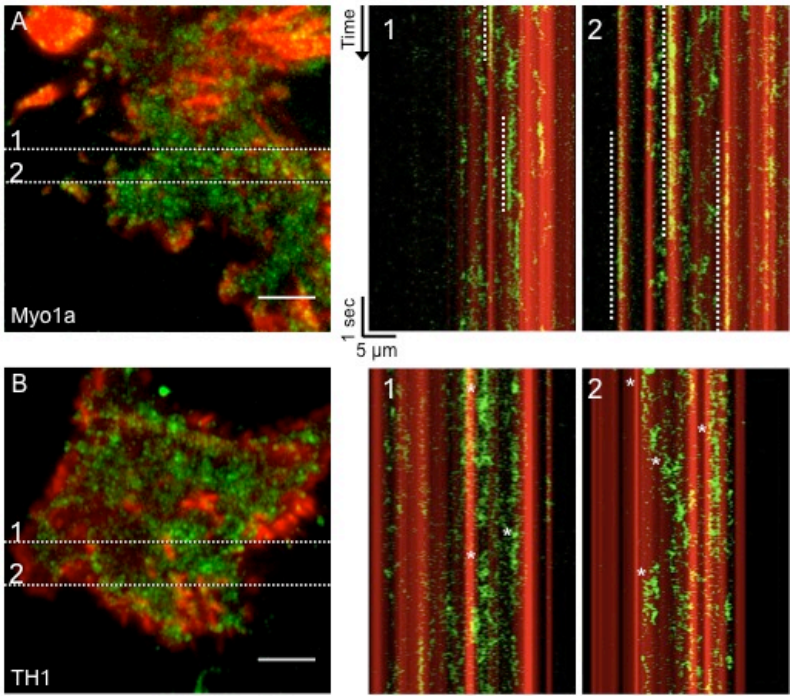

Figure 4-3. Kymograph analysis of Myo1a and Myo1a-TH1. Kymographs, right, show 3x-Citrine tagged Myo1a (green, A) or Myo1a-TH1 (green, B) merged with the mCherry-Espin (red) image from each corresponding cell. Cell images, left, are max projections of image stacks. Dashed lines in left image represent cellular location of the corresponding kymograph. Dashed lines in (A) show actin bound Myo1a molecules and asterisks in (B) denote mobile TH1 molecules. Bars are 5 μm.

membrane binding motifs are required for steady-state targeting of TH1 and Myo1a, and disruption of either of these regions results in decreased membrane bound lifetimes in cells (Mazerik and Tyska, 2012). We investigated the effects of mutations to these motifs (K847A/K858A, NTM and K1031A/K1032A/K1033A, CTM) on the lateral mobility of TH1 and full length Myo1a. Strikingly, membrane binding mutations to either the NTM or CTM affected TH1 and Myo1a in a similar manner, significantly reducing mobility in both cases (Fig. 4-5). These results were intriguing because our previous studies show that in the context of TH1, these mutations reduce membrane bound lifetime and steady

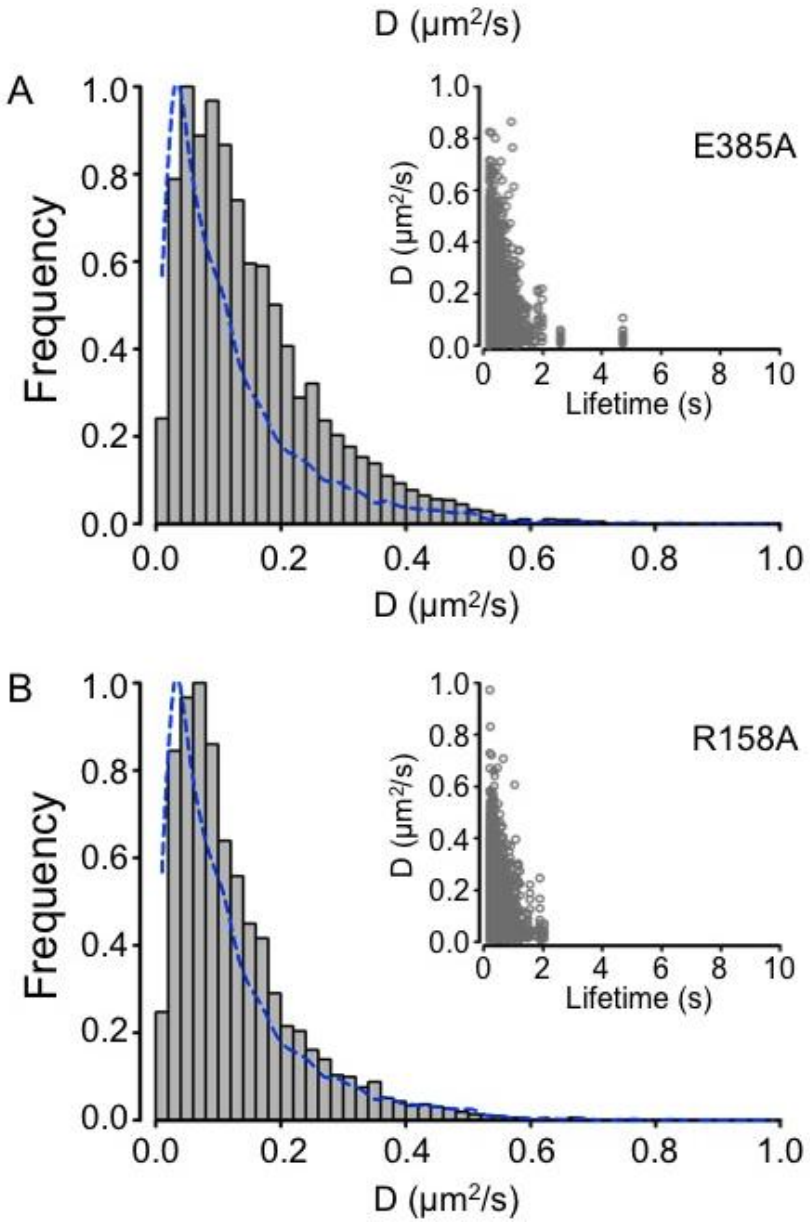

Figure 4-4. Comparing the dynamics of weak actin binding mutants Myo1a-E385A and Myo1a-R15A. Histograms of D values for Myo1a-E385A (A) and Myo1a-R15A (B). Inset, plots of D versus lifetime associated with each trajectory fit to obtain D values. Long-lived events were lost and the numbers of near-immobile events were reduced for both mutant constructs. The E385A and R158A mutations caused the overall distribution of D values to shift toward higher mobility. Blue dashed lines are traced outlines of Myo1a histogram density.

state targeting (Mazerik and Tyska, 2012). These data therefore suggest that membrane bound lifetime can be uncoupled from mobility (i.e. low mobility events do not have to be long-lived). The shift toward lower mobility for Myo1a-NTM, Myo1a-CTM, TH1-NTM and TH1-CTM indicated that TH1 plays an important role in maintaining the diffusion behavior that is characteristic to wild type Myo1a by allowing the molecule to sample a high mobility state. When membrane binding mutations are introduced, a patch of electrostatic charge is lost from TH1. Having multiple electrostatic binding sites might allow TH1 to 'surf' along the membrane surface by sampling multiple binding orientations.

A functional lever arm is required for low mobility behavior displayed by Myo1a

To complete our analysis of domain contributions to Myo1a dynamics, the effects of altering the lever arm were determined. To this end, we deleted the three IQ motifs (amino acid residues 695-764) from full length Myo1a, which resulted in a molecule that had completely functional motor and TH1 domains, but lacked the neck region. We called this mutant Myo1a-Neckless. We expressed Myo1a-Neckless in polarized CL4 epithelial cells and analyzed brush border localization. Using our previously published assay to quantify microvillar targeting, -Fold enrichment in microvilli (FEM) (Mazerik and Tyska, 2012), we determined that Myo1a-Neckless is unable to target properly at steady state (FEM = 0.85 ± 0.13; proteins that are normally enriched in the brush border have a FEM > 1). We then analyzed Myo1a-Neckless dynamics. Myo1a-Neckless exhibited high mobility diffusion similar to TH1 (Fig. 4-6 A). Long-lived, low D binding events that were characteristic to Myo1a were noticeably absent from Myo1a-Neckless trajectories (Fig. 4-6 A, inset). Together with our targeting FEM analysis, the absence of these

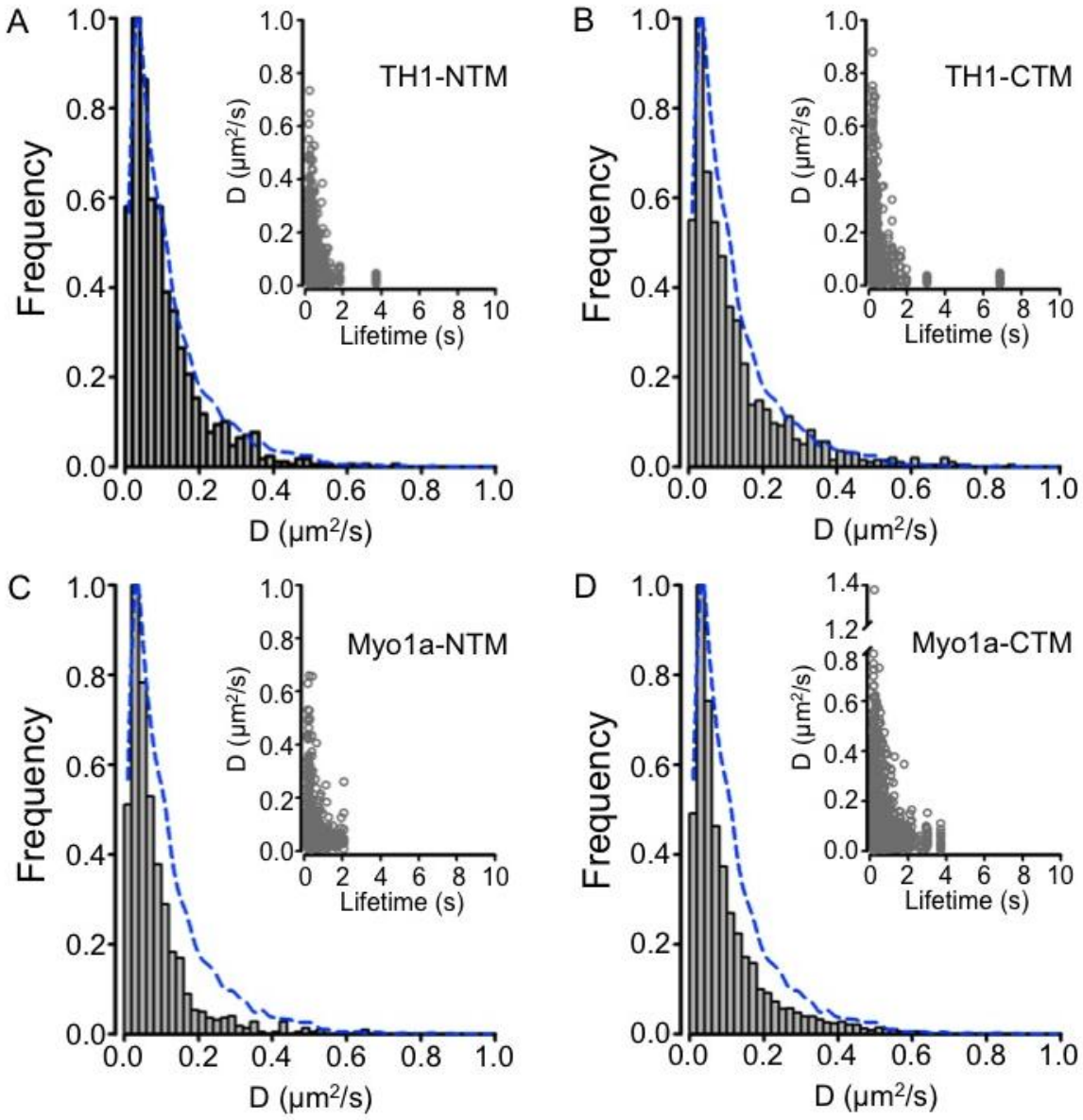

Figure 4-5. Comparing the dynamics of membrane binding mutants TH1-NTM, TH1-CTM, Myo1a-NTM and Myo1a-CTM. Histograms of D values for TH1-NTM (A), TH1-CTM (B), Myo1a-NTM (C) and Myo1a-CTM (D). Inset, plots of D versus lifetime associated with each trajectory fit to obtain D values. Membrane binding mutations for both full-length Myo1a and TH1 resulted in loss of long-lived events and drastic shifts toward low mobility in the overall distribution of D values. Blue dashed lines are traced outlines of Myo1a histogram density.

events might suggest that Myo1a-Neckless has a defect in lifetime, a result that is unexpected given the presence of TH1. Kymograph analysis of Myo1a-Neckless showed traces that resembled TH1, and lacked the long-lived actin localized events that were abundant in Myo1a records (Fig. 4-6 B). These results clearly indicated that intact motor and tail binding activities are not sufficient to enable wild type Myo1a diffusion behavior. Moreover, the neck region plays an essential role in transmitting information between these two domains to promote proper binding activities and dynamics.

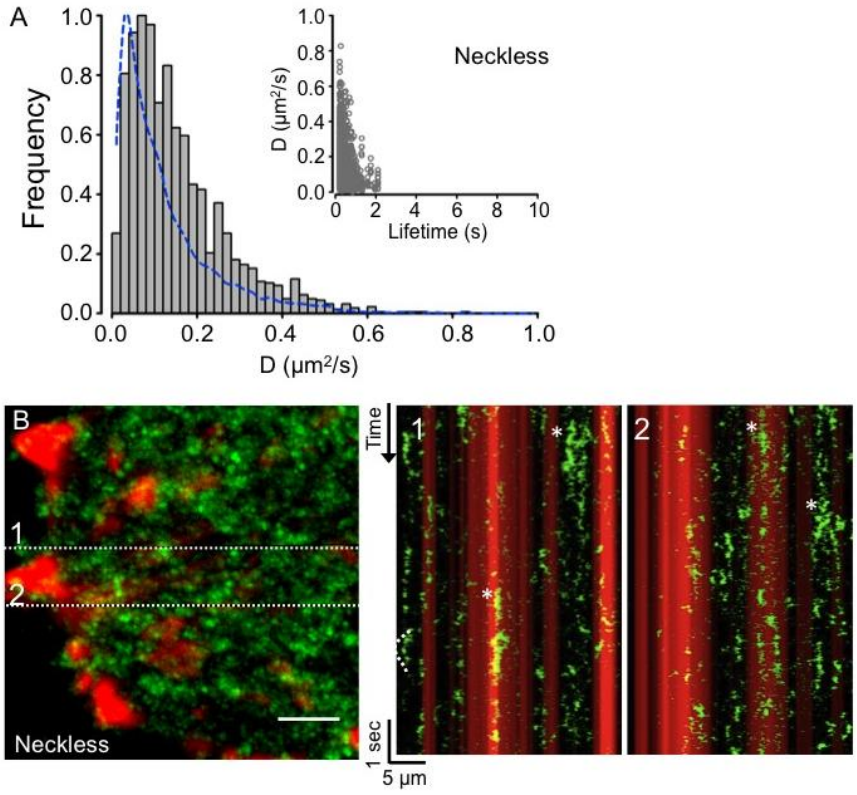

Figure 4-6. The Myo1a neck region is necessary for immobilization. A, Histogram of D values for Myo1a-Neckless. Inset, plot of D versus lifetime associated with each trajectory fit to obtain D values. Inset shows that long-lived events were not detected for this Myo1a-Neckless. The neck deletion resulted in a shift toward high mobility in the overall distribution of D values and a loss of the near-immobile population. Blue dashed lines are traced outlines of Myo1a histogram density. B, Kymograph analysis of Myo1a-Neckless. Kymographs, right, show 3x-Citrine tagged Myo1a-Neckless (green) merged with the mCherry-Espin (red) image from each corresponding cell. Cell images, left, are max projections of image stacks. Dashed lines represent cellular location of the corresponding kymograph. Bars are 5 μm.

Discussion

The studies presented here are the first to investigate the single molecule dynamics of a class I myosin. Previous studies used fluorescence recovery after photobleaching (FRAP) to measure ensemble dynamics for Myo1a and TH1 in the brush border of epithelial cells (Tyska and Mooseker, 2002). However, the analysis of FRAP data is model dependent. Our single molecule analysis allowed us to directly measure physical parameters (D) that are model-independent. Therefore, our analysis provides an unbiased approach to determining how specific sub-domains of Myo1a govern dynamics at the cell membrane.

Analysis of diffusion coefficients revealed that Myo1a displays limited dynamics relative to TH1 and Lact-C2 (Fig. 4-2). Kymograph analysis also revealed that Myo1a molecules co-localize on actin filaments for several seconds (Fig. 4-3 A), and intact motor/actin interactions are required for low mobility (Fig. 4-2 A, red arrowhead). These results were surprising for two reasons: (1) previous studies had established the importance of TH1/membrane interactions in sub-cellular targeting, and (2) solution kinetic measurements have determined that the motor/actin interaction for strongly bound Myo1a is short-lived (~50 ms) (Jontes et al., 1997). Together, our results show that Myo1a motor domain makes an unexpected contribution to overall dynamics.

The intact motor/actin interaction required for normal Myo1a dynamics might have implications for tension sensing. Myo1a produces its working stroke in two steps and might respond to mechanical load by lengthening its actin bound duration (Veigel et al., 1999). Indeed, this is the case for Myo1b, which has similar two-step kinetics and under load can remain bound to actin for ~50 sec (Laakso et al., 2008). Myo1c shares

the ensemble solution kinetic properties of Myo1a and Myo1b, and under load in optical trapping assays Myo1c actin detachment kinetics are slowed and it transitions to a high duty ratio motor (Greenberg et al., 2012). Myo1a has not been tested at the single molecule level *in vitro*; it is unknown how its kinetics would be altered under opposing force. Based on results obtained with other class I myosins in optical trapping assays, we predict that in our SM-TIRF assay, force sensing events would be long-lived, have low mobility, and require intact motor and neck domains. Indeed, we observed long-lived, low D events for Myo1a (Fig. 4-2, red arrowhead and inset; Fig. 4-3) that were lost when mutations were introduced to the motor domain or the neck region was eliminated (Figs. 4-4, 4-5, and 4-6). Although it is intriguing to speculate that Myo1a responds to load, force was not directly applied in this experiment and tension imparted onto the molecules would have to come from a cellular process or from inherent thermal fluctuations.

Our previous single molecule analysis detected increases in the detachment rates for TH1 when NTM and CTM are mutated and indicated that both binding motifs are required for long membrane attachment durations in cells (Mazerik and Tyska, 2012). We therefore expected these mutations to have detrimental effects on Myo1a mobility as well. Myo1a- NTM, Myo1a-CTM, TH1-NTM and TH1-CTM all exhibited lower mobility than their wild type counterparts (Fig. 4-5). These results suggest that lifetime and mobility are uncoupled and low mobility is achievable even during fast collisions with the membrane. One possible explanation for these data is that multiple electrostatic sites (i.e., NTM and CTM) in TH1 keep Myo1a in close proximity to the membrane and facilitate reduced dimensionality diffusion. This could allow TH1 (in the

context of full length Myo1a or as an independent membrane binding protein) to sample multiple binding orientations and remain in close proximity to the membrane while diffusing. Similar mechanisms have been proposed for MCAK, a kinesin motor that uses electrostatic interactions to quickly diffuse along spindle microtubules to achieve plus end localization (Helenius et al., 2006), and DNA binding proteins, which use this mechanism to quickly find their promoter regions and associated binding partners (Gorman and Greene, 2008). Experiments aimed to measure the lifetimes for the full length variants will provide further information about the interplay between lifetime and mobility in controlling overall dynamics for Myo1a.

Together, the data presented here indicate that both the motor/actin interaction and the tail/membrane interaction are necessary for the low mobility diffusion characteristic to Myo1a, and that the neck region coordinates synergistic binding between the motor and TH1 domains. Future experiments will require measuring the dynamics of Myo1b and Myo1c using SM-TIRF. Given that tension sensing is dependent on neck length (Laakso et al., 2010), investigating a Myo1a variant with a long neck will also be informative. Eventually, the force sensing kinetic properties of Myo1a will need to be determined using optical trapping experiments.

CHAPTER V.

THE MYO1A NECK REGION PLAYS A REGULATORY ROLE IN LOCALIZATION

Introduction

All molecular motors, including Myo1a, transduce energy from ATP hydrolysis into mechanical work. To avoid wasting energy, most ATP-consuming processes are regulated in some manner. In some motor proteins, the lever arms regulate activity. Myosins V, VII, X, and II (actin-based motors) undergo a conformational change in the neck region: they are folded when inactive, but when work is required, these molecules extend into active structures (Ikebe, 2008; Sellers and Knight, 2007; Taylor, 2007; Umeki et al., 2011; Umeki et al., 2009; Yang et al., 2009). *In vitro* studies suggest that Myosin V folding is mediated by CaM/Ca^{2+} interactions with the neck region (Krementsov et al., 2004; Li et al., 2006; Trybus, 2008; Wang et al., 2004). Folding of the neck region results in an inactive conformation of Myosin VIIa that is stabilized through an ionic interaction between the tail domain and motor domain (Umeki et al., 2009; Yang et al., 2009). A head-tail interaction also regulates folding for Myosin X; upon lipid (cargo) binding, this inhibition is abolished (Umeki et al., 2011). In Myosin II, light chain/neck region interactions result in a conformational change that inhibits activity by ~1000-fold (Ikebe, 2008; Li et al., 2000; Sellers and Adelstein, 1985). In motors such as Kinesins-1 (KIF5s), microtubule binding is prevented by conformational changes in the neck regions that are stabilized through head-tail interactions (Adio et al., 2006; Hirokawa and Noda, 2008). Together, these studies show that in a variety of molecular motors, the neck region acts as a regulatory domain.

The neck conformations of some myosin motors are altered and thereby regulate molecular function through interactions between Ca^{2+} and CaM light chains. The effects of Ca^{2+} on myosin-1 ATPase and mechanotransduction are well characterized. Generally, Ca^{2+} increases the ATPase activity of these motors while inhibiting their ability to move actin filaments (Collins et al., 1990; Swanljung-Collins and Collins, 1991; Wolenski et al., 1993a). This response, while differential, indicates Ca^{2+} regulates both motor domain dependent activities, ATPase and mechanical movement of filaments. Both effects are thought to be mediated by the dissociation of at least one CaM, as motility is restored by addition of exogenous CaM (Collins et al., 1990; Manceva et al., 2007; Swanljung-Collins and Collins, 1991; Wolenski et al., 1993a; Zhu et al., 1998). While the regulatory effects of Ca^{2+}/CaM on force producing and transducing activities of myosin-1 are well studied *in vitro,* the *in vivo* effects of alterations such as CaM dissociation have not been studied. Specifically, the role of the neck region and the effects of Ca^{2+}/CaM interactions on membrane targeting activity in cells are unknown.

This chapter describes experiments designed to: (1) to determine if the neck region regulates Myo1a targeting activity and (2) identify the molecular mechanism(s) through which regulation is conferred. Our results show Myo1a and TH1 display differential targeting in epithelial cells and in Cos-7 cells. TH1 enrichment is enhanced relative to full-length Myo1a in microvilli and at the plasma membrane, indicating that in the context of the full-length molecule, TH1 membrane binding activity is down-regulated. Full-length Myo1a mutant molecules that lack the entire neck region do not target to microvilli and labeling of EGFP-Myo1a with an antibody targeted towards the motor domain reveals two populations in epithelial cells, one in microvilli that is detected

by the antibody, and one outside microvilli that is not detectable. The position of the epitope suggests that conformational changes to bound CaM or the neck region itself could prevent antibody binding, further implicating this region as a major regulator of microvillar targeting. Size exclusion chromatography reveals a Ca^{2+}-induced change in the Myo1a Stokes radius, suggesting that CaM binding to the neck region may play a regulatory role by altering the shape of the molecule. Together, these data indicate the neck plays an important role in governing Myo1a localization and that Ca^{2+}/CaM interactions may confer this regulation.

Results

Myo1a and TH1 display differential localization

Published studies from our laboratory have established that FL-Myo1a and TH1 demonstrate differential apical membrane targeting abilities (Chapter III, Fig. 3-3) (Mazerik and Tyska, 2012). To further investigate this phenomenon in a simple model system, we co-expressed EGFP-Myo1a and RFP-TH1 in Cos-7 cells. Surprisingly, RFP-TH1 displayed strong enrichment at the membrane, while EGFP-Myo1a localized to membrane ruffles in some cells but was cytosolic compared to RFP-TH1 (Fig. 5-1 A). To ensure RFP-TH1 was not out-competing EGFP-Myo1a for membrane binding sites, we expressed EGFP-Myo1a and EGFP-TH1 separately in Cos-7 cells. Again, EGFP-TH1 was enriched at the membrane, while EGFP-Myo1a localization at the periphery of cells was far less striking (Fig. 5-1, B and C). These results suggest that TH1 domain membrane binding activity may be regulated in the context of the FL- Myo1a molecule.

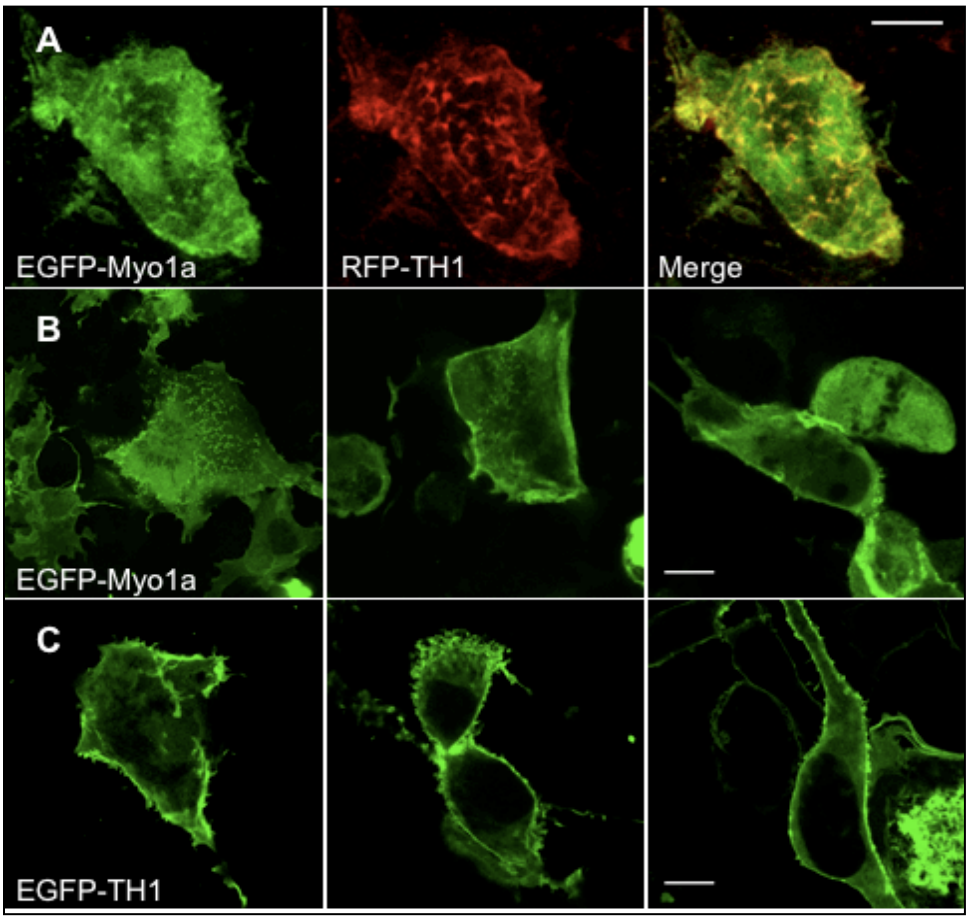

Figure 5-1. TH1 displays enrichment at the plasma membrane in Cos-7 cells.
A, Co-expression of EGFP-Myo1a and RFP-TH1 revealed that Myo1a localizes to some prominent membrane ruffles but has a comparatively high cytosolic distribution, while TH1 displays a more striking localization at the plasma membrane and in apical membrane ruffles. EGFP-Myo1a (B) and EGFP-TH1 (C) display differential localization at the membrane and cell periphery when expressed individually. Bars are 10 μM.

Myo1a neck region is required for proper targeting to microvilli

Because Myo1a and TH1 display clear differential localizations, and because the neck region is a regulatory switch for activity in many other molecular motors (Ikebe, 2008; Krementsov et al., 2004; Li et al., 2008; Sellers and Knight, 2007; Taylor, 2007; Trybus, 2008; Umeki et al., 2009; Wang et al., 2004; Yang et al., 2009), we hypothesized that the neck region might play a role in regulating the tail/membrane

interaction in Myo1a in cells. To test this possibility, we designed a Myo1a construct lacking the neck region. This molecule consists of the entire motor and TH1 domains, but the IQ motifs (residues 694-764) have been removed. We expressed EGFP-tagged "neckless" Myo1a (Myo1a-Neckless) in polarized CL4 cells and strikingly, the mutant did not target to microvilli (Fig. 5-2). In comparison to Myo1a, Myo1a-Neckless appeared soluble and microvillar enrichment was lost (FEM = 0.85 ± 0.13). These data show that the neck region is critical for proper localization in epithelial cells, and further support the idea that it may confer a regulatory effect on Myo1a.

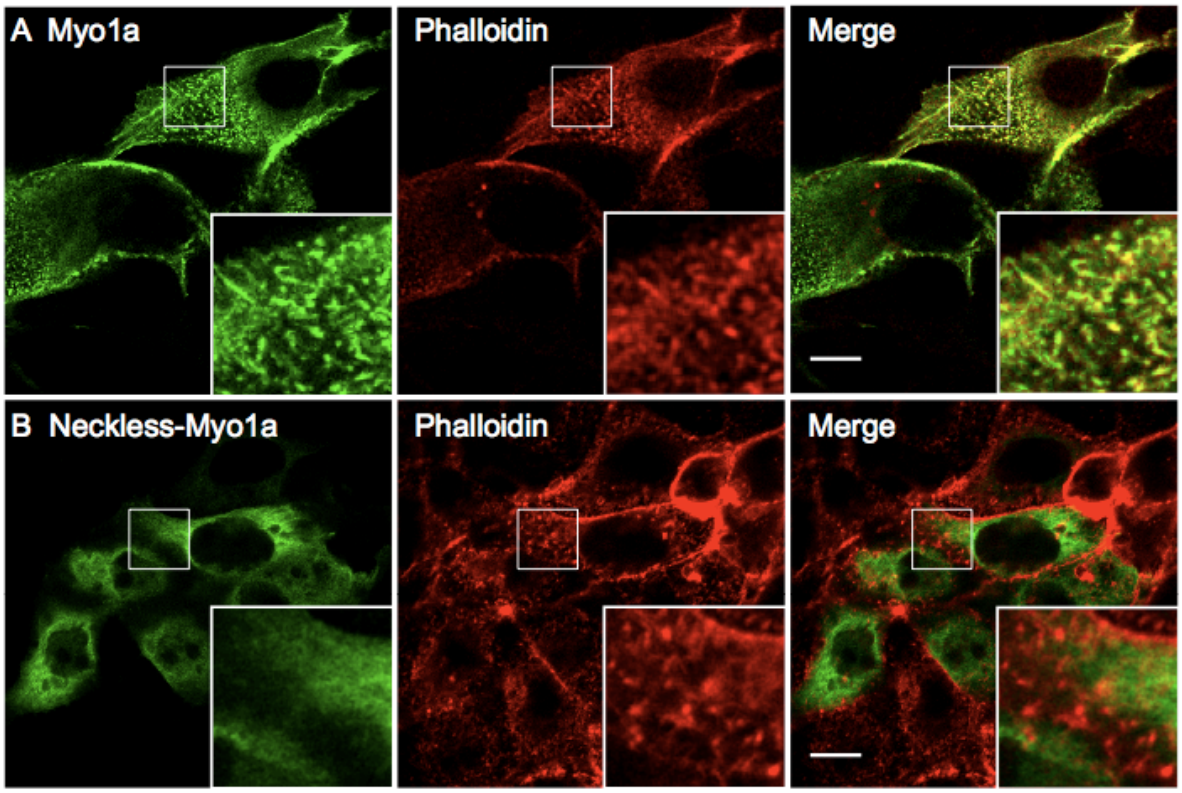

Figure 5-2. Myo1a neck region is critical for microvillar targeting.
EGFP-Myo1a (A) and EGFP-neckless-Myo1a (B) were expressed in CL4 cells, co-labeled with phalloidin-568 to mark F-actin and imaged using confocal microscopy. A, Apical view of EGFP-Myo1a. Punctate localization shows targeting to microvilli; notice co-localization of Myo1a with actin in merge. B, Apical view of EGFP-neckless-Myo1a, which does not target to microvilli; notice lack of punctate colocalization with actin. Bars are 10 μm.

Epithelial cells have two spatially distinct Myo1a populations

As a research tool for studying Myo1a, rabbit polyclonal antibody against the N-terminal amino acid sequence of the motor domain, residues 1-14, was generated. This peptide is located opposite the actin-binding interface on the back of the motor domain. To test the specificity of the antibody (called 4P1) it was applied to CL4 cells expressing EGFP-Myo1a and fluorescently labeled with a 568-conjugated anti-rabbit secondary. The cells were imaged using confocal microscopy.

Surprisingly, although EGFP-Myo1a clearly localized throughout the cell body and at the basolateral membrane, 4P1 only detected the population of EGFP-Myo1a in

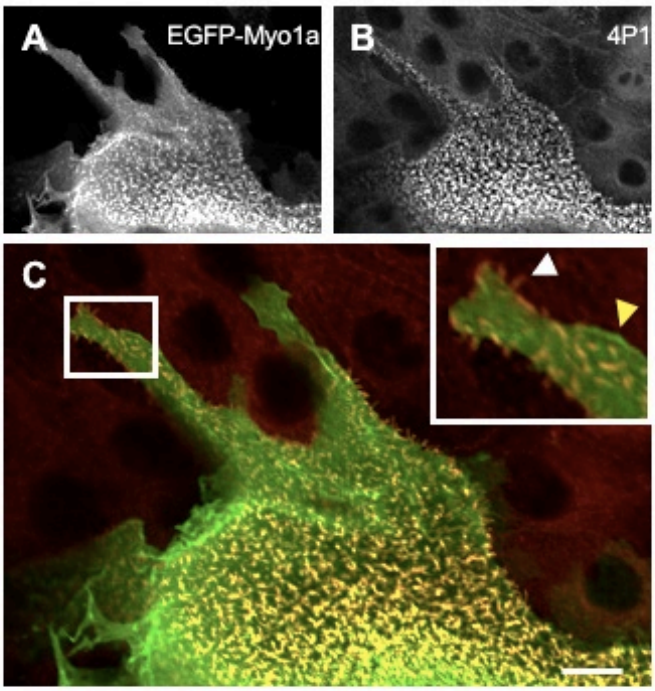

Figure 5-3. Antibody staining reveals two distinct populations of Myo1a in CL4 epithelial cells.
A, EGFP-Myo1a, and B, anti-Myo1a antibody, 4P1, conjugated to Alexa 568. C, Merged EGFP-Myo1a and antibody labeled Myo1a reveals that the antibody only recognizes the population of Myo1a in microvilli (white arrowhead, yellow colocalization), and cannot recognize the cytosolic and basolateral populations of EGFP-Myo1a (yellow arrowhead). Bar is 10 μm.

microvilli (Fig. 5-3). These data suggest that the antibody binding site is masked when Myo1a is outside the microvillar environment, and provide evidence that in cells, Myo1a exists in at least two distinct structural states. An interesting possibility is that molecules in microvilli are properly localized and therefore might represent an active or functional population.

Ca^{2+} alters chromatography properties of Myo1a

IQ motifs in the Myo1a neck region are targets for Ca^{2+}/CaM interactions. These interactions have substantial effects on myosin-I motor function *in vitro* and are essential for regulating the ATPase of other myosin superfamily members. We sought to determine if the Myo1a neck region was a putative regulatory target by testing the effects of Ca^{2+} on the overall size and shape of the molecule. To this end, we purified full length Myo1a, loaded it with exogenous CaM, and subjected the purified protein to size exclusion chromatography in the presence or absence of 1 mM $CaCl_2$. We used a DuoFlow FPLC system (BioRad) to run the protein through the HiLoad 16/60 Superdex 200 prep grade column (GE Healthcare Biosciences). Analysis of column fractions using SDS-PAGE and Coomassie Blue staining revealed that Ca^{2+} increased retention time of Myo1a (Fig. 5-4 A). In the absence of Ca^{2+}, Myo1a Stokes radius was 65Å. When Ca^{2+} was added, the Myo1a Stokes radius was 58Å, indicating either a shift to a more globular conformation or a change in molecular weight, possibly due to a loss of multiple CaM molecules (Fig. 5-4, A and B). These data indicate that interactions between Ca^{2+}/CaM are capable of modulating the size of Myo1a, further suggesting that the neck region may play an important role in regulating this molecule.

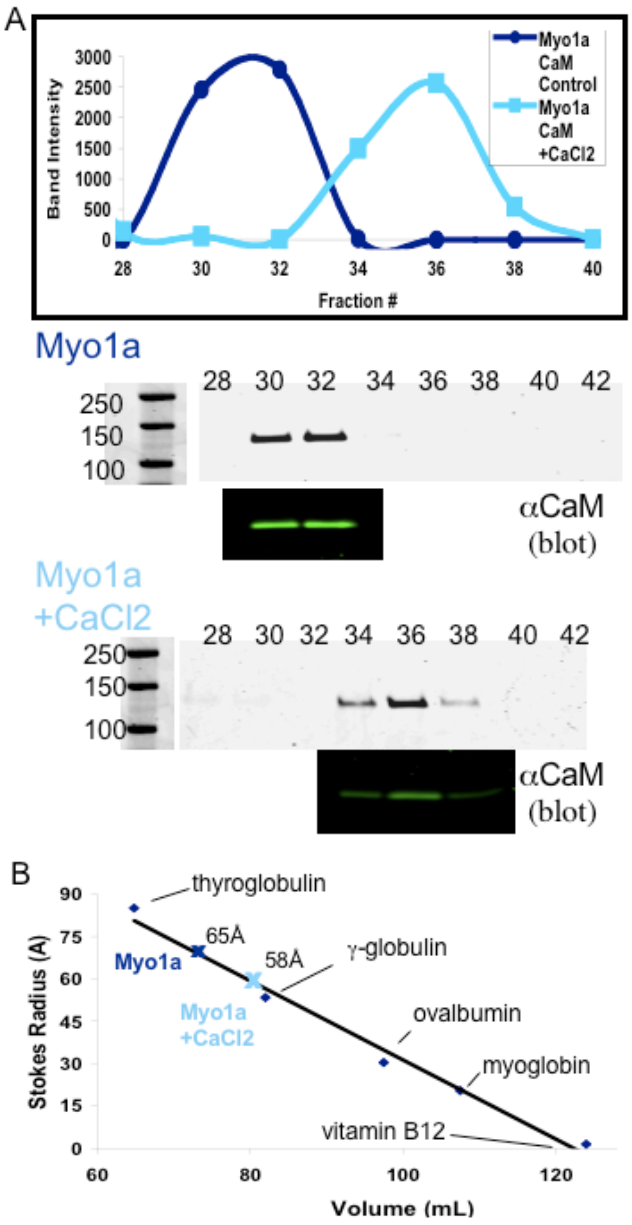

Figure 5-4. Gel filtration reveals a calcium-dependent shift in Myo1a elution.
A, Myo1a was expressed in and purified from SF9 insect cells, loaded with exogenous CaM, and run through a Superdex 200 column in the absence (navy blue) and presence (light blue) of Ca^{2+}. Protein gels of eluted fractions stained with Coomassie Blue revealed Myo1a shifted to higher fractions in the presence of Ca^{2+}. Top panel, Band intensities were analyzed using ImageJ and plotted in Excel. Lower panels, Fractions containing Myo1a were blotted for CaM using an α CaM monoclonal antibody conjugated to α mouse 680 secondary and visualized using an Odyssey imaging system. B, Globular protein standards of known Stokes radii (BioRad) were run on Superdex 200 and gel filtration data were used to calculate Stokes radii of Myo1a populations. These data revealed a change in Myo1a Stokes radius in the presence of Ca^{2+}.

Summary

Since it was identified as a plus-end directed actin-activated ATPase in 1989, most studies on Myo1a have aimed at understanding the motor domain (Mooseker and Coleman, 1989). Recent studies from our lab have focused on the lipid-binding activities and targeting of TH1 to microvilli (Mazerik and Tyska, 2012). However, studies to date have not unified these domain-specific findings to develop a comprehensive view of how the full-length molecule is regulated in cells. Our data suggest that in the context of the full-length molecule, membrane binding is regulated, and the neck region plays an important role in proper localization of Myo1a. TH1 alone has a higher targeting capacity than Myo1a (Fig. 5-1). These data suggest that in the absence of the neck and motor domains, TH1 binds membrane in an unregulated manner, but in full-length Myo1a, membrane binding activity and/or localization is regulated. Myo1a-Neckless does not target microvilli, indicating the neck is essential to facilitate functional membrane targeting (Fig. 5-2).

From these studies it is still unclear why the neck is critical for proper localization. One possibility is that alterations to the normal neck length (~60 amino acids) result in a loss of targeting due to the inability of the shorter molecule to “reach” the exact distance between the membrane and the core actin bundle in microvilli. Alternatively, Ca^{2+}/CaM interactions with the IQ motifs might be required to activate or ‘prime’ the molecule for targeting. In this scenario, CaM may act as an additional adapter by binding to another protein, or saturating CaM may be required to attain certain rigidity necessary to retain Myo1a in microvilli. Alternatively, a lipid modified CaM-like molecule might bind the

neck region in the absence of CaM and facilitate membrane interactions. Further studies are needed to address these possibilities.

The antibody masking experiment suggests that two populations of Myo1a are present in epithelial cells (Fig. 5-3). These data are intriguing, and might suggest that an "active" form of Myo1a is found in microvilli where it is needed for proper physiological functions, while the soluble cytosolic pool may be "inactive" (i.e., not membrane- or actin-bound and not hydrolyzing ATP). Because 4P1 recognizes an epitope on the back of the motor domain, and because our data suggest the neck region is required for targeting, one potential explanation is that the neck region can undergo a Ca^{2+}/CaM- induced conformational change, such that Myo1a in microvilli is open, while the soluble population is folded, causing an intramolecular change to mask the antibody binding site. Alternatively, the molecule could be oligomerizing or binding to another protein at the basolateral membrane, two intermolecular interactions that would also prevent antibody binding. However, the inherent ease with which the neck region responds to CaM/ Ca^{2+} interactions makes regulation through the neck a more attractive model. Indeed, our gel filtration data may support this idea (Fig. 5-4), but it is still unknown whether the size shift we observe in the presence of Ca^{2+} is large enough to represent a conformational change in Myo1a. An alternative possibility is that Myo1a-bound CaM undergoes a conformational change but remains bound to provide regulation. For example, in the presence of Ca^{2+}, CaM becomes extended and might hinder antibody binding. This change in shape to CaM could also cause Myo1a to move through the column at a slightly different rate and thus provide an explanation for the small shift in Stokes' radius observed during gel filtration experiments. Indeed, a caveat

to the gel filtration experiment is that the observed change in size for Myo1a might be an underestimate. Myosins are elongated proteins and might move through the column differently than the available protein standards, which are globular. For example, an elongated myosin molecule might behave like a protein with a Stokes' radius much larger than its molecular weight suggests, while a folded myosin would behave more like a true globular protein. Future studies will need to address whether or not the molecule can actually take on a folded conformation, and if this putative change corresponds to membrane targeting potential.

The data presented here suggest that the neck region plays an important role in Myo1a targeting in cells. Although the specific ways in which the neck controls localization are still unknown, this regulation may be a mechanism to prevent non-productive membrane binding activity. If membrane binding serves as an activator for Myo1a, the regulation conferred through the neck region could prevent unnecessary ATP hydrolysis when the molecule is outside of microvilli.

CHAPTER VI.

FUTURE DIRECTIONS

Exploring the tail/membrane interaction

Our studies revealed that Myo1a interacts with PS in microvilli of pig kidney epithelial cells (Chapter III). However, studies using brush border membranes from pig enterocytes, pig kidney epithelial cells, and mouse enterocytes all estimate that PS makes up <10% of the total membrane lipid (Billington and Nayudu, 1978; Christiansen and Carlsen, 1981; Parkin et al., 2001). Based on the results of our co-sedimentation assays, such a low concentration of PS is unlikely to support a Myo1a interaction with the affinity necessary to retain the motor in the brush border. Therefore, other negatively charged lipid species must contribute to the electrostatic interaction between Myo1a and the membrane. Determining other anionic lipids present in the brush border that could serve as potential targets for Myo1a is an interesting follow-up study. Because many anionic lipid species are rare and often exist only transiently, they are difficult to detect. This might explain why previous studies only reported major lipid species (Billington and Nayudu, 1978; Christiansen and Carlsen, 1981; Parkin et al., 2001). Future studies need to extensively analyze the lipid composition of brush border membranes from rats, mice, and human models (Caco-2_{BBE} cells). Current mass spectrometry techniques using the proper lipid standards will detect negatively charged lipid species, even at low abundances. Phosphatidic acid, phosphatidylglycerol, and phosphoinositide species including $PI(4,5)P_2$ and $PI(3,4,5)P_3$ are potentially present in

microvilli and could increase the negative charge on the inner leaflet to facilitate Myo1a membrane binding.

Determining if polarized lipid distribution exists within microvilli is another experimental avenue worth pursing. Such distinct lipid pools exist in bullfrog stereocilia, the actin-based structures in the inner ear that share structural and proteomic features with microvilli. $PI(4,5)P_2$ is found in the distal half of stereocilia, while PS is distributed along the axes of these structures (Hirono et al., 2004). Although microvilli are much smaller structures and distributions might prove more difficult to detect, lipid labeling in combination with super resolution imaging will determine if similar distributions are present in microvilli.

Experiments aimed to solve the brush border lipidome and determine if lipid distributions along the microvillar axis exist are novel and informative in their own right. Whether or not the lipid composition and distribution within microvilli changes in enterocytes in Myo1a knockout mice is a comparative study that will shed light on the mechanisms underlying Myo1a localization and function in normal brush borders. If lipid sorting exists in the brush border, and if it is a protein-dependent process, we expect Myo1a knockout brush borders to have disordered lipid compartmentalization. Alternatively, lipid species might inherently sort independent of proteins, and might influence differential protein localization.

One differential protein distribution that exists in brush borders is that between Myo1a and Myo1d. Although Myo1a is the most abundant class I myosin in the brush border, multiple others, including Myo1d, Myo1c and Myo1e (albeit at very low levels) are present. While Myo1c has the capacity to redistribute and occupy the brush border

to a greater extent in Myo1a knockout intestinal tissue (Tyska et al., 2005), the two main occupants in normal microvilli are Myo1a and Myo1d (Benesh et al., 2010). It is clear from previous studies that Myo1a is distributed along the microvillar axis (Heintzelman et al., 1994; Skowron and Mooseker, 1999), while Myo1d localizes in two distinct populations at the tips of microvilli and in the terminal web (Benesh et al., 2010). In normal tissue, Myo1a outcompetes Myo1d for binding sites along the microvillar axis in part because Myo1a is more immobile that Myo1d and has a greater affinity for actin in the presence of ATP. In tissue from Myo1a knockout animals, Myo1d redistributes to the position where Myo1a is normally found (Benesh et al., 2010). It is unknown if differential lipid binding or compartmentalization plays a role in properly distributing these two motors in normal tissue. The molecular basis of this differential localization might provide clues to the mechanisms that underlie the physiological consequences of disturbing their distribution (i.e., misregulated vesicle shedding in Myo1a knockout animals (McConnell et al., 2009)).

For instance, lipid compartmentalization and differential binding might determine how these motors distribute in microvilli. In light of our studies showing that Myo1a binds electrostatically to membrane and that its localization is at least partially driven by an interaction with PS (Mazerik and Tyska, 2012), it will be informative to subject Myo1d to a comparative lipid binding analysis. Currently, the mechanism of membrane binding and affinities associated with these interactions are unknown for Myo1d. Interestingly, the Myo1d tail contains the conserved Myo1PH region and an additional basic residue that is found in the beta 3 loop and shared only with Myo1g, a motor that requires an intact PH domain for targeting (Hokanson et al., 2006; Patino-Lopez et al., 2010).

However, the role of the Myo1PH or this basic residue in membrane localization for Myo1d remains unknown.

In our investigation of how Myo1a targets to the brush border, we took a protein-centric approach by identifying multiple regions in TH1 required for targeting, and tested a limited number of lipid species for interactions with Myo1a (Mazerik and Tyska, 2012). A more rigorous lipid binding analysis on Myo1a will also provide useful information. Our unpublished results using PIP strips revealed that Myo1a might have a strong preference for PA. *In vitro* liposome binding studies using Myo1c and Myo1e showed that including physiologically relevant lipid mixes enhance the liposome-bound lifetimes of these molecules (McKenna and Ostap, 2009). Given the inherent cholesterol-rich environment of the brush border, similar experiments will determine if including cholesterol or other raft lipids such as sphingomyelin in liposomes affects Myo1a or Myo1d membrane interactions. By defining the lipid species that are necessary for Myo1d to bind membrane, and comparing these to a full set of lipids to which Myo1a binds, we will learn more about the roles of and relationship between these two class I myosins in the brush border. For example, if lipid distribution studies show that $PI(4,5)P_2$ is found at the tips of microvilli, and Myo1d binds preferentially to this lipid, these results might help explain how Myo1a and Myo1d sort within this structure.

Curvature sensing is another alternative mechanism that might contribute to differential protein localization along the microvillar axis. Experiments to determine if Myo1a or Myo1d can sense curvature are also interesting, especially considering the highly curved geometry of microvilli and the specific compartmentalization of Myo1d at the concave tips. Expanding our studies to include lipid binding analysis and curvature

sensing analysis of Myo1d will enhance our overall understanding of how these proteins distribute in relation to each other in microvilli.

The motor/actin interaction: A reinvigoration

Vertebrate class I myosins are low duty ratio motors and spend only a short duration during their ATPase cycles strongly bound to actin (De La Cruz and Ostap, 2004). Although in some cases the motor domain enhances localization, this domain alone is not sufficient for targeting, and most class I myosins are dependent on their tail domains for proper localization in cells (Benesh et al., 2010; Olety et al., 2010; Patino-Lopez et al., 2010; Tang and Ostap, 2001; Tyska and Mooseker, 2002). Therefore, in hopes of learning more about *in vivo* functional properties of these motors, some recent studies have focused on the tail domains of class I myosins. Interestingly, single molecule TIRF analysis of full-length Myo1a molecules in cells revealed two intriguing findings (Chapter IV). First, Myo1a can immobilize itself at the membrane/cytoskeletal interface for several seconds at a time. Second, the motor/actin interaction dominates these unique local dynamics. These findings suggest that motor domain plays a more significant role than we originally suspected in regulating the dynamics of this myosin.

In vitro experiments using optical trapping assays revealed that class I myosins have the ability to sense tension and transition to high duty ratio motors under applied forces (Greenberg et al., 2012; Laakso et al., 2008). Early biochemical studies of Myo1a indicated that this motor produces its working stroke in two steps; this led researchers to hypothesize that Myo1a might also have altered kinetics when a load is applied (Veigel et al., 1999). If Myo1a can transition to a high duty ratio state in a manner similar to Myo1b (large increases to the duration to the strongly bound state), it is possible that

the motor-dependent immobilization observed in our TIRF assay represent tension sensing. Manipulating the Myo1a neck region and then using TIRF to assay for these events will help determine if they represent molecules under load. The tension properties of Myo1b are dependent on neck length; load dependent actin attached durations decrease with decrease in neck length (Laakso et al., 2010). Indeed, Myo1a-Neckless appears to diffuse more freely than wild type Myo1a and does not exhibit long-lived events (Chapter IV). It will therefore be informative to complete this data set and also test the effects of shortening or lengthening the Myo1a neck. A chimeric Myo1a molecule with the Myo1b neck region also needs to be tested; this alteration is expected to drive a larger population of these molecules into an immobile, strongly bound state because the Myo1b neck is nearly double the length of the Myo1a neck (3 versus 6 IQ motifs).

Although Myo1a has biochemical properties that are amenable to force sensing, this feature has not been directly tested. Because Myo1b and Myo1c share similar solution kinetics yet behave much differently under load, further investigations will require directly testing the kinetics of Myo1a under load using optical trapping assays to determine if it behaves more similarly to Myo1b or Myo1c, or completely differently than both. These *in vitro* experiments will ultimately complement our single molecule findings in cells. Along these lines, performing single molecule TIRF experiments using *in vitro* reconstitution will also be informative. The dynamics for purified Myo1a or mutant Myo1a molecules on actin bundles and supported lipid bilayers need to be measured. This simplified system will allow us the flexibility to change the lipid composition and determine how different lipid species, such as cholesterol, affect the

dynamics of Myo1a. These experiments will provide insight as to how this molecule might function in cells as a dynamic cross linker at the actin/membrane interface.

A major future goal is to use single molecule TIRF imaging to compare the dynamics of Myo1a to those of the other class I myosins. Comparison with Myo1b and Myo1c are at the top of the list, as these two proteins have been well characterized at the single molecule level *in vitro* using optical trapping experiments. Comprehensive class-wide studies will give the field a broad view of how each myosin's *in vitro* biochemical properties relate to its dynamic behavior in cells. These studies will provide insight as to how differential properties of all the myosins-I might influence their various independent *in vivo* functions.

The neck region links it back together

Preliminary observations suggest that in the full-length Myo1a molecule, TH1 membrane targeting is regulated (Chapter V). Our data and other published studies on myosin motors suggest that regulation is conferred through the neck region (Collins and Matsudaira, 1991; Collins et al., 1990; Gillespie and Cyr, 2002; Manceva et al., 2007; Swanljung-Collins and Collins, 1991; Wolenski et al., 1993a). One possibility for Myo1a is that the length of the neck region might maintain the optimal distance between the motor domain and TH1 to enable efficient and simultaneous actin and membrane binding within the microvillus. To determine if Myo1a targeting depends solely on neck length, independent of CaM interactions, the IQ motifs can be replaced with a stable single a-helix (SAH). This is an α-helical domain that is present in myosins VI, VII, and X, is stabilized through intrahelical bonds, and does not bind light chains (Baboolal et al., 2009; Knight et al., 2005). The SAH consists of repeats of highly charged sequence

(alternating glutamic acid residues and basic residues). Replacing Myo1a IQ motifs with varying numbers of SAH repeats to obtain varying Myo1a neck lengths and assaying for targeting to microvilli will determine the importance of neck length for targeting.

Myo1a is the most abundant CaM binding protein in the brush border. CaM functions to buffer Ca^{2+} levels, which fluctuate significantly in the gut during cycles of feeding and fasting (Bronner, 2003, 2009). In the presence of Ca^{2+}, CaM dissociates from and exposes the α-helical neck region of Myo1a (Jontes and Milligan, 1997c). The neck is required for proper microvillar targeting, therefore a second possibility is that functional interactions between CaM and IQ motifs in the neck may be critical for regulating this process (Collins et al., 1990; Coluccio and Bretscher, 1987; Swanljung-Collins and Collins, 1991). Mutating residues known to be critical for IQ/CaM interactions (Li and Sacks, 2003) or systematically deleting each IQ motif alone or in combination will disrupt CaM binding to individual IQ motifs. Using this approach will allow direct assessment of how each IQ motif contributes to microvillar targeting.

A conformational change in the Myo1a neck region might modulate a folding event; this represents a third possible mechanism by which the neck might control targeting and activity. The ability of Myo1a to undergo a conformational change could explain many of the results discussed in Chapter V. This regulatory mechanism would require proper neck length and regulation by Ca^{2+}/CaM interactions, and therefore this hypothesis also provides a unifying model for our data and the other two possible mechanisms proposed within this chapter. Subjecting purified Myo1a or mutant Myo1a molecules discussed above to negative stain electron microscopy in the presence and absence of Ca^{2+} will determine if Myo1a undergoes a conformational change. With

rigorous averaging and molecular modeling, this method will allow us to visualize the protein and detect different conformations under various conditions, if they exist.

We expect that Myo1a targeting to microvilli will require three fully functional IQ motifs. Even if the molecule does not undergo a large regulatory conformational change, full occupancy of these motifs by CaM would enable maximum extension of the a-helical neck region (Jontes and Milligan, 1997c). If Myo1a-SAH does not target and full CaM occupancy is not necessary for targeting, this would suggest that the neck region plays a role beyond separating the motor and tail domains by the appropriate distance. For example, one or more of the IQ motifs may bind to a 'receptor' on the microvillar membrane. A similar idea has been proposed for Myo1c (Cyr et al., 2002). Pull-down assays from cells expressing EGFP-Myo1a or EGFP-neckless-Myo1a could test this idea by using shotgun mass spectrometry to identify binding partners in the presence and absence of the neck region. Any putative interactions could be further confirmed using immunoprecipitation assays.

Overall, these future studies will provide insight as to how Myo1a finds its unique place in microvilli among other proteins present in these small structures, how tension sensing may play a role in retaining Myo1a at the membrane/ cytoskeletal interface, and whether Myo1a targeting to microvilli is regulated intramolecularly. Future studies should also comparatively investigate the properties and behaviors of other class I myosins, as this will aid in our understanding of how these motors achieve differential functions *in vivo*.

CHAPTER VII.

CONCLUDING REMARKS

The results presented in this thesis provide several novel insight regarding the mechanistic behavior of Myo1a. Our first new discovery is that unlike most other class I myosins, Myo1a does not depend on the Myo1-PH to target membrane (Chapter III). This finding underscores the importance of the diversity of the tail domains of these motors. The differences in membrane binding mechanisms between myosins-I might help explain their differential localizations and functions in cells.

These studies also revealed a paradigm-shifting discovery: the Myo1a motor domain contributes significantly to overall dynamics of the molecule in cells (Chapter IV). Single particle tracking and means squared displacement analysis of strategic structural mutants allowed us to propose a model that unifies our findings with published properties of the tail domain. In this model, TH1 is required for global localization to the membrane, and once in place, the motor domain takes over and restricts local diffusion through interactions with the actin cytoskeleton. Together, the motor and tail synergistically regulate Myo1a dynamics.

A final unique aspect of these new experiments is that we investigated biophysical and biochemical findings using cell based assays. This approach taught us more about how the properties of this Myo1a are influenced by a complex cellular system. An important avenue for future studies is to focus on how the mechanistic properties described here relate to the motor's functional roles in vesicle shedding and tension regulation in intestinal brush borders.

REFERENCES

Adamek, N., Coluccio, L.M., Geeves, M.A., 2008. Calcium sensitivity of the cross-bridge cycle of Myo1c, the adaptation motor in the inner ear. Proceedings of the National Academy of Sciences of the United States of America 105, 5710-5715.

Adams, R.J., Pollard, T.D., 1989. Binding of myosin I to membrane lipids. Nature 340, 565-568.

Adio, S., Reth, J., Bathe, F., Woehlke, G., 2006. Review: regulation mechanisms of Kinesin-1. J Muscle Res Cell Motil 27, 153-160.

Albanesi, J.P., Coue, M., Fujisaki, H., Korn, E.D., 1985a. Effect of actin filament length and filament number concentration on the actin-activated ATPase activity of Acanthamoeba myosin I. The Journal of biological chemistry 260, 13276-13280.

Albanesi, J.P., Fujisaki, H., Korn, E.D., 1985b. A kinetic model for the molecular basis of the contractile activity of Acanthamoeba myosins IA and IB. The Journal of biological chemistry 260, 11174-11179.

Albanesi, J.P., Hammer, J.A., 3rd, Korn, E.D., 1983. The interaction of F-actin with phosphorylated and unphosphorylated myosins IA and IB from Acanthamoeba castellanii. The Journal of biological chemistry 258, 10176-10181.

Almeida, C.G., Yamada, A., Tenza, D., Louvard, D., Raposo, G., Coudrier, E., 2011. Myosin 1b promotes the formation of post-Golgi carriers by regulating actin assembly and membrane remodelling at the trans-Golgi network. Nature cell biology 13, 779-789.

Baboolal, T.G., Sakamoto, T., Forgacs, E., White, H.D., Jackson, S.M., Takagi, Y., Farrow, R.E., Molloy, J.E., Knight, P.J., Sellers, J.R., Peckham, M., 2009. The SAH

domain extends the functional length of the myosin lever. Proc Natl Acad Sci U S A 106, 22193-22198.

Bagshaw, C.R., Eccleston, J.F., Eckstein, F., Goody, R.S., Gutfreund, H., Trentham, D.R., 1974. The magnesium ion-dependent adenosine triphosphatase of myosin. Two-step processes of adenosine triphosphate association and adenosine diphosphate dissociation. The Biochemical journal 141, 351-364.

Bahler, M., Kroschewski, R., Stoffler, H.E., Behrmann, T., 1994. Rat myr 4 defines a novel subclass of myosin I: identification, distribution, localization, and mapping of calmodulin-binding sites with differential calcium sensitivity. J Cell Biol 126, 375-389.

Balla, T., Varnai, P., 2009. Visualization of cellular phosphoinositide pools with GFP-fused protein-domains. Curr Protoc Cell Biol Chapter 24, Unit 24 24.

Bates, J.M., Akerlund, J., Mittge, E., Guillemin, K., 2007. Intestinal alkaline phosphatase detoxifies lipopolysaccharide and prevents inflammation in zebrafish in response to the gut microbiota. Cell host & microbe 2, 371-382.

Batters, C., Arthur, C.P., Lin, A., Porter, J., Geeves, M.A., Milligan, R.A., Molloy, J.E., Coluccio, L.M., 2004. Myo1c is designed for the adaptation response in the inner ear. EMBO J 23, 1433-1440.

Bement, W.M., Mooseker, M.S., 1995. TEDS rule: a molecular rationale for differential regulation of myosins by phosphorylation of the heavy chain head. Cell motility and the cytoskeleton 31, 87-92.

Benesh, A.E., Fleming, J.T., Chiang, C., Carter, B.D., Tyska, M.J., 2012. Expression and localization of myosin-1d in the developing nervous system. Brain research 1440, 9-22.

Benesh, A.E., Nambiar, R., McConnell, R.E., Mao, S., Tabb, D.L., Tyska, M.J., 2010. Differential localization and dynamics of class I myosins in the enterocyte microvillus. Mol Biol Cell 21, 970-978.

Billington, T., Nayudu, P.R., 1978. Studies on the brush border membrane on mouse duodenum: lipids. The Australian journal of experimental biology and medical science 56, 25-29.

Boguslavsky, S., Chiu, T., Foley, K.P., Osorio-Fuentealba, C., Antonescu, C.N., Bayer, K.U., Bilan, P.J., Klip, A., 2012. Myo1c binding to submembrane actin mediates insulin-induced tethering of GLUT4 vesicles. Mol Biol Cell 23, 4065-4078.

Bose, A., Guilherme, A., Robida, S.I., Nicoloro, S.M., Zhou, Q.L., Jiang, Z.Y., Pomerleau, D.P., Czech, M.P., 2002. Glucose transporter recycling in response to insulin is facilitated by myosin Myo1c. Nature 420, 821-824.

Bose, A., Robida, S., Furcinitti, P.S., Chawla, A., Fogarty, K., Corvera, S., Czech, M.P., 2004. Unconventional myosin Myo1c promotes membrane fusion in a regulated exocytic pathway. Mol Cell Biol 24, 5447-5458.

Bronner, F., 2003. Mechanisms and functional aspects of intestinal calcium absorption. J Exp Zool A Comp Exp Biol 300, 47-52.

Bronner, F., 2009. Recent developments in intestinal calcium absorption. Nutr Rev 67, 109-113.

Brzeska, H., Guag, J., Preston, G.M., Titus, M.A., Korn, E.D., 2012. Molecular basis of dynamic relocalization of Dictyostelium myosin IB. J Biol Chem 287, 14923-14936.

Brzeska, H., Guag, J., Remmert, K., Chacko, S., Korn, E.D., 2010. An experimentally based computer search identifies unstructured membrane-binding sites in proteins:

application to class I myosins, PAKS, and CARMIL. The Journal of biological chemistry 285, 5738-5747.

Brzeska, H., Hwang, K.J., Korn, E.D., 2008. Acanthamoeba myosin IC colocalizes with phosphatidylinositol 4,5-bisphosphate at the plasma membrane due to the high concentration of negative charge. The Journal of biological chemistry 283, 32014-32023.

Cai, D., McEwen, D.P., Martens, J.R., Meyhofer, E., Verhey, K.J., 2009. Single molecule imaging reveals differences in microtubule track selection between Kinesin motors. PLoS Biol 7, e1000216.

Cai, D., Verhey, K.J., Meyhofer, E., 2007. Tracking single Kinesin molecules in the cytoplasm of mammalian cells. Biophys J 92, 4137-4144.

Chase, S.E., Encina, C.V., Stolzenburg, L.R., Tatum, A.H., Holzman, L.B., Krendel, M., 2012. Podocyte-specific knockout of myosin 1e disrupts glomerular filtration. American journal of physiology. Renal physiology 303, F1099-1106.

Chen, C.L., Wang, Y., Sesaki, H., Iijima, M., 2012. Myosin I links PIP3 signaling to remodeling of the actin cytoskeleton in chemotaxis. Science signaling 5, ra10.

Chen, X.W., Leto, D., Chiang, S.H., Wang, Q., Saltiel, A.R., 2007. Activation of RalA is required for insulin-stimulated Glut4 trafficking to the plasma membrane via the exocyst and the motor protein Myo1c. Developmental cell 13, 391-404.

Cheng, J., Grassart, A., Drubin, D.G., 2012. Myosin 1E coordinates actin assembly and cargo trafficking during clathrin-mediated endocytosis. Mol Biol Cell 23, 2891-2904.

Christiansen, K., Carlsen, J., 1981. Microvillus membrane vesicles from pig small intestine. Purity and lipid composition. Biochimica et biophysica acta 647, 188-195.

Chuang, C.H., Carpenter, A.E., Fuchsova, B., Johnson, T., de Lanerolle, P., Belmont, A.S., 2006. Long-range directional movement of an interphase chromosome site. Curr Biol 16, 825-831.

Collins, J.H., Borysenko, C.W., 1984. The 110,000-dalton actin- and calmodulin-binding protein from intestinal brush border is a myosin-like ATPase. The Journal of biological chemistry 259, 14128-14135.

Collins, K., Matsudaira, P., 1991. Differential regulation of vertebrate myosins I and II. 14:11-6, 11-16.

Collins, K., Sellers, J.R., Matsudaira, P., 1990. Calmodulin dissociation regulates brush border myosin I (110-kD- calmodulin) mechanochemical activity in vitro. J Cell Biol 110, 1137-1147.

Coluccio, L.M., 2008. Myosin I. Springer.

Coluccio, L.M., Bretscher, A., 1987. Calcium-regulated cooperative binding of the microvillar 110K-calmodulin complex to F-actin: formation of decorated filaments. J Cell Biol 105, 325-333.

Conzelman, K.A., Mooseker, M.S., 1987. The 110-kD protein-calmodulin complex of the intestinal microvillus is an actin-activated MgATPase. The Journal of cell biology 105, 313-324.

Coudrier, E., Almeida, C.G., 2011. Myosin 1 controls membrane shape by coupling F-Actin to membrane. Bioarchitecture 1, 230-235.

Crothers, D.M., Metzger, H., 1972. The influence of polyvalency on the binding properties of antibodies. Immunochemistry 9, 341-357.

Cyr, J.L., Dumont, R.A., Gillespie, P.G., 2002. Myosin-1c interacts with hair-cell receptors through its calmodulin-binding IQ domains. J Neurosci 22, 2487-2495.

Czech, M.P., Corvera, S., 1999. Signaling mechanisms that regulate glucose transport. J Biol Chem 274, 1865-1868.

Dai, J., Sheetz, M.P., 1995. Regulation of endocytosis, exocytosis, and shape by membrane tension. Cold Spring Harbor symposia on quantitative biology 60, 567-571.

Dai, J., Ting-Beall, H.P., Hochmuth, R.M., Sheetz, M.P., Titus, M.A., 1999. Myosin I contributes to the generation of resting cortical tension. Biophys J 77, 1168-1176.

De La Cruz, E.M., Ostap, E.M., 2004. Relating biochemistry and function in the myosin superfamily. Curr Opin Cell Biol 16, 61-67.

De La Cruz, E.M., Ostap, E.M., 2009. Kinetic and equilibrium analysis of the myosin ATPase. Methods Enzymol 455, 157-192.

Donaudy, F., Ferrara, A., Esposito, L., Hertzano, R., Ben-David, O., Bell, R.E., Melchionda, S., Zelante, L., Avraham, K.B., Gasparini, P., 2003. Multiple mutations of MYO1A, a cochlear-expressed gene, in sensorineural hearing loss. American journal of human genetics 72, 1571-1577.

Dzijak, R., Yildirim, S., Kahle, M., Novak, P., Hnilicova, J., Venit, T., Hozak, P., 2012. Specific nuclear localizing sequence directs two myosin isoforms to the cell nucleus in calmodulin-sensitive manner. PloS one 7, e30529.

Fairn, G.D., Hermansson, M., Somerharju, P., Grinstein, S., 2011a. Phosphatidylserine is polarized and required for proper Cdc42 localization and for development of cell polarity. Nat Cell Biol 13, 1424-1430.

Fairn, G.D., Schieber, N.L., Ariotti, N., Murphy, S., Kuerschner, L., Webb, R.I., Grinstein, S., Parton, R.G., 2011b. High-resolution mapping reveals topologically distinct cellular pools of phosphatidylserine. The Journal of cell biology 194, 257-275.

Fan, Y., Eswarappa, S.M., Hitomi, M., Fox, P.L., 2012. Myo1c facilitates G-actin transport to the leading edge of migrating endothelial cells. J Cell Biol 198, 47-55.

Feeser, E.A., Ignacio, C.M., Krendel, M., Ostap, E.M., 2010. Myo1e binds anionic phospholipids with high affinity. Biochemistry 49, 9353-9360.

Ferguson, K.M., Lemmon, M.A., Schlessinger, J., Sigler, P.B., 1995. Structure of the high affinity complex of inositol trisphosphate with a phospholipase C pleckstrin homology domain. Cell 83, 1037-1046.

Frost, A., Perera, R., Roux, A., Spasov, K., Destaing, O., Egelman, E.H., De Camilli, P., Unger, V.M., 2008. Structural basis of membrane invagination by F-BAR domains. Cell 132, 807-817.

Fujisaki, H., Albanesi, J.P., Korn, E.D., 1985. Experimental evidence for the contractile activities of Acanthamoeba myosins IA and IB. The Journal of biological chemistry 260, 11183-11189.

Geisterfer-Lowrance, A.A., Kass, S., Tanigawa, G., Vosberg, H.P., McKenna, W., Seidman, C.E., Seidman, J.G., 1990. A molecular basis for familial hypertrophic cardiomyopathy: a beta cardiac myosin heavy chain gene missense mutation. Cell 62, 999-1006.

Gillespie, P.G., Cyr, J.L., 2002. Calmodulin binding to recombinant myosin-1c and myosin-1c IQ peptides. BMC Biochem 3, 31.

Gillespie, P.G., Cyr, J.L., 2004. Myosin-1c, the hair cell's adaptation motor. Annu Rev Physiol 66, 521-545.

Gillespie, P.G., Muller, U., 2009. Mechanotransduction by hair cells: models, molecules, and mechanisms. Cell 139, 33-44.

Gorelik, R., Yang, C., Kameswaran, V., Dominguez, R., Svitkina, T., 2011. Mechanisms of plasma membrane targeting of formin mDia2 through its amino terminal domains. Mol Biol Cell 22, 189-201.

Gorman, J., Greene, E.C., 2008. Visualizing one-dimensional diffusion of proteins along DNA. Nature structural & molecular biology 15, 768-774.

Greenberg, M.J., Lin, T., Goldman, Y.E., Shuman, H., Ostap, E.M., 2012. Myosin IC generates power over a range of loads via a new tension-sensing mechanism. Proceedings of the National Academy of Sciences of the United States of America 109, E2433-2440.

Greenberg, M.J., Ostap, E.M., 2013. Regulation and control of myosin-I by the motor and light chain-binding domains. Trends in cell biology 23, 81-89.

Grosshans, B.L., Grotsch, H., Mukhopadhyay, D., Fernandez, I.M., Pfannstiel, J., Idrissi, F.Z., Lechner, J., Riezman, H., Geli, M.I., 2006. TEDS site phosphorylation of the yeast myosins I is required for ligand-induced but not for constitutive endocytosis of the G protein-coupled receptor Ste2p. J Biol Chem 281, 11104-11114.

Hayden, S.M., Wolenski, J.S., Mooseker, M.S., 1990. Binding of brush border myosin I to phospholipid vesicles. The Journal of cell biology 111, 443-451.

Heintzelman, M.B., Hasson, T., Mooseker, M.S., 1994. Multiple unconventional myosin domains of the intestinal brush border cytoskeleton. Journal of cell science 107 (Pt 12), 3535-3543.

Helenius, J., Brouhard, G., Kalaidzidis, Y., Diez, S., Howard, J., 2006. The depolymerizing kinesin MCAK uses lattice diffusion to rapidly target microtubule ends. Nature 441, 115-119.

Hirokawa, N., Noda, Y., 2008. Intracellular transport and kinesin superfamily proteins, KIFs: structure, function, and dynamics. Physiol Rev 88, 1089-1118.

Hirono, M., Denis, C.S., Richardson, G.P., Gillespie, P.G., 2004. Hair cells require phosphatidylinositol 4,5-bisphosphate for mechanical transduction and adaptation. Neuron 44, 309-320.

Hokanson, D.E., Laakso, J.M., Lin, T., Sept, D., Ostap, E.M., 2006. Myo1c binds phosphoinositides through a putative pleckstrin homology domain. Mol Biol Cell 17, 4856-4865.

Hokanson, D.E., Ostap, E.M., 2006. Myo1c binds tightly and specifically to phosphatidylinositol 4,5-bisphosphate and inositol 1,4,5-trisphosphate. Proceedings of the National Academy of Sciences of the United States of America 103, 3118-3123.

Holt, J.R., Gillespie, S.K., Provance, D.W., Shah, K., Shokat, K.M., Corey, D.P., Mercer, J.A., Gillespie, P.G., 2002. A chemical-genetic strategy implicates myosin-1c in adaptation by hair cells. Cell 108, 371-381.

Houdusse, A., Cohen, C., 1995. Target sequence recognition by the calmodulin superfamily: implications from light chain binding to the regulatory domain of scallop

myosin. Proceedings of the National Academy of Sciences of the United States of America 92, 10644-10647.

Hozumi, S., Maeda, R., Taniguchi, K., Kanai, M., Shirakabe, S., Sasamura, T., Speder, P., Noselli, S., Aigaki, T., Murakami, R., Matsuno, K., 2006. An unconventional myosin in Drosophila reverses the default handedness in visceral organs. Nature 440, 798-802.

Hozumi, S., Maeda, R., Taniguchi-Kanai, M., Okumura, T., Taniguchi, K., Kawakatsu, Y., Nakazawa, N., Hatori, R., Matsuno, K., 2008. Head region of unconventional myosin I family members is responsible for the organ-specificity of their roles in left-right polarity in Drosophila. Developmental dynamics : an official publication of the American Association of Anatomists 237, 3528-3537.

Huber, L.A., Fialka, I., Paiha, K., Hunziker, W., Sacks, D.B., Bahler, M., Way, M., Gagescu, R., Gruenberg, J., 2000. Both calmodulin and the unconventional myosin Myr4 regulate membrane trafficking along the recycling pathway of MDCK cells. Traffic 1, 494-503.

Hudspeth, A.J., 2005. How the ear's works work: mechanoelectrical transduction and amplification by hair cells. Comptes rendus biologies 328, 155-162.

Hwang, K.J., Mahmoodian, F., Ferretti, J.A., Korn, E.D., Gruschus, J.M., 2007. Intramolecular interaction in the tail of Acanthamoeba myosin IC between the SH3 domain and a putative pleckstrin homology domain. Proc Natl Acad Sci U S A 104, 784-789.

Ihnatovych, I., Migocka-Patrzalek, M., Dukh, M., Hofmann, W.A., 2012. Identification and characterization of a novel myosin Ic isoform that localizes to the nucleus. Cytoskeleton (Hoboken) 69, 555-565.

Ikebe, M., 2008. Regulation of the function of mammalian myosin and its conformational change. Biochem Biophys Res Commun 369, 157-164.

Ishikawa, T., Cheng, N., Liu, X., Korn, E.D., Steven, A.C., 2004. Subdomain organization of the Acanthamoeba myosin IC tail from cryo-electron microscopy. Proc Natl Acad Sci U S A 101, 12189-12194.

Johnson, K.A., Taylor, E.W., 1978. Intermediate states of subfragment 1 and actosubfragment 1 ATPase: reevaluation of the mechanism. Biochemistry 17, 3432-3442.

Jontes, J.D., Milligan, R.A., 1997a. Brush border myosin-I structure and ADP-dependent conformational changes revealed by cryoelectron microscopy and image analysis. The Journal of cell biology 139, 683-693.

Jontes, J.D., Milligan, R.A., 1997b. Three-dimensional structure of Brush Border Myosin-I at approximately 20 A resolution by electron microscopy and image analysis. Journal of molecular biology 266, 331-342.

Jontes, J.D., Milligan, R.A., 1997c. Three-dimensional structure of Brush Border Myosin-I at approximately 20 A resolution by electron microscopy and image analysis. 266, 331-342.

Jontes, J.D., Milligan, R.A., Pollard, T.D., Ostap, E.M., 1997. Kinetic characterization of brush border myosin-I ATPase. Proceedings of the National Academy of Sciences of the United States of America 94, 14332-14337.

Jontes, J.D., Ostap, E.M., Pollard, T.D., Milligan, R.A., 1998. Three-dimensional structure of Acanthamoeba castellanii myosin-IB (MIB) determined by cryoelectron microscopy of decorated actin filaments. The Journal of cell biology 141, 155-162.

Jontes, J.D., Wilson-Kubalek, E.M., Milligan, R.A., 1995. A 32 degree tail swing in brush border myosin I on ADP release. Nature 378, 751-753.

Jung, G., Remmert, K., Wu, X., Volosky, J.M., Hammer, J.A., 3rd, 2001. The Dictyostelium CARMIL protein links capping protein and the Arp2/3 complex to type I myosins through their SH3 domains. J Cell Biol 153, 1479-1497.

Jung, G., Wu, X., Hammer, J.A., 3rd, 1996. Dictyostelium mutants lacking multiple classic myosin I isoforms reveal combinations of shared and distinct functions. J Cell Biol 133, 305-323.

Kaksonen, M., Toret, C.P., Drubin, D.G., 2006. Harnessing actin dynamics for clathrin-mediated endocytosis. Nat Rev Mol Cell Biol 7, 404-414.

Kambara, T., Rhodes, T.E., Ikebe, R., Yamada, M., White, H.D., Ikebe, M., 1999. Functional significance of the conserved residues in the flexible hinge region of the myosin motor domain. The Journal of biological chemistry 274, 16400-16406.

Kay, J.G., Koivusalo, M., Ma, X., Wohland, T., Grinstein, S., 2012. Phosphatidylserine dynamics in cellular membranes. Mol Biol Cell 23, 2198-2212.

Khoroshev, M.I., Munson, S.J., Bikle, D.D., 1999. Six putative IQ motifs of the recombinant chicken intestinal brush border myosin I are involved in calmodulin binding. Arch Biochem Biophys 361, 94-100.

Kim, S.V., Flavell, R.A., 2008. Myosin I: from yeast to human. Cellular and molecular life sciences : CMLS 65, 2128-2137.

Kim, S.V., Mehal, W.Z., Dong, X., Heinrich, V., Pypaert, M., Mellman, I., Dembo, M., Mooseker, M.S., Wu, D., Flavell, R.A., 2006. Modulation of cell adhesion and motility in the immune system by Myo1f. Science 314, 136-139.

Knight, J.D., Falke, J.J., 2009. Single-molecule fluorescence studies of a PH domain: new insights into the membrane docking reaction. Biophys J 96, 566-582.

Knight, J.D., Lerner, M.G., Marcano-Velazquez, J.G., Pastor, R.W., Falke, J.J., 2010. Single molecule diffusion of membrane-bound proteins: window into lipid contacts and bilayer dynamics. Biophys J 99, 2879-2887.

Knight, P.J., Thirumurugan, K., Xu, Y., Wang, F., Kalverda, A.P., Stafford, W.F., 3rd, Sellers, J.R., Peckham, M., 2005. The predicted coiled-coil domain of myosin 10 forms a novel elongated domain that lengthens the head. J Biol Chem 280, 34702-34708.

Kohler, D., Ruff, C., Meyhofer, E., Bahler, M., 2003. Different degrees of lever arm rotation control myosin step size. The Journal of cell biology 161, 237-241.

Kollmar, M., Durrwang, U., Kliche, W., Manstein, D.J., Kull, F.J., 2002. Crystal structure of the motor domain of a class-I myosin. EMBO J 21, 2517-2525.

Komaba, S., Coluccio, L.M., 2010. Localization of myosin 1b to actin protrusions requires phosphoinositide binding. The Journal of biological chemistry 285, 27686-27693.

Koyama, I., Matsunaga, T., Harada, T., Hokari, S., Komoda, T., 2002. Alkaline phosphatases reduce toxicity of lipopolysaccharides in vivo and in vitro through dephosphorylation. Clinical biochemistry 35, 455-461.

Krementsov, D.N., Krementsova, E.B., Trybus, K.M., 2004. Myosin V: regulation by calcium, calmodulin, and the tail domain. The Journal of cell biology 164, 877-886.

Krendel, M., Mooseker, M.S., 2005. Myosins: tails (and heads) of functional diversity. Physiology (Bethesda) 20, 239-251.

Krendel, M., Osterweil, E.K., Mooseker, M.S., 2007. Myosin 1E interacts with synaptojanin-1 and dynamin and is involved in endocytosis. FEBS Lett 581, 644-650.

Laakso, J.M., Lewis, J.H., Shuman, H., Ostap, E.M., 2008. Myosin I can act as a molecular force sensor. Science 321, 133-136.

Laakso, J.M., Lewis, J.H., Shuman, H., Ostap, E.M., 2010. Control of myosin-I force sensing by alternative splicing. Proceedings of the National Academy of Sciences of the United States of America 107, 698-702.

Leibler, S., Huse, D.A., 1993. Porters versus rowers: a unified stochastic model of motor proteins. The Journal of cell biology 121, 1357-1368.

Lewis, J.H., Greenberg, M.J., Laakso, J.M., Shuman, H., Ostap, E.M., 2012. Calcium regulation of myosin-I tension sensing. Biophys J 102, 2799-2807.

Lewis, J.H., Lin, T., Hokanson, D.E., Ostap, E.M., 2006. Temperature dependence of nucleotide association and kinetic characterization of myo1b. Biochemistry 45, 11589-11597.

Li, X.D., Jung, H.S., Mabuchi, K., Craig, R., Ikebe, M., 2006. The globular tail domain of myosin Va functions as an inhibitor of the myosin Va motor. J Biol Chem 281, 21789-21798.

Li, X.D., Jung, H.S., Wang, Q., Ikebe, R., Craig, R., Ikebe, M., 2008. The globular tail domain puts on the brake to stop the ATPase cycle of myosin Va. Proc Natl Acad Sci U S A 105, 1140-1145.

Li, X.D., Saito, J., Ikebe, R., Mabuchi, K., Ikebe, M., 2000. The interaction between the regulatory light chain domains on two heads is critical for regulation of smooth muscle myosin. Biochemistry 39, 2254-2260.

Li, Z., Sacks, D.B., 2003. Elucidation of the interaction of calmodulin with the IQ motifs of IQGAP1. J Biol Chem 278, 4347-4352.

Lin, T., Greenberg, M.J., Moore, J.R., Ostap, E.M., 2011. A hearing loss-associated myo1c mutation (R156W) decreases the myosin duty ratio and force sensitivity. Biochemistry 50, 1831-1838.

Lin, T., Tang, N., Ostap, E.M., 2005. Biochemical and motile properties of Myo1b splice isoforms. The Journal of biological chemistry 280, 41562-41567.

Loomis, P.A., Zheng, L., Sekerkova, G., Changyaleket, B., Mugnaini, E., Bartles, J.R., 2003. Espin cross-links cause the elongation of microvillus-type parallel actin bundles in vivo. The Journal of cell biology 163, 1045-1055.

Lymn, R.W., Taylor, E.W., 1971. Mechanism of adenosine triphosphate hydrolysis by actomyosin. Biochemistry 10, 4617-4624.

Lynch, T.J., Brzeska, H., Miyata, H., Korn, E.D., 1989. Purification and characterization of a third isoform of myosin I from Acanthamoeba castellanii. The Journal of biological chemistry 264, 19333-19339.

Malo, M.S., Alam, S.N., Mostafa, G., Zeller, S.J., Johnson, P.V., Mohammad, N., Chen, K.T., Moss, A.K., Ramasamy, S., Faruqui, A., Hodin, S., Malo, P.S., Ebrahimi, F., Biswas, B., Narisawa, S., Millan, J.L., Warren, H.S., Kaplan, J.B., Kitts, C.L., Hohmann, E.L., Hodin, R.A., 2010. Intestinal alkaline phosphatase preserves the normal homeostasis of gut microbiota. Gut 59, 1476-1484.

Manceva, S., Lin, T., Pham, H., Lewis, J.H., Goldman, Y.E., Ostap, E.M., 2007. Calcium regulation of calmodulin binding to and dissociation from the myo1c regulatory domain. Biochemistry 46, 11718-11726.

Matsudaira, P.T., Burgess, D.R., 1979. Identification and organization of the components in the isolated microvillus cytoskeleton. J Cell Biol 83, 667-673.

Mazerik, J.N., Tyska, M.J., 2012. Myosin-1A targets to microvilli using multiple membrane binding motifs in the tail homology 1 (TH1) domain. The Journal of biological chemistry 287, 13104-13115.

Mazzolini, R., Dopeso, H., Mateo-Lozano, S., Chang, W., Rodrigues, P., Bazzocco, S., Alazzouzi, H., Landolfi, S., Hernandez-Losa, J., Andretta, E., Alhopuro, P., Espin, E., Armengol, M., Tabernero, J., Ramon y Cajal, S., Kloor, M., Gebert, J., Mariadason, J.M., Schwartz, S., Jr., Aaltonen, L.A., Mooseker, M.S., Arango, D., 2012. Brush border myosin Ia has tumor suppressor activity in the intestine. Proceedings of the National Academy of Sciences of the United States of America 109, 1530-1535.

Mazzolini, R., Rodrigues, P., Bazzocco, S., Dopeso, H., Ferreira, A.M., Mateo-Lozano, S., Andretta, E., Woerner, S.M., Alazzouzi, H., Landolfi, S., Hernandez-Losa, J., Macaya, I., Suzuki, H., Ramon, Y.C.S., Mooseker, M.S., Mariadason, J.M., Gebert, J., Hofstra, R.M., Reventos, J., Yamamoto, H., Schwartz, S., Jr., Arango, D., 2013. Brush border myosin Ia inactivation in gastric but not endometrial tumors. International journal of cancer. Journal international du cancer 132, 1790-1799.

McConnell, R.E., Higginbotham, J.N., Shifrin, D.A., Jr., Tabb, D.L., Coffey, R.J., Tyska, M.J., 2009. The enterocyte microvillus is a vesicle-generating organelle. The Journal of cell biology 185, 1285-1298.

McConnell, R.E., Tyska, M.J., 2007. Myosin-1a powers the sliding of apical membrane along microvillar actin bundles. The Journal of cell biology 177, 671-681.

McConnell, R.E., Tyska, M.J., 2010. Leveraging the membrane - cytoskeleton interface with myosin-1. Trends in cell biology 20, 418-426.

McKenna, J.M., Ostap, E.M., 2009. Kinetics of the interaction of myo1c with phosphoinositides. The Journal of biological chemistry 284, 28650-28659.

McLaughlin, S., Aderem, A., 1995. The myristoyl-electrostatic switch: a modulator of reversible protein-membrane interactions. Trends Biochem Sci 20, 272-276.

McLaughlin, S., Wang, J., Gambhir, A., Murray, D., 2002. PIP(2) and proteins: interactions, organization, and information flow. Annu Rev Biophys Biomol Struct 31, 151-175.

McNally, E.M., Bravo-Zehnder, M.M., Leinwand, L.A., 1991. Identification of sequences necessary for the association of cardiac myosin subunits. The Journal of cell biology 113, 585-590.

Mele, C., Iatropoulos, P., Donadelli, R., Calabria, A., Maranta, R., Cassis, P., Buelli, S., Tomasoni, S., Piras, R., Krendel, M., Bettoni, S., Morigi, M., Delledonne, M., Pecoraro, C., Abbate, I., Capobianchi, M.R., Hildebrandt, F., Otto, E., Schaefer, F., Macciardi, F., Ozaltin, F., Emre, S., Ibsirlioglu, T., Benigni, A., Remuzzi, G., Noris, M., 2011. MYO1E mutations and childhood familial focal segmental glomerulosclerosis. The New England journal of medicine 365, 295-306.

Milligan, R.A., 1996. Protein-protein interactions in the rigor actomyosin complex. Proc Natl Acad Sci U S A 93, 21-26.

Miyata, H., Bowers, B., Korn, E.D., 1989. Plasma membrane association of Acanthamoeba myosin I. The Journal of cell biology 109, 1519-1528.

Mooseker, M.S., 1985. Organization, chemistry, and assembly of the cytoskeletal apparatus of the intestinal brush border. Annu Rev Cell Biol 1, 209-241.

Mooseker, M.S., Cheney, R.E., 1995. Unconventional myosins. Annu Rev Cell Dev Biol 11, 633-675.

Mooseker, M.S., Coleman, T.R., 1989. The 110-kD protein-calmodulin complex of the intestinal microvillus (brush border myosin I) is a mechanoenzyme. 108, 2395-2400.

Mooseker, M.S., Tilney, L.G., 1975. Organization of an actin filament-membrane complex. Filament polarity and membrane attachment in the microvilli of intestinal epithelial cells. The Journal of cell biology 67, 725-743.

Nagata, K., Zheng, L., Madathany, T., Castiglioni, A.J., Bartles, J.R., Garcia-Anoveros, J., 2008. The varitint-waddler (Va) deafness mutation in TRPML3 generates constitutive, inward rectifying currents and causes cell degeneration. Proceedings of the National Academy of Sciences of the United States of America 105, 353-358.

Nambiar, R., McConnell, R.E., Tyska, M.J., 2009. Control of cell membrane tension by myosin-I. Proceedings of the National Academy of Sciences of the United States of America 106, 11972-11977.

Nambiar, R., McConnell, R.E., Tyska, M.J., 2010. Myosin motor function: the ins and outs of actin-based membrane protrusions. Cell Mol Life Sci 67, 1239-1254.

Novak, K.D., Peterson, M.D., Reedy, M.C., Titus, M.A., 1995. Dictyostelium myosin I double mutants exhibit conditional defects in pinocytosis. J Cell Biol 131, 1205-1221.

Novak, K.D., Titus, M.A., 1997. Myosin I overexpression impairs cell migration. J Cell Biol 136, 633-647.

Novak, K.D., Titus, M.A., 1998. The myosin I SH3 domain and TEDS rule phosphorylation site are required for in vivo function. Mol Biol Cell 9, 75-88.

Nowak, G., Pestic-Dragovich, L., Hozak, P., Philimonenko, A., Simerly, C., Schatten, G., de Lanerolle, P., 1997. Evidence for the presence of myosin I in the nucleus. J Biol Chem 272, 17176-17181.

Odronitz, F., Kollmar, M., 2007. Drawing the tree of eukaryotic life based on the analysis of 2,269 manually annotated myosins from 328 species. Genome Biol 8, R196.

Olety, B., Walte, M., Honnert, U., Schillers, H., Bahler, M., 2010. Myosin 1G (Myo1G) is a haematopoietic specific myosin that localises to the plasma membrane and regulates cell elasticity. FEBS Lett 584, 493-499.

Parkin, E.T., Turner, A.J., Hooper, N.M., 2001. Differential effects of glycosphingolipids on the detergent-insolubility of the glycosylphosphatidylinositol-anchored membrane dipeptidase. The Biochemical journal 358, 209-216.

Patino-Lopez, G., Aravind, L., Dong, X., Kruhlak, M.J., Ostap, E.M., Shaw, S., 2010. Myosin 1G is an abundant class I myosin in lymphocytes whose localization at the plasma membrane depends on its ancient divergent pleckstrin homology (PH) domain (Myo1PH). The Journal of biological chemistry 285, 8675-8686.

Percipalle, P., Farrants, A.K., 2006. Chromatin remodelling and transcription: be-WICHed by nuclear myosin 1. Current opinion in cell biology 18, 267-274.

Pestic-Dragovich, L., Stojiljkovic, L., Philimonenko, A.A., Nowak, G., Ke, Y., Settlage, R.E., Shabanowitz, J., Hunt, D.F., Hozak, P., de Lanerolle, P., 2000. A myosin I isoform in the nucleus. Science 290, 337-341.

Petzoldt, A.G., Coutelis, J.B., Geminard, C., Speder, P., Suzanne, M., Cerezo, D., Noselli, S., 2012. DE-Cadherin regulates unconventional Myosin ID and Myosin IC in Drosophila left-right asymmetry establishment. Development 139, 1874-1884.

Philimonenko, V.V., Zhao, J., Iben, S., Dingova, H., Kysela, K., Kahle, M., Zentgraf, H., Hofmann, W.A., de Lanerolle, P., Hozak, P., Grummt, I., 2004. Nuclear actin and myosin I are required for RNA polymerase I transcription. Nature cell biology 6, 1165-1172.

Pollard, T.D., Korn, E.D., 1973. Acanthamoeba myosin. I. Isolation from Acanthamoeba castellanii of an enzyme similar to muscle myosin. The Journal of biological chemistry 248, 4682-4690.

Pyrpassopoulos, S., Feeser, E.A., Mazerik, J.N., Tyska, M.J., Ostap, E.M., 2012. Membrane-bound myo1c powers asymmetric motility of actin filaments. Curr Biol 22, 1688-1692.

Pyrpassopoulos, S., Shuman, H., Ostap, E.M., 2010. Single-molecule adhesion forces and attachment lifetimes of myosin-I phosphoinositide interactions. Biophys J 99, 3916-3922.

Rando, O.J., Zhao, K., Crabtree, G.R., 2000. Searching for a function for nuclear actin. Trends Cell Biol 10, 92-97.

Raucher, D., Sheetz, M.P., 2000. Cell spreading and lamellipodial extension rate is regulated by membrane tension. J Cell Biol 148, 127-136.

Rayment, I., Rypniewski, W.R., Schmidt-Base, K., Smith, R., Tomchick, D.R., Benning, M.M., Winkelmann, D.A., Wesenberg, G., Holden, H.M., 1993. Three-dimensional structure of myosin subfragment-1: a molecular motor. Science 261, 50-58.

Redowicz, M.J., 2001. Regulation of nonmuscle myosins by heavy chain phosphorylation. Journal of muscle research and cell motility 22, 163-173.

Ricci, A.J., Wu, Y.C., Fettiplace, R., 1998. The endogenous calcium buffer and the time course of transducer adaptation in auditory hair cells. J Neurosci 18, 8261-8277.

Richards, T.A., Cavalier-Smith, T., 2005. Myosin domain evolution and the primary divergence of eukaryotes. Nature 436, 1113-1118.

Roy, A., Kucukural, A., Zhang, Y., 2010. I-TASSER: a unified platform for automated protein structure and function prediction. Nat Protoc 5, 725-738.

Ruppert, C., Godel, J., Muller, R.T., Kroschewski, R., Reinhard, J., Bahler, M., 1995. Localization of the rat myosin I molecules myr 1 and myr 2 and in vivo targeting of their tail domains. J Cell Sci 108 (Pt 12), 3775-3786.

Ruppert, C., Kroschewski, R., Bahler, M., 1993. Identification, characterization and cloning of myr 1, a mammalian myosin-I. J Cell Biol 120, 1393-1403.

Salas-Cortes, L., Ye, F., Tenza, D., Wilhelm, C., Theos, A., Louvard, D., Raposo, G., Coudrier, E., 2005. Myosin Ib modulates the morphology and the protein transport within multi-vesicular sorting endosomes. J Cell Sci 118, 4823-4832.

Sasaki, N., Ohkura, R., Sutoh, K., 2003. Dictyostelium myosin II mutations that uncouple the converter swing and ATP hydrolysis cycle. Biochemistry 42, 90-95.

Saxton, M.J., 1997. Single-particle tracking: the distribution of diffusion coefficients. Biophys J 72, 1744-1753.

Schietroma, C., Yu, H.Y., Wagner, M.C., Umbach, J.A., Bement, W.M., Gundersen, C.B., 2007. A role for myosin 1e in cortical granule exocytosis in Xenopus oocytes. J Biol Chem 282, 29504-29513.

Sellers, J.R., Adelstein, R.S., 1985. The mechanism of regulation of smooth muscle myosin by phosphorylation. 27, 51-62.

Sellers, J.R., Knight, P.J., 2007. Folding and regulation in myosins II and V. J Muscle Res Cell Motil 28, 363-370.

Sherr, E.H., Joyce, M.P., Greene, L.A., 1993. Mammalian myosin I alpha, I beta, and I gamma: new widely expressed genes of the myosin I family. J Cell Biol 120, 1405-1416.

Shifrin, D.A., Jr., McConnell, R.E., Nambiar, R., Higginbotham, J.N., Coffey, R.J., Tyska, M.J., 2012. Enterocyte microvillus-derived vesicles detoxify bacterial products and regulate epithelial-microbial interactions. Curr Biol 22, 627-631.

Shimada, T., Sasaki, N., Ohkura, R., Sutoh, K., 1997. Alanine scanning mutagenesis of the switch I region in the ATPase site of Dictyostelium discoideum myosin II. Biochemistry 36, 14037-14043.

Skowron, J.F., Mooseker, M.S., 1999. Cloning and characterization of mouse brush border myosin-I in adult and embryonic intestine. J Exp Zool 283, 242-257.

Sokac, A.M., Schietroma, C., Gundersen, C.B., Bement, W.M., 2006. Myosin-1c couples assembling actin to membranes to drive compensatory endocytosis. Developmental cell 11, 629-640.

Speder, P., Adam, G., Noselli, S., 2006. Type ID unconventional myosin controls left-right asymmetry in Drosophila. Nature 440, 803-807.

Speder, P., Noselli, S., 2007. Left-right asymmetry: class I myosins show the direction. Current opinion in cell biology 19, 82-87.

Stauffer, E.A., Scarborough, J.D., Hirono, M., Miller, E.D., Shah, K., Mercer, J.A., Holt, J.R., Gillespie, P.G., 2005. Fast adaptation in vestibular hair cells requires myosin-1c activity. Neuron 47, 541-553.

Stoffler, H.E., Bahler, M., 1998. The ATPase activity of Myr3, a rat myosin I, is allosterically inhibited by its own tail domain and by Ca2+ binding to its light chain calmodulin. The Journal of biological chemistry 273, 14605-14611.

Sun, Y., Martin, A.C., Drubin, D.G., 2006. Endocytic internalization in budding yeast requires coordinated actin nucleation and myosin motor activity. Developmental cell 11, 33-46.

Swanljung-Collins, H., Collins, J.H., 1991. Ca2+ stimulates the Mg2(+)-ATPase activity of brush border myosin I with three or four calmodulin light chains but inhibits with less than two bound. 266, 1312-1319.

Szentpetery, Z., Balla, A., Kim, Y.J., Lemmon, M.A., Balla, T., 2009. Live cell imaging with protein domains capable of recognizing phosphatidylinositol 4,5-bisphosphate; a comparative study. BMC Cell Biol 10, 67.

Tang, N., Lin, T., Ostap, E.M., 2002. Dynamics of myo1c (myosin-ibeta) lipid binding and dissociation. The Journal of biological chemistry 277, 42763-42768.

Tang, N., Ostap, E.M., 2001. Motor domain-dependent localization of myo1b (myr-1). Curr Biol 11, 1131-1135.

Taylor, K.A., 2007. Regulation and recycling of myosin V. Current opinion in cell biology 19, 67-74.

Thompson, R.F., Langford, G.M., 2002. Myosin superfamily evolutionary history. Anat Rec 268, 276-289.

Titus, M.A., 2006. Myosin I and actin dynamics: the frogs weigh in. Developmental cell 11, 594-595.

Titus, M.A., Wessels, D., Spudich, J.A., Soll, D., 1993. The unconventional myosin encoded by the myoA gene plays a role in Dictyostelium motility. Mol Biol Cell 4, 233-246.

Toprak, E., Kural, C., Selvin, P.R., 2010. Super-accuracy and super-resolution getting around the diffraction limit. Methods Enzymol 475, 1-26.

Toyoda, T., An, D., Witczak, C.A., Koh, H.J., Hirshman, M.F., Fujii, N., Goodyear, L.J., 2011. Myo1c regulates glucose uptake in mouse skeletal muscle. J Biol Chem 286, 4133-4140.

Trybus, K.M., 2008. Myosin V from head to tail. Cell Mol Life Sci 65, 1378-1389.

Tyska, M.J., Mackey, A.T., Huang, J.D., Copeland, N.G., Jenkins, N.A., Mooseker, M.S., 2005. Myosin-1a is critical for normal brush border structure and composition. Mol Biol Cell 16, 2443-2457.

Tyska, M.J., Mooseker, M.S., 2002. MYO1A (brush border myosin I) dynamics in the brush border of LLC-PK1-CL4 cells. Biophys J 82, 1869-1883.

Tyska, M.J., Mooseker, M.S., 2004. A role for myosin-1A in the localization of a brush border disaccharidase. The Journal of cell biology 165, 395-405.

Umeki, N., Jung, H.S., Sakai, T., Sato, O., Ikebe, R., Ikebe, M., 2011. Phospholipid-dependent regulation of the motor activity of myosin X. Nature structural & molecular biology 18, 783-788.

Umeki, N., Jung, H.S., Watanabe, S., Sakai, T., Li, X.D., Ikebe, R., Craig, R., Ikebe, M., 2009. The tail binds to the head-neck domain, inhibiting ATPase activity of myosin VIIA. Proc Natl Acad Sci U S A 106, 8483-8488.

Uyeda, T.Q., Ruppel, K.M., Spudich, J.A., 1994. Enzymatic activities correlate with chimaeric substitutions at the actin-binding face of myosin. Nature 368, 567-569.

Vale, R.D., Milligan, R.A., 2000. The way things move: looking under the hood of molecular motor proteins. Science 288, 88-95.

Vallotton, P., Ponti, A., Waterman-Storer, C.M., Salmon, E.D., Danuser, G., 2003. Recovery, visualization, and analysis of actin and tubulin polymer flow in live cells: a fluorescent speckle microscopy study. Biophys J 85, 1289-1306.

van Meer, G., de Kroon, A.I., 2011. Lipid map of the mammalian cell. Journal of cell science 124, 5-8.

van Meer, G., Voelker, D.R., Feigenson, G.W., 2008. Membrane lipids: where they are and how they behave. Nat Rev Mol Cell Biol 9, 112-124.

Varnai, P., Balla, T., 1998. Visualization of phosphoinositides that bind pleckstrin homology domains: calcium- and agonist-induced dynamic changes and relationship to myo-[3H]inositol-labeled phosphoinositide pools. J Cell Biol 143, 501-510.

Veigel, C., Coluccio, L.M., Jontes, J.D., Sparrow, J.C., Milligan, R.A., Molloy, J.E., 1999. The motor protein myosin-I produces its working stroke in two steps. Nature 398, 530-533.

Wang, F., Thirumurugan, K., Stafford, W.F., Hammer, J.A., 3rd, Knight, P.J., Sellers, J.R., 2004. Regulated conformation of myosin V. J Biol Chem 279, 2333-2336.

Wessels, D., Murray, J., Jung, G., Hammer, J.A., 3rd, Soll, D.R., 1991. Myosin IB null mutants of Dictyostelium exhibit abnormalities in motility. Cell motility and the cytoskeleton 20, 301-315.

Whittaker, M., Milligan, R.A., 1997. Conformational changes due to calcium-induced calmodulin dissociation in brush border myosin I-decorated F-actin revealed by cryoelectron microscopy and image analysis. Journal of molecular biology 269, 548-557.

Williams, R., Coluccio, L.M., 1994. Novel 130-kDa rat liver myosin-1 will translocate actin filaments. Cell motility and the cytoskeleton 27, 41-48.

Wolenski, J.S., Hayden, S.M., Forscher, P., Mooseker, M.S., 1993a. Calcium-calmodulin and regulation of brush border myosin-I MgATPase and mechanochemistry. J Cell Biol 122, 613-621.

Wolenski, J.S., Hayden, S.M., Forscher, P., Mooseker, M.S., 1993b. Calcium-calmodulin and regulation of brush border myosin-I MgATPase and mechanochemistry. The Journal of cell biology 122, 613-621.

Yang, Y., Baboolal, T.G., Siththanandan, V., Chen, M., Walker, M.L., Knight, P.J., Peckham, M., Sellers, J.R., 2009. A FERM domain autoregulates Drosophila myosin 7a activity. Proc Natl Acad Sci U S A 106, 4189-4194.

Yap, K.L., Ames, J.B., Swindells, M.B., Ikura, M., 1999. Diversity of conformational states and changes within the EF-hand protein superfamily. Proteins 37, 499-507.

Ye, J., Zhao, J., Hoffmann-Rohrer, U., Grummt, I., 2008. Nuclear myosin I acts in concert with polymeric actin to drive RNA polymerase I transcription. Genes & development 22, 322-330.

Yengo, C.M., Ananthanarayanan, S.K., Brosey, C.A., Mao, S., Tyska, M.J., 2008. Human deafness mutation E385D disrupts the mechanochemical coupling and subcellular targeting of myosin-1a. Biophys J 94, L5-7.

Yeung, T., Gilbert, G.E., Shi, J., Silvius, J., Kapus, A., Grinstein, S., 2008. Membrane phosphatidylserine regulates surface charge and protein localization. Science 319, 210-213.

Yeung, T., Heit, B., Dubuisson, J.F., Fairn, G.D., Chiu, B., Inman, R., Kapus, A., Swanson, M., Grinstein, S., 2009. Contribution of phosphatidylserine to membrane surface charge and protein targeting during phagosome maturation. The Journal of cell biology 185, 917-928.

Yip, M.F., Ramm, G., Larance, M., Hoehn, K.L., Wagner, M.C., Guilhaus, M., James, D.E., 2008. CaMKII-mediated phosphorylation of the myosin motor Myo1c is required for insulin-stimulated GLUT4 translocation in adipocytes. Cell metabolism 8, 384-398.

Zadro, C., Alemanno, M.S., Bellacchio, E., Ficarella, R., Donaudy, F., Melchionda, S., Zelante, L., Rabionet, R., Hilgert, N., Estivill, X., Van Camp, G., Gasparini, P., Carella, M., 2009. Are MYO1C and MYO1F associated with hearing loss? Biochimica et biophysica acta 1792, 27-32.

Zhang, P., Wang, Y., Sesaki, H., Iijima, M., 2010. Proteomic identification of phosphatidylinositol (3,4,5) triphosphate-binding proteins in Dictyostelium discoideum. Proc Natl Acad Sci U S A 107, 11829-11834.

Zhang, Y., 2008. I-TASSER server for protein 3D structure prediction. BMC Bioinformatics 9, 40.

Zhu, T., Beckingham, K., Ikebe, M., 1998. High affinity Ca2+ binding sites of calmodulin are critical for the regulation of myosin Ibeta motor function. J Biol Chem 273, 20481-20486.

Zhu, T., Sata, M., Ikebe, M., 1996. Functional expression of mammalian myosin I beta: analysis of its motor activity. Biochemistry 35, 513-522.